NASA CONTRACTOR REPORT

NASA CR-1689

PARAMETRIC ANALYSIS OF MICROWAVE AND LASER SYSTEMS FOR COMMUNICATION AND TRACKING

Volume IV - Operational Environment and System Implementation

Prepared by
HUGHES AIRCRAFT COMPANY
Culver City, Calif. 90230
for Goddard Space Flight Center

NATIONAL AERONAUTICS AND SPACE ADMINISTRATION • WASHINGTON, D. C. • FEBRUARY 1971

1. Report No.	2. Government Accession No.	3. Recipient's Catalog No.
NASA CR-1689		

4. Title and Subtitle
Parametric Analysis of Microwave and Laser Systems for Communication and Tracking; Volume IV - Operational Environment and System Implementation

5. Report Date
February 1971

6. Performing Organization Code

7. Author(s)

8. Performing Organization Report No.

9. Performing Organization Name and Address
Hughes Aircraft Company
Culver City, California

10. Work Unit No.

11. Contract or Grant No.
NAS 5-9637

12. Sponsoring Agency Name and Address
National Aeronautics and Space Administration
Washington, D. C. 20546

13. Type of Report and Period Covered
Contractor Report

14. Sponsoring Agency Code

15. Supplementary Notes Prepared in cooperation with all the available experts at the Hughes Aircraft Company and edited jointly by L. S. Stokes, the Program Manager, K. L. Brinkman, the Associate Program Manager, and Dr. F. Kalil, the NASA-GSFC Technical Monitor, with L. S. Stokes being the primary contributing editor.

16. Abstract

Present and future space programs are requiring progressively higher communication rates. For instance, the Earth Resources Technology Satellite-A requires about 70 MHz total bandwidth in its S-Band downlink spectra, and it appears likely that future earth observation satellites will require more bandwidth because of the larger number of sensors and higher sensor resolutions. On the other hand, the frequency bands allocated via international agreements for space use are limited, and hence, the r-f spectrum is becoming crowded. However, the advent of the C-W laser systems offered a "new" and wide electromagnetic spectrum for use in space telecommunications. Although the laser systems offered this "new" capability, their technological development was also new. Therefore, this study was undertaken to make a comparative analysis of microwave and laser space telecommunication systems. A fundamental objective of the study was to provide the mission planner and designer with reference data (weight, volume, reliability, and costs), supplementary material, and a trade-off methodology for selecting the system (microwave or optical) which best suits his requirements. This report is the final report of that study. Because of the large amount of material, the report is presented in four volumes. This volume, Volume IV, "Operational Environment and System Implementation," has three major parts: Background Radiation and Atmospheric Propagation, Ground Receiving Facilities, and System Implementation. Background Radiation and Atmospheric Propagation deals with interfering signals that compete with both laser and microwave communication. Further the atmospheric attenuation as a function of frequency and weather condition is given. The ground receiving facilities part contains a brief description of current world wide networks such as the MSFN, DSIF, and STADAN. System Implementation describes the communications systems of several successful spacecraft. These may be used as a reference and comparison for future design.

17. Key Words (Selected by Author(s))	18. Distribution Statement
Background Radiation/Noise Atmospheric Propagation Earth Receiving Facilities	Unclassified - Unlimited

19. Security Classif. (of this report)	20. Security Classif. (of this page)	21. No. of Pages	22. Price*
Unclassified	Unclassified	227	$3.00

*For sale by the National Technical Information Service, Springfield, Virginia 22151

PARAMETRIC ANALYSIS OF MICROWAVE AND LASER SYSTEMS FOR COMMUNICATION AND TRACKING

VOLUME I	SUMMARY
VOLUME II	SYSTEM SELECTION
VOLUME III	REFERENCE DATA FOR ADVANCED SPACE COMMUNICATION AND TRACKING SYSTEMS
VOLUME IV	**OPERATIONAL ENVIRONMENT AND SYSTEM IMPLEMENTATION**

ACKNOWLEDGEMENT

The material for Background Radiation and Atmospheric Propagation and the material for Earth Receiving Facilities were largely prepared by Mr. James R. Sullivan formerly with Hughes Aircraft Company and presently with Systems Associates.

BRIEF INDEX OF VOLUME IV

PART 1 BACKGROUND RADIATION AND ATMOSPHERIC PROPAGATION

PART 2 EARTH RECEIVING FACILITIES

PART 3 SYSTEMS IMPLEMENTATION

OPERATIONAL ENVIRONMENT AND SYSTEM IMPLEMENTATION

DETAILED INDEX OF VOLUME IV

PART 1 BACKGROUND RADIATION AND ATMOSPHERIC PROPAGATION

DETAILED INDEX OF VOLUME IV (Continued)

PART 1 BACKGROUND RADIATION AND ATMOSPHERIC PROPAGATION

INTRODUCTION

Background radiation and atmospheric propagation can seriously degrade space communications.

The effect of external noise is of great significance in determining ultimate communication system performance. Such information as is currently available concerning external noise sources relevant to optical and microwave space communication systems is given in the following sections. The principal types of noise encountered are:

1. Cosmic noise, originating outside the solar system
2. Terrestrial noise, originating from the earth or its surrounding atmosphere
3. Solar system noise, other than terrestrial, originating from the sun, the planets, or their satellites.

Unless otherwise stated, all measurements of extraterrestrial radio and optical background are corrected for atmospheric attenuation and refraction.

Subsequent to the discussion of external noise is a discussion of propagation of radio frequency and optical radiation through the terrestrial atmosphere. These include effects of atmospheric anomalies in introducing phase and polarization changes, beam scanning, and scintillation is considered.

Background Radiation and Atmospheric Propagation

SUMMARY

Background radiation competes with the desired signal, both are attenuated by the earth's atmosphere.

Two major considerations are described in this part: the energy which may compete with a desired signal, background radiation and the attenuation of a desired signal (or background energy) by the earth's atmosphere. Other atmospheric effects are discussed briefly.

The background radiation enters an optical or radio receiver which has a particular antenna area, antenna field of view, and bandwidth. Since these three receiver parameters vary with each receiving site, measurements of background radiation have been usually normalized with respect to all three. Thus it is common to see the optical energy from a background source expressed as:

$$\frac{\text{watts}}{(\text{cm}^2)\ (\text{Steradian})\ (\text{micron})}$$

and energy from radio sources expressed as:

$$\frac{\text{watts}}{(\text{Cm}^2)\ (\text{Steradian})\ (\text{Hz})}$$

In order to find the interfering power it is necessary to multiply these normalized values by the area of the antennas, the field of view and the optical or radio bandwidth.

Care must be exercised in the case of the field of view. If the background angular extent is greater than the field of view of the receiving aperture, then the receiving field of view is used. If the angular extent of the background is less than the receiving field of view then the angular dimensions of the source are used.

Propagation losses reduce the signal strength of the desired and in most cases the background energy. The loss is wavelength sensitive and is given per unit of range and for total loss through the earth's atmosphere as a function of zenith angle.

SUMMARY

In RF receivers, the background noise is usually equated in terms of an antenna noise temperature. That is, the total system noise temperature measured at the receiver input terminal is

$$T_{system} = \frac{T_{ant}}{L} + \left(1 - \frac{1}{L}\right) + T_{eff,\ rcvr}$$

where

T_{ant} = effective antenna noise temperature resulting from the background radiation which gets into the antenna feeds via the lobes or other optical paths, *i. e.* via the main lobe, sidelobes, backlobes in the case of mesh antennas, and spill-over

T_L = temperature of the lines from the antenna to the receiver input terminals

L = line losses

$T_{eff,\ rcvr}$ = T_o (N. F. - 1), effective receiver noise temperature discussed in part 3 of Volume III

N. F. = receiver noise figure

T_o = 290^oK

BACKGROUND RADIATION AND ATMOSPHERIC PROPAGATION

Radio Frequency Background

ANTENNA NOISE POWER AND NOISE TEMPERATURE[1]

The brightness of external noise is related to the antenna gain pattern to determine the total power received from a noise source.

Relative contributions to microwave receiving system noise may be conveniently compared in terms of noise temperature. The concept of noise temperature is related to the Rayleigh-Jeans approximation for power density radiated by a black body cavity. The power density emanating from a unit solid angle per cycle of bandwidth (watts $m^{-2}ster^{-1}(Hz)^{-1}$) is called brightness. The brightness, B', is given rigorously for a Lambertian surface radiating into a hemisphere from Planck's equation by:

$$B' = \frac{2hf}{\lambda^2 \left(e^{\frac{hf}{kT}} - 1 \right)} \tag{1}$$

f = frequency (Hz)

h = Planck's constant (6.624×10^{-34} joule sec)

k = Boltzmann's constant (1.38×10^{-23} joules/^{o}K)

T = temperature (^{o}K)

λ = wavelength (m)

The Rayleigh-Jeans approximation to Planck's equation gives

$$B = \frac{2kT}{\lambda^2} \tag{2}$$

which is valid for $hf/kT \ll 1$.

Consider the calculation of the noise power available to a receiving antenna in the frequency interval f to f + β, where β is the bandwidth (Hz). The contribution to the available noise power from an elemental solid angle, $d\Omega$, is obtained by multiplying the effective area of the antenna in the direction of the solid angle, by the incident power density (watts m^{-2}) having the same polarization as the antenna and originating from that elemental solid angle.

---

[1] Evans, A., Brchyuski, M. P., and Wacker, A. G., "The Radio Spectrum in Aerospace Communications," Technical Report ASD-TR-61-589; IV, Absorption in Planetary Atmospheres and Sources of Noise, RCA Victor Company Ltd., Montreal Canada, pp. 115-132, August 1962.

That is

$$dP = \{A(\theta_1, \phi_1)\} \{\gamma\beta B(\theta_1, \phi_1)\, d\Omega\} \tag{3}$$

where

dP = the elemental available power received by the antenna from the solid angle, $d\Omega$ (watts)

β = the bandwidth in question (Hz)

$A(\theta_1, \phi_1)$ = the effective area of the antenna in the direction of the solid angle $d\Omega$ (m^2)

$B(\theta_1, \phi_1)$ = the brightness in the direction of the solid angle $d\Omega$. (watts m^{-2} $ster^{-1}$ Hz^{-1})

γ = the polarization coefficient ($\gamma = 1/2$ if the receiving antenna is linearly polarized and the incident electromagnetic radiation is randomly polarized, since only 1/2 the power in a randomly polarized electromagnetic wave can be intercepted by a linearly polarized antenna).

θ_1 and ϕ_1 = are particular values of the spatial coordinate angles θ and ϕ (i. e., the values of θ and ϕ in the direction of the solid angle $d\Omega$).

Equation (3) can be considered to define the effective area of an antenna.

To obtain the total available power P, the contribution from all directions must be added. This superposition of power is permissible provided that the contributions from the various directions are uncorrelated as is usually the case for noise. Thus

$$P = \iint_{4\pi} \gamma\beta A(\theta, \phi) B(\theta, \phi)\, d\Omega \tag{4}$$

where

$A(\theta, \phi)$ is the effective area of the antenna as a function of the direction and will be referred to as the effective area function of the antenna

and

$B(\theta, \phi)$ is the brightness of the antenna surroundings as a function of direction and will be referred to as the brightness function of the source.

ANTENNA NOISE POWER AND NOISE TEMPERATURE

The antenna gain function is defined as

$$G(\theta,\phi) = \frac{4\pi P(\theta,\phi)}{\iint_{4\pi} P(\theta,\phi)\, d\Omega} \tag{5}$$

where

$P(\theta,\phi)$ = the power radiated per unit solid angle as a function of the coordinates

The effective area function of an antenna is related to the antenna gain function $G(\theta,\phi)$ by

$$A(\theta,\phi) = \frac{\lambda^2}{4\pi} G(\theta,\phi) \tag{6}$$

In the direction of maximum gain (6) becomes

$$A = \frac{\lambda^2}{4\pi} G \tag{7}$$

where

G = the maximum antenna gain

A = the maximum effective area.

The antenna beamwidth Ω_a is defined as

$$\Omega_a = \frac{4\pi}{G} \tag{8}$$

The beamwidth Ω_a is the solid angle through which all the power radiated from an antenna would stream, if the power per unit solid angle equalled the maximum value over the beamwidth. Inherent in the use of beamwidth is the assumption that the gain and effective area functions are constant over the beamwidth with values of G and A respectively and zero elsewhere. Furthermore, the concept is applicable only to antennas that have only one principle lobe in the radiation pattern.

The derived expression for the available power is general. If the antenna is placed in a black body cavity the brightness function is

constant and is given by (2) (classically) or (1) (quantum mechanically). Using the classical equation and $\gamma = 1/2$, the available power, P_b, is

$$P_b = \iint_{4\pi} \frac{1}{2}\beta A(\theta,\phi) \frac{2kT}{\lambda^2} \, d\Omega \tag{9}$$

If the effective area function is expressed in terms of the gain function this reduces to

$$P_b = \frac{kT\beta}{4\pi} \iint_{4\pi} G(\theta,\phi) \, d\Omega \tag{10}$$

Since gain function of an antenna integrated over 4π steradians is 4π, the available power in a black body cavity is

$$P_b = kT\beta \text{ (classically)} \tag{11}$$

and

$$P'_b = \frac{hf\beta}{e^{\frac{hf}{kT}} - 1} \text{ (quantum mechanically).} \tag{12}$$

Consider the problem of calculating the noise power available to an antenna in its actual surroundings. For the lower frequencies, the classical approximation for the brightness in a black body cavity is sufficiently accurate for almost all practical purposes. Furthermore, if the actual environment exhibits a variation of brightness and if the antenna exchanges radiation on a black body basis (i. e., none of the radiation leaving the antenna ever returns to it) then Equation (10) is still valid provided that the directional variation of the brightness is ascribed to the temperature. Hence, provided the classical approximation is valid and assuming γ is $1/2$, the power available to an antenna in its actual environment is

$$P = k \frac{1}{4\pi} \iint_{4\pi} G(\theta,\phi)T(\theta,\phi) \, d\Omega \tag{13}$$

ANTENNA NOISE POWER AND NOISE TEMPERATURE

The quantity $T(\theta, \phi)$ is the brightness temperature as a function of the coordinates. In practice, the antenna and its surroundings do not necessarily radiate like black bodies and hence, $T(\theta, \phi)$ is replaced by an effective brightness temperature $T_e(\theta, \phi)$. The effective temperature takes the emissivity and reflectivity of the antenna environment into consideration. Replacing $T(\theta, \phi)$ in (13) by $T_e(\theta, \phi)$ we have for the available power

$$P = k\beta \frac{1}{4\pi} \iint_{4\pi} G(\theta, \phi) T_e(\theta, \phi) \, d\Omega \tag{14}$$

Comparing this equation with (10) we can define an effective antenna noise temperature T_{eff} as

$$T_{eff} = \frac{1}{4\pi} \iint_{4\pi} G(\theta, \phi) T_e(\theta, \phi) \, d\Omega \tag{15}$$

It is apparent that if the antenna were immersed in a black body cavity whose temperature is T_{eff}, then the noise power which would be received by the antenna from the black body is identical to the noise power received by the antenna from its actual surroundings. It is in this sense that physical significance can be attached to the effective antenna noise temperature. In low noise receiving systems the earth, which subtends approximately 2π sterradians with respect to a surface antenna, contributes significantly to the antenna temperature through the antenna backlobes with an effective $T_{eff} = 300^{o}K$.

If the frequency is sufficiently high, then practical temperatures may be so low that the Rayleigh-Jeans approximation is no longer valid and the expression based on Planck's equation should be used. It is still possible under these circumstances to define an effective antenna noise temperature. However, the concept of effective antenna noise temperature, as defined for the quantum mechanical case is of limited utility. In the classical case, the total input noise power to a receiver can be specified in terms of an effective temperature which is just the sum of the effective noise temperatures of the individual sources of noise. It is this additive property that makes the concept of effective temperatures very useful in the classical case. In the quantum mechanical case the effective noise temperatures are no longer additive because the noise powers are no longer linearly related to the effective noise temperatures.

CALCULATION OF THE ANTENNA NOISE POWER FOR SOME PRACTICAL CASES

The antenna noise power is derived for certain cases where the noise source is in the main lobe of the antenna.

The total noise power, P, received by an antenna, as noted previously, is given by:

$$P = \int\int_{4\pi} \gamma\beta A(\theta,\phi) B(\theta,\phi)\, d\Omega \qquad (1)$$

where

$A(\theta,\phi)$ is the effective area of the antenna as a function of the direction and will be referred to as the effective area function of the antenna.

and

$B(\theta,\phi)$ is the brightness of the antenna surroundings as a function of direction and will be referred to as the brightness function of the source.

β is bandwidth in Hz.

γ is the polarization coefficient.

$d\Omega$ is the incremental solid angle.

The integration of Equation (1) to obtain the total available noise power is quite difficult in practice. Not only are the effective area and brightness complicated functions of the coordinates but usually they are known only approximately, at least for certain values of θ and ϕ. In practice, Equation (1) is usually evaluated by the summation of a finite number of terms. Certain practical cases have been considered. The results are given below in terms of both brightness and effective brightness temperatures.

1. The solid angle subtended by the source (Ω_s) is less than the antenna beamwidth (i.e., $\Omega_s < \Omega_a$). Assume that the angular coordinates of the source center are θ_1 and ϕ_1.

a. Assume that the brightness of the source, $B(\theta_1,\phi_1)$, and the effective area of the antenna, $A(\theta,\phi)$, are constant over the solid angle subtended by the source (Ω_s) and that the brightness is zero elsewhere. That is $B(\theta,\phi) = B$ (a constant) within the solid angle Ω_s. $B(\theta,\phi) = O$ outside the solid angle Ω_s.

and

$$A(\theta,\phi) = A(\theta_1,\phi_1) \text{ (a constant)}$$

where

$A(\theta_1,\phi_1)$ is the effective area in the particular direction θ_1,ϕ_1.

Substituting those quantities in Equation (1) and integrating we have an expression for the available power.

$$P = \gamma\beta A(\theta_1,\phi_1)B\Omega_s \tag{2}$$

If the main beam is pointed in the direction of the source, then the effective area in the direction of the source is A and the available power is

$$P = \gamma\beta A\Omega_s \tag{3}$$

Expressing the effective area in terms of the antenna beamwidth, Equation (3) becomes

$$P = \gamma\beta\lambda^2 B\frac{\Omega_s}{\Omega_a} \tag{4}$$

where

λ is the wavelength

Ω_a is the antenna solid angle

If the constant brightness, B, is expressed in terms of a constant effective brightness temperature T_e, (4) can be written as

$$P = \gamma\beta 2kT_e\frac{\Omega_a}{\Omega_s} \tag{5}$$

In practice, the case of $\Omega_s < \Omega_a$ often occurs for such noise sources as the sun. Actually both the brightness and effective area functions will usually vary somewhat over the solid angle subtended by the source but they can frequently be approximated by a constant representing a suitable average. This is particularly true if the source is much smaller than the antenna beamwidth.

CALCULATION OF THE ANTENNA NOISE POWER FOR SOME PRACTICAL CASES

b. A point source corresponds to the limiting case of $\Omega_s < \Omega_a$. Practical sources are radio stars, since their angular extent is extremely small. For a true point source it is not possible to specify the brightness and angular extend individually since as $\Omega_s \to 0$ $B \to \infty$. Hence, for point sources, the flux density

$$S = \iint_{\Omega_s} B(\theta,\phi)\, d\Omega \ (\text{watts m}^{-2}(\text{cps})^{-1})$$

is usually given. Then

$$P = \gamma\beta A(\theta,\phi)S \tag{6}$$

2. The solid angle subtended by the source is greater than the beamwidth ($\Omega_s > \Omega_a$).

The brightness is constant over the whole solid angle of 4π steradians. That is $B(\theta,\phi) = B$ (a constant) for all θ and ϕ. As already mentioned this is the situation that prevails inside a black body cavity provided $\gamma = 1/2$. In general for any γ and with constant brightness, Equation (1) for the available noise power yields

$$P = \gamma\beta B \iint_{4\pi} A_e(\theta,\phi)\, d\Omega \tag{7}$$

Now the integral of the effective area over the whole solid angle is just λ^2. Therefore,

$$P = \gamma\beta\lambda^2 B \tag{8}$$

This can again be written in terms of the effective brightness temperature. Hence, the available power for this case in terms of brightness temperature is given by

$$P = \gamma 2kT_e B \tag{9}$$

By setting $\Omega_s = \Omega_a$, this equation can also be obtained from Equation (5) which is based on the concept of beamwidth. It is therefore apparent that although the concept of beamwidth is an approximation, the correct result is still obtained for the particular case of constant brightness. Equation (9) is also a good approximation if the brightness is constant over the beamwidth of the antenna and the contribution from the side lobes is small.

NOISE CONTRIBUTION DUE TO ANTENNA BACKLOBES[1]

A noise temperature contribution in the order of 30°K from antenna backlobes is not unusual for an earth antenna.

The basic equation required to calculate antenna temperature is

$$T_a = \frac{\int_\psi T(\theta,\phi)G(\theta,\phi)\, dS}{\int_\psi G(\theta,\phi)\, dS} \qquad (1)$$

where

$\int_\psi$ = a space integral;

$T(\theta,\phi)$ = temperature as a function of elevation and azimuth angle;

$G(\theta,\phi)$ = gain as a function of elevation and azimuth angle;

dS = solid angle element.

The numerator may be evaluated by subdividing it as shown in (2). T_a then becomes

$$T_a = \frac{\int_{\psi me} T_e G_m\, dS + \int_{\psi ms} T_s G_m\, dS + \int_{\psi b} T_b G_b\, dS}{\int_\psi G\, dS} \qquad (2)$$

where

$\int_{\psi me}$ = space integral over the minor lobe with an earth background.

$\int_{\psi ms}$ = space integral over the minor lobe with a sky background.

$\int_{\psi b}$ = space integral over the main lobe.

T_e = earth temperature.

T_s = sky temperature.

---

[1]Grimm, H.H., "Fundamental Limitations of External Noise," IRE Trans. Instrumentation pp.97-103, December 1959.

T_b = main lobe temperature.

G_m = minor lobe gain.

G_b = main lobe gain.

It can be seen that the first two integrals in the numerator of (2) cover the space occupied by the minor lobes in the lower and upper hemisphere except for a small beam angle which is represented by the third integral.

If the antenna could be pointed to a region of space which is at a temperature of absolute zero, then the temperature of the main beam, $T_b \rightarrow 0$ and $G_b T_b \rightarrow 0$. In addition, if it is assumed that G_m, T_e and T_s are invariant, then the equation for T_a becomes

$$T_a = \frac{G_m \left[T_e \int_{\psi me} dS + T_s \int_{\psi ms} dS \right]}{\int_{\psi} G \, dS} \tag{3}$$

But, the angle integrals in (3) are essentially hemispheres; i.e.,

$$\int_{\psi me} dS \approx 2\pi$$

and

$$\int_{\psi ms} dS \approx 2\pi$$

When G is properly normalized

$$\int_{\psi} G \, dS = 4\pi,$$

then

$$T_a \rightarrow G_m (0.5 T_e + 0.5 T_s).$$

NOISE CONTRIBUTION DUE TO ANTENNA BACKLOBES[1]

This shows the dependence of the antenna temperature on the average minor lobe gain, G_m. The factors of 0.5 merely state that essentially one half of the space surrounding the antenna has an earth background while the other half consists of a sky background. Note that if $G_m = 0.2$, as it can be for a good antenna, and if $T_s = 0$, then $T_a = 0.1\ T_e$. Since the earth temperature, T_e, is about 300°K the backlobes can have a significant effect on the overall noise temperature of low noise systems.

[1] Grimm, H. H., "Fundamental Limitations of External Noise," IRE Trans. Instrumentation pp. 97-103, December 1959.

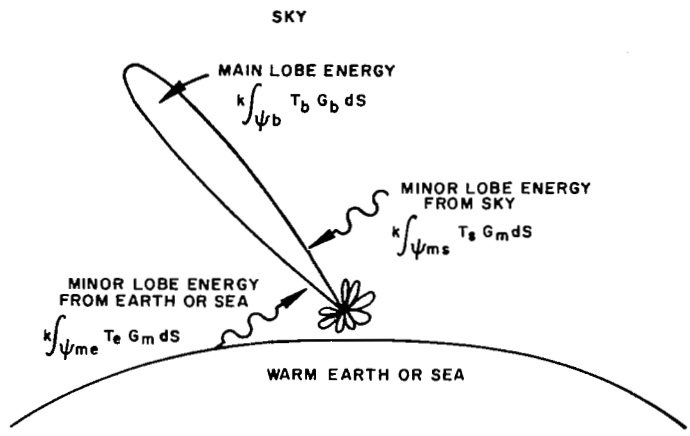

Factors Contributing to Antenna Noise Temperature

COSMIC DIFFUSE BACKGROUND

Measured values of the cosmic radio background are given. This energy is frequency dependent, decreasing to insignificant values in the 2-3 GHz region.

A survey of diffuse radio sources in the galaxy has been made by Ko[1]. Figures A through H summarize the most reliable measurements of galactic noise spatial distributions over the frequency range 60 to 910 MHz. The isophotes give sky brightness, temperatures in degrees Kelvin and are plotted in celestial coordinates Epoch 1950. The relative accuracy within each map is stated to be 5 percent to 20 percent.

The maps have general similarities but differ in local structure. The general structure of the isophotes may be conveniently represented as a superposition of symmetrical and non-symmetrical distributions. There are three symmetrical distributions:

1. A narrow bright belt of radiation about 3 degrees wide lies in the galactic plane and is concentrated toward the galactic center. This belt dominates entirely above 400 MHz.

2. A very broad band of radiation is concentrated within about 15 to 30 degrees of galactic latitude and has its maximum brightness in the region of the galactic center. The brightness is an inverse function of frequency. This band dominates at frequencies below 250 MHz and decreases to insignificance above 400 MHz.

3. There is a roughly isotropic component of radiation disbributed over the entire celestial sphere. The brightness of this component varies inversely with frequency. Above 200 MHz, the brightness is so low that measurement becomes difficult.

Above 1 GHz the background galactic brightness temperature is very low and exclusively concentrated in the galactic center. Brown and Hazard[2] quote 17°K at 1.2 GHz with a 2.8° beam and 2.6°K at 3 GHz with a 3.4-degree beam.

The data presented in Figures A through H as discussed above is summarized in Figure I[3]. Figure I depicts noise temperature (°K) versus frequency for the galactic center and for one of the coldest regions of the radio sky. Space communication systems can expect noise temperatures near the minimum value for most regions of the sky. It is

---

[1] Ko, H.C., "The Distribution of Cosmic Radio Background Radiation," Proceedings of the IRE, 46, No. 1, pp. 218-215, January 1958.

[2] Brown, R., Hanbury and Hazard, C., "A Model of Radio-Frequency Radiation from the Galaxy," Philosophical Magazine, 44, No. 7, pp. 939-936, September 1953.

[3] Stephenson, R.G., "External Noise," Space Communications, Edited by A. V. Balikrishnan, McGraw-Hill Book Company, Inc.

apparent from Figures A through I that the average galactic background temperature varies inversely with frequency. Several investigators[4,5] have concluded that the brightness spectrum is of the form

$$B \propto \lambda^{n} \tag{1}$$

where n is approximately 2.5 over most of the spectrum.

Of particular interest in space communications is the level of galactic noise along the ecliptic plane. The majority of more distant space missions will presumably occur in or near the ecliptic plane and hence it is the ecliptic noise level which will be present as an interfering background. Figure J[6] shows curves of the ecliptic noise level for three different frequencies, 81, 100, and 600 MHz. Extrapolations to higher frequencies may be made by means of the aforementioned frequency dependence of Equation (1).

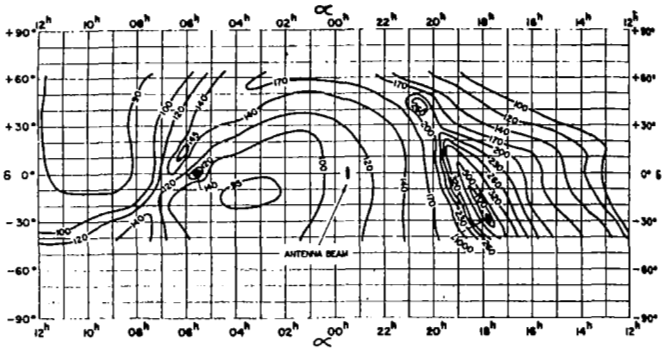

Figure A. Map of Radio Sky Background at 64 MHz (After Hey, Parsons, and Phillips)

The contours give the absolute brightness temperature of the radio sky in degrees Kelvin.

---

[4] Cottony, H.V., and Johler, J.R., "Cosmic Radio Noise Intensities in the UHF Band," Proceedings of the IRE, 40, pp. 1487-1489, 1946.

[5] Piddington, J.H., and Trent, G.H., "A Survey of Cosmic Radio Emission at 600 mc," Australian Journal of Physics, 9, pp. 481-493, December 1956.

[6] Smith, A.G., "Extraterrestrial Noise as a Factor in Space Communications," Proceedings of the IRE, 48, No. 4, pp. 594, April 1960.

COSMIC DIFFUSE BACKGROUND

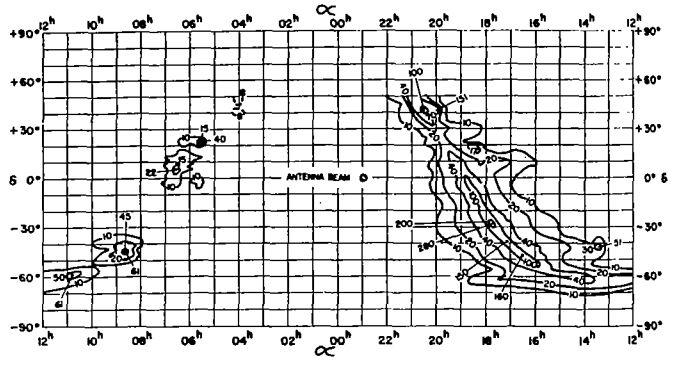

Figure B. Map of Radio Sky Background at 100 MHz (After Bolton and Westfold)

The contours give the absolute brightness temperature of the radio sky in degrees Kelvin.

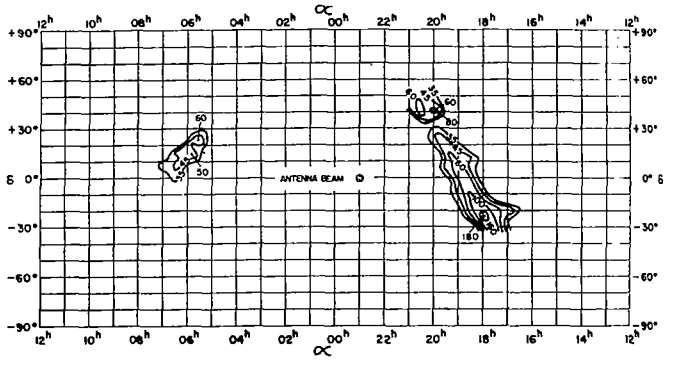

Figure C. Map of Radio Sky Background at 81 MHz (After Baldwin)

The contours give the absolute brightness temperature of the radio sky in degrees Kelvin.

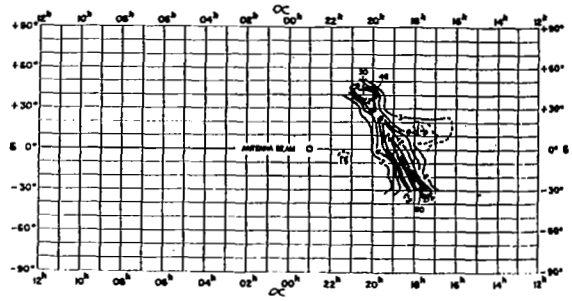

Figure D. Map of Radio Sky Background at 160 MHz (After Reber)

The contours give the absolute brightness temperature of the radio sky in degrees Kelvin.

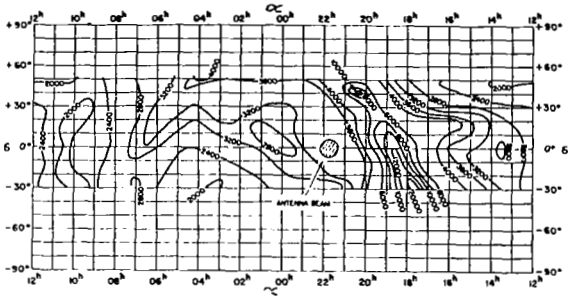

Figure E. Map of Radio Sky Background at 250 MHz (After Ko and Kraus)

The contours give the absolute brightness temperature of the radio sky in degrees Kelvin.

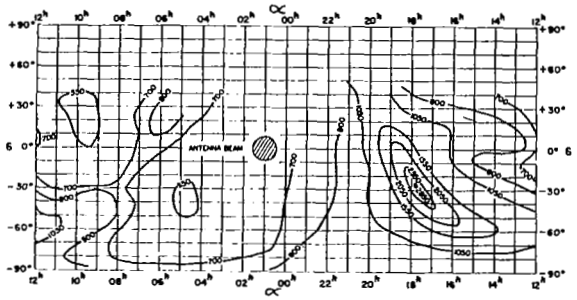

Figure F. Map of Radio Sky Background at 600 MHz (After Piddington and Trent)

The contours give the absolute brightness temperature of the radio sky in degrees Kelvin.

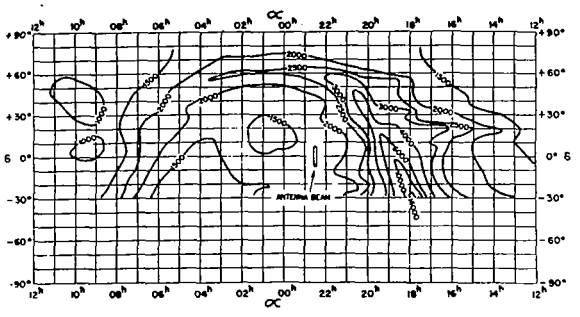

Figure G. Map of Radio Sky Background at 480 MHz (After Reber)

The contours give the absolute brightness temperature of the radio sky in degrees Kelvin.

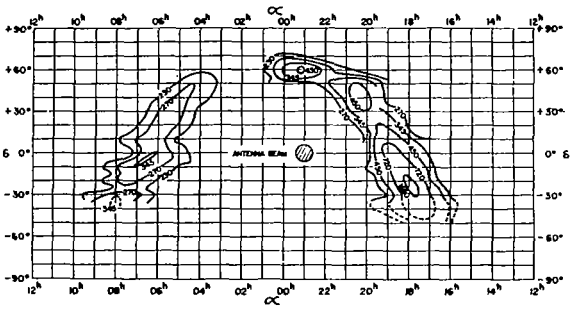

Figure H. Map of Radio Sky Background at 910 MHz (After Denisse, Leroux, and Steinberg)

The contours give the absolute brightness temperature of the radio sky in degrees Kelvin.

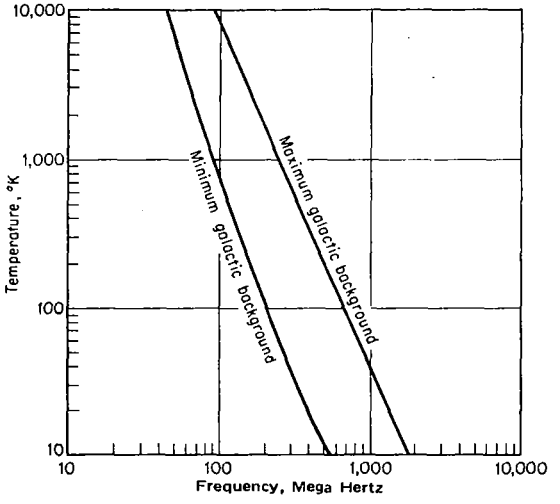

Figure I. Galactic Noise Temperature

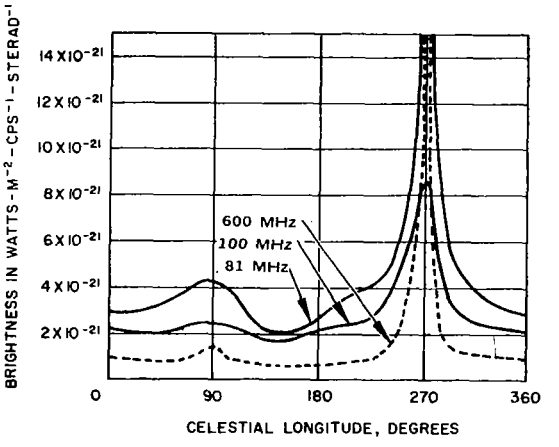

Figure J. Galactic Noise Along the Ecliptic at Three Frequencies

The 600 MHz peak extends to a height of 21 units and the 81-MHz peak to 27 units.

RADIO STARS

Radio stars generally have low enough energies at frequencies of concern and are few enough that they do not represent a significant source of interference.

Superimposed on the general galactic background radiation are numerous discrete sources, generally less than 1 degree in extent. Since the majority of these sources cannot be identified with visible objects they are known as radio stars. The strongest of these sources tend to occur near the galactic plane. Figure A[1] locates the ten strongest radio stars in equatorial coordinates and gives their noise temperatures at 378 MHz. Figure B[2] for comparison purposes locates most of these same sources in celestial coordinates.

The spectral irradiance of the four brightest radio stars outside the terrestrial atmosphere in terms of flux density is shown in Figure C[3]. Spectra of radio stars have been found to fall into one of three categories. Two categories, Class S and Class C, follow a power law relation of the form

$$\text{Log } B = -\alpha \log f + \text{constant}$$

where α is called the spectral index. Class S sources have constant spectral indices within experimental accuracy below 1420 MHz. Class C sources have spectral indices which vary with frequency. Class T sources have a thermal spectrum. Of 158 sources for which information is available 134 are Class S, 19 are Class C, and the remaining 5 are Class T. Spectra have been tabulated for all 158 sources by Conway, Kellerman and Long[3].

For a receiving system in the 10 GHz to 300 GHz region, the contribution of radio stars to the total noise power can in general be neglected. Not only is the contribution small when they are directly in the main beam, but because of their discrete nature they can easily be avoided.

---

[1]Stephenson, R.G., "External Noise," Space Communications, Edited by A. V. Balikrishnan, McGraw-Hill Book Company, Inc.

[2]Ko, H.C., "The Distribution of Cosmic Radio Background Radiation," Proceedings of the IRE, 46, No. 1, pp. 218-215, January 1958.

[3]Conway, R.G., Kellerman, K.I., and Long, R.F., "The Radio Frequency Spectra of Discrete Radio Sources," Monthly Notices of the Royal Astronomical Society, 125, pp. 268-269, 1963.

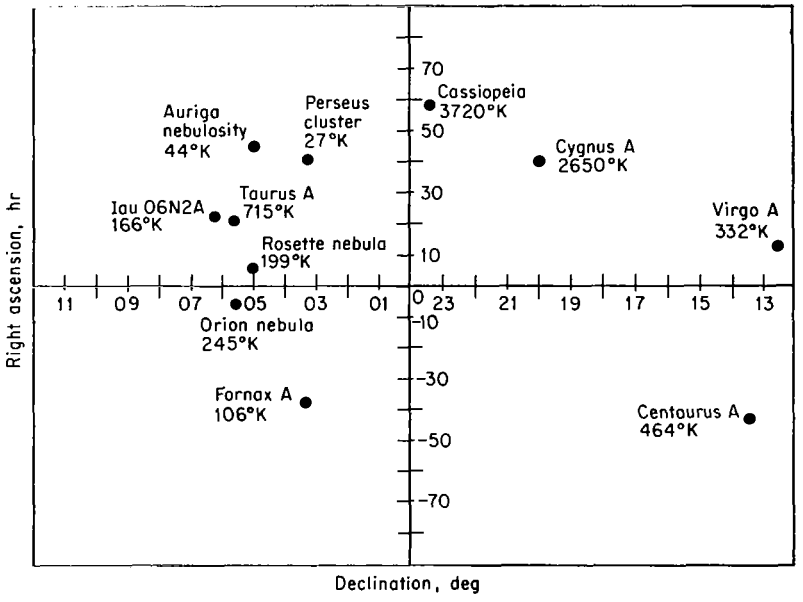

Figure A. Radio Stars at 378 MHz

RADIO STARS

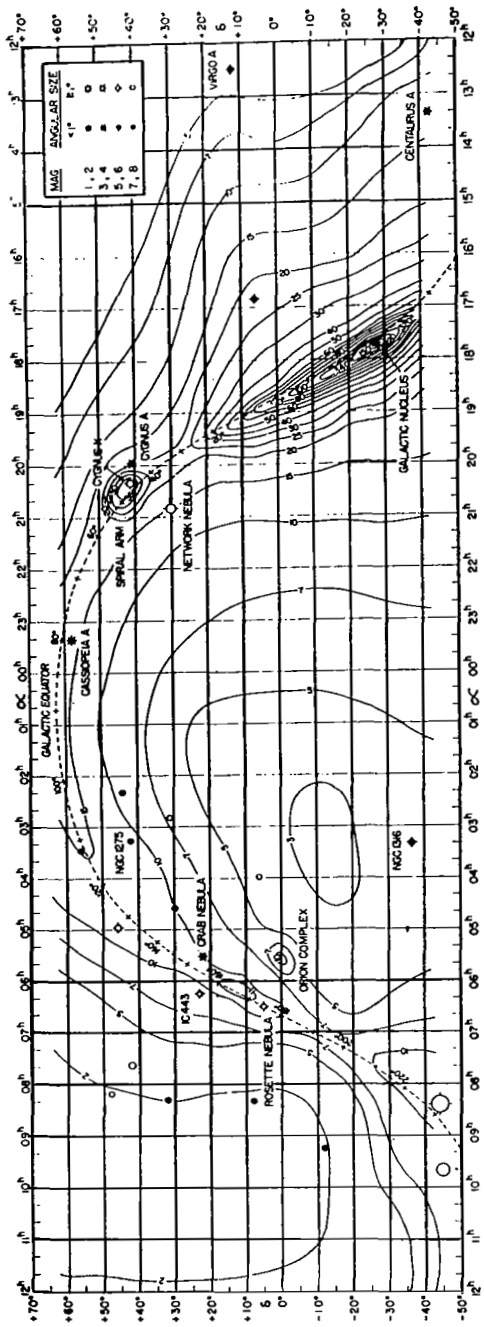

Figure B. The Most Prominent Radio Stars Superimposed on the Radio Sky Background Map at 250 MHz

Brightness temperatures of the isophotes are in degrees Kelvin.

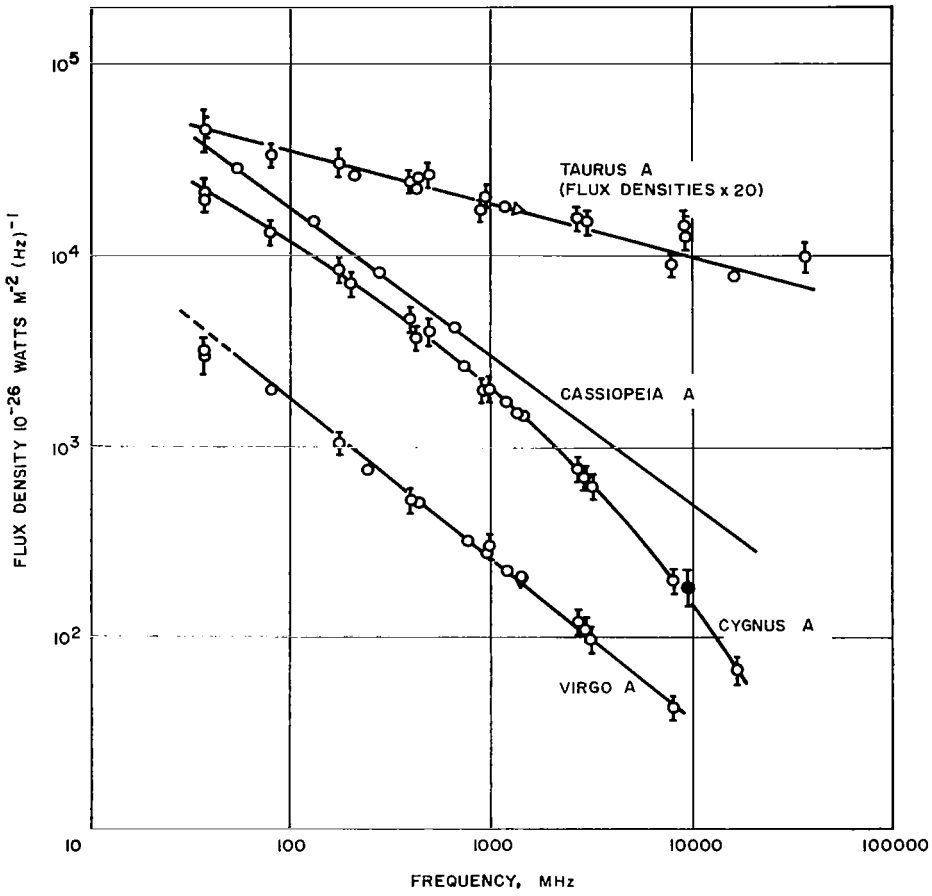

Figure C. Spectra of the Most Prominent Radio Stars

HYDROGEN LINE EMISSION BY INTERSTELLAR GAS CLOUDS

Hydrogen-line emission while containing significant energy need not be a significant source of interference due to its narrow spectral distribution.

Radio astronomers have detected an essentially monochromatic spectrum line due to the radiation of atomic hydrogen at a wavelength of 21 cm (1.42 GHz). The hydrogen line emission is a maximum along the Milky Way with a distribution over the sky roughly similar to the general galactic background. It has a maximum brightness temperature of 100°K and maximum brightness of 6×10^{-20} watts/m^2 steradian per cps[1]. This is well in excess of the general galactic background at that frequency. However, since this is limited to a single wavelength, it is unimportant as a source of interference for deep space communication.

---

[1] Smith, A. G., "Extraterrestrial Noise as a Factor in Space Communications," Proceedings of the IRE, Volume 48, No. 4, pp. 594, April 1960.

SOLAR RADIATION

Calculated and measured values of the sun's temperature and irradiance are given.

The sun is an extremely important noise source for certain frequencies. For example, Mercury is never more than 28° from the sun when viewed from the earth and while earth as viewed from Jupiter it is always within 11° of the sun.

The r-f radiation from the sun can be classified into five categories:

a. The thermal or basic component.

b. The slowly varying component which is associated with sunspots and has a period of approximately 27 days (the mean solar rotation period).

c. Noise storms, consisting of trains of bursts together with enhancement of the general radiation; these last for hours or days and show strong circular polarization.

d. Outbursts associated with flares which can be very intense and last for a number of minutes.

e. Isolated bursts lasting for 5 to 10 seconds.

In the frequency range, 30 to 300 GHz, the sun radiates essentially as a black body (thermal component) at a temperature of 6000° to 7000°K. There is some slight enhancement due to the solar flares.

In the 0.3 to 30 GHz frequency range the solar radiation is more intense than for a black body at 6000 to 7000°K. In addition, the radiation exhibits temporal effects as the contribution of sunspots and flares (particularly sunspots) becomes more important; at 10 GHz enhancements of the order of 2 occur. This is a small enhancement compared with enhancements of the order of 1000 at meter wavelengths[1]. The observed values of sun temperature between 0.3 GHz and 35 GHz follow closely the relationship

$$\frac{T_s}{290} = \frac{.675}{f}\left[1 + \frac{1}{2.3}\sin 2\pi \frac{\log_{10} 6(f - 0.1)}{2.3}\right] \qquad (1)$$

where T_s is the apparent sun temperature in °K and f is the frequency in GHz. Equation (1) is plotted in Figure A[2].

---

[1] Evans, A., Brchyuski, M.P., and Wacker, A.G., "The Radio Spectrum in Aerospace Communications," Technical Report ASD-TR-61-589, IV, Absorption in Planetary Atmospheres and Sources of Noise, RCA Victor Company Ltd., Montreal, Canada, pp. 115-132, August 1962.

[2] Hogg, D.C., and Mumford, W.W., "The Effective Noise Temperature of the Sky," Microwave Journal, 3, pp. 80-84, March 1960.

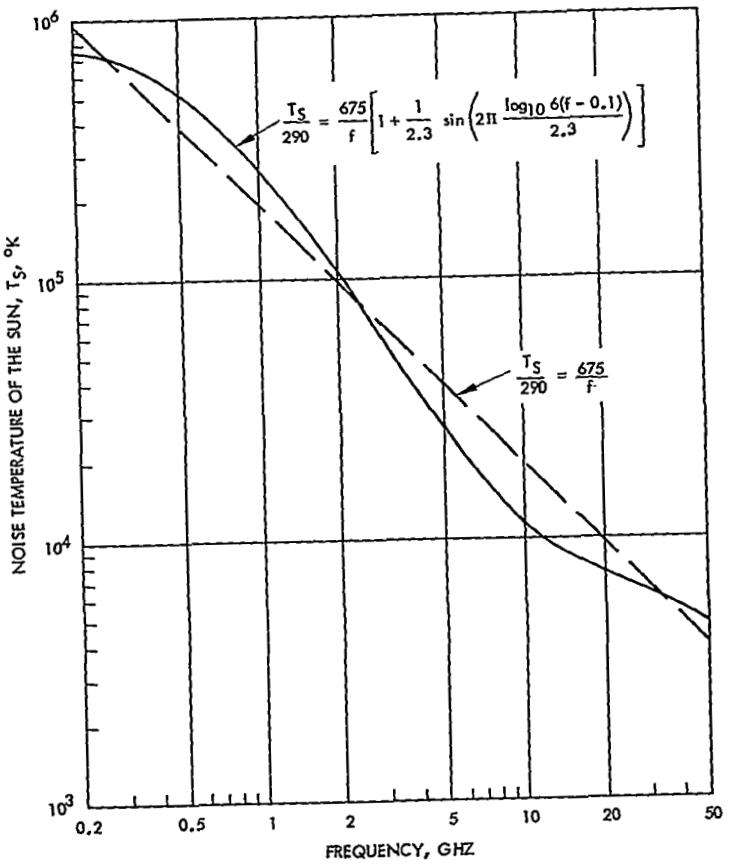

Figure A. Sun Noise Temperature Versus Frequency

SOLAR RADIATION

From earth, the sun subtends a solid angle, Ω_s, of about 7.6×10^{-5} steradians. The temperature given by the above equation will be observed by an antenna having a beamwidth, Ω_a, equal to or less than this. For antennas having beamwidth greater than this, the apparent temperature is decreased by the ratio of the sun angular substense to the antenna beamwidth. Measured solar irradiance levels outside the earth's atmosphere are depicted in Figure B[3].

[3] Malitson, H.H., "The Solar Energy Spectrum," Sky and Telescope, pp. 162-165, March 1965.

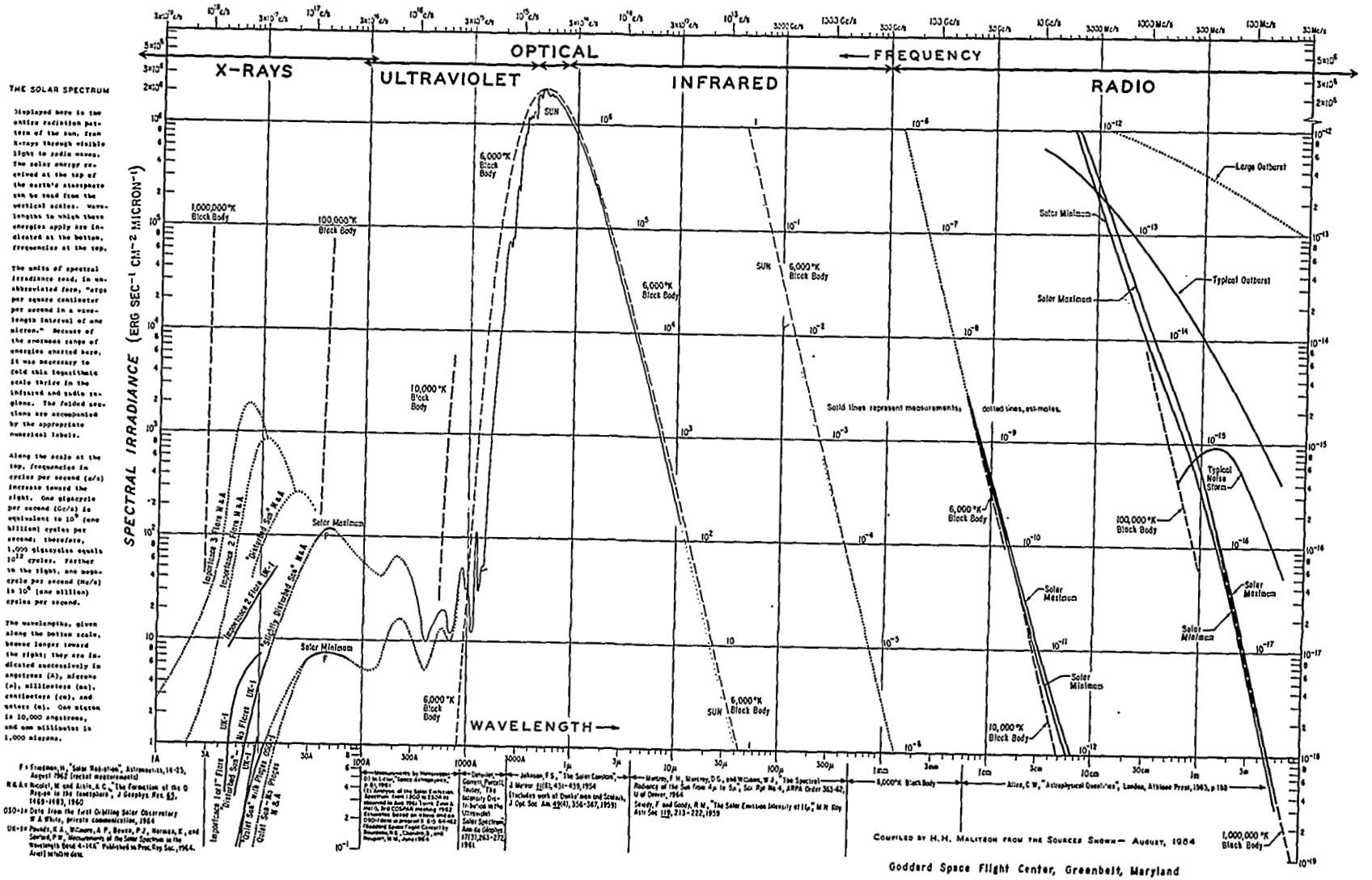

Figure B. Solar Spectral Irradiance Outside the Earth's Atmosphere

PLANETARY RADIATION

The radiation in watts/m^2/Hz is given for the planets.

For low noise space receiving systems in the vicinity of a planet, the planetary radiation must be taken into consideration. However, to an earth based receiving system, the planets contribute negligible noise power even if the planet is in the main beam of the antenna. This is because the solid angles subtended by the planets at earth are so small that they fill only a small part of the antenna beam.

Thermal radiation from Venus, Mars and Jupiter has been measured by Mayer and others.[2] (See the table)

The figure[1] shows the theoretical maximum thermal radiation outside the earth's atmosphere based on planetary temperature estimates. These are essential in agreement with infrared measurements except in the cases of Jupiter and Venus.

The discrepancy between the microwave and infrared temperatures of Venus is customarily explained by assuming that microwaves penetrate the atmosphere of the planet more readily than infrared rays. Hence, the infrared temperature is the temperature of the atmosphere whereas the microwave temperature is that of the actual surface. In the case of Jupiter the discrepancy is believed due to radiation by synchrotron radiation by high energy electrons trapped in the planetary magnetic field. This theory is supported by observations by Radhakreshnan and Roberts of CIT that the signals are linearly polarized and come from an area larger than the solid disc of the planet.

In addition to the above mentioned steady state thermal radiation, several planets notably Jupiter, Saturn and Venus exhibit strong sporadic bursts of clearly non-thermal radiation; typical peak intensities observed to date include 10^{-19} watt m^{-2} $(Hz)^{-1}$ at 19.6 MHz (Jupiter), 6×10^{-21} watt m^{-2} $(Hz)^{-1}$ at 22 MHz (Saturn), and 9×10^{-22} watt m^{-2} $(Hz)^{-1}$ at 26.7 MHz (Venus).[3] In no instance have these impulsive signals been observed at frequencies above 43 MHz.

---

[1] Mayer, C. H., "Thermal Radio Radiation from the Moon and Planets," IEEE Transactions on Antennas and Propagation, AP 12, No. 7, pp. 902-913, December 1964.

[2] Mayer, C. H., McCullough, T. P., and Sloanaker, R. M., "Measurements of Planetary Radiation at Centimeter Wavelengths," Proceedings of the IRE, 46, No. 1, pp. 260-266, January 1958.

[3] Smith, A. G., "Extraterrestrial Noise as a Factor in Space Communications," Proceedings of the IRE, 48, No. 4, pp. 594, April 1960.

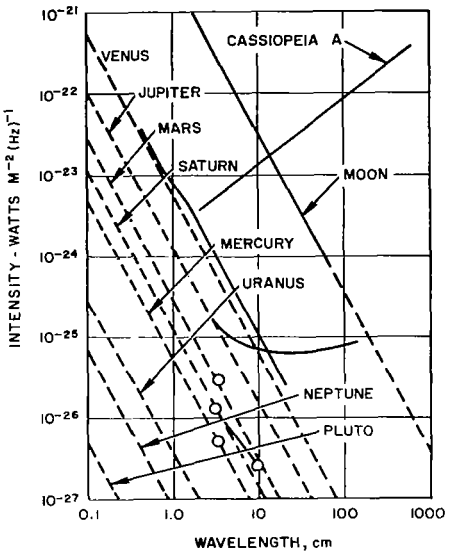

Predicted Intensity of Planetary Thermal Radio Radiation when Planet is Near Closest Approach to Earth (Dashed Lines), and Measured Intensity of Radiation from the Planets, the Moon, and the Nonthermal Radio Source, Cassiopeia A (Solid Lines and Points)

Planetary Radiation

Planet	Infrared Temperature (°K)	f(GHz)	λ(cm)	Equivalent Radio Blackbody Temperature (°K)
Mercury			4	400°K (Planet at greatest elongation)
Venus	240	35	0.86	410°K
			2-21	620°K
Mars	260	9.5	3.15	211°K
Jupiter	130		3-8	145°K
		2.9	10	600°K
		1.4	21	2000°K
		0.97	31	5000°K
		0.94	136	50000°K
Saturn	150	8.7	3.45	106°K
		2.9	10	140°K
			Highly polarized	200°K

LUNAR RADIATION

Lunar Radiation produces an effective noise temperature of approximately 200°K. This is a significant noise contribution especially for earth stations tracking lunar probes.

The thermal noise flux from the moon is considerably greater than that from the planets. Furthermore, the moon subtends an angle of approximately 0.5 degrees at the earth, and hence, practical antennas in the mm region can have beamwidths less than the solid angle subtended by the moon (6×10^{-5} steradians). This means, provided the earth's atmosphere permits, such an antenna based on earth can "see" the moon directly. Thus for certain frequencies in the 10-300 GHz region, where atmospheric effects are smallest, the moon can make a significant contribution to the noise temperature of an antenna pointed at the moon. Gibson has found that at 35 GHz the brightness temperature of the moon varies with phase between the limits of 145°K and 220°K as shown in the figure[1]. The corresponding flux densities at earth are 4×10^{-21} watts m^{-2} $(Hz)^{-1}$. The brightness temperatures determined by Gibson should be reasonably valid throughout the whole frequency range of 10-300 GHz, and hence can be used to calculate the noise contribution from the moon for any particular case. Lunar surface temperatures as determined by infrared measurements vary from 120°K to 400°K and are observed to lag the microwave temperatures by approximately 45 degrees. This feature may be accounted for by postulating a thin layer of lunar surface dust which is transparent to microwaves but effectively insulates an underlying rock surface. At frequencies less than 1.4 GHz the radiation temperature is a constant 250°K[2].

---

[1] Gibson, J. E., "Lunar Thermal Radiation at 35 kmc," Proceedings of the IRE, 46, No. 1, pp. 280-286, January 1958.

[2] Stevenson, R. G., "External Noise," Space Communications, Edited by A. V. Balikrishnan, McGraw-Hill Book Co. Inc. New York, N. Y.

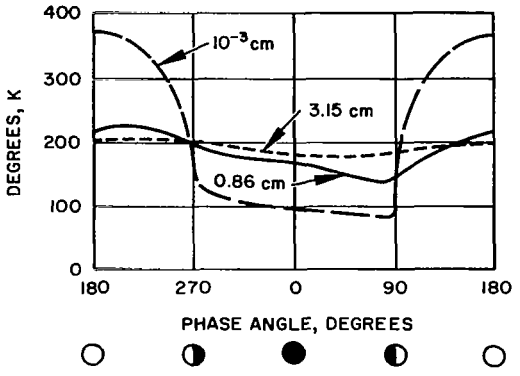

Brightness Temperature of Center of Disk of Moon as Function of the Phase of Solar Illumination

Long dashes - brightness temperature corresponding to the infrared radiation as approximated by the calculated surface temperature of Wesselink.* Solid line - brightness temperature corresponding to the 8.6-mm radiation measured by Gibson.** Short dashes - brightness temperature corresponding to the 3.15 cm radiation measured by Mayer, McCullough, and Sloanaker.***

*Bull, Astron, Inst. Neth., 10, pp. 351-363; April 1948.

**Proc. IRE, 46, pp. 280-286, January 1958.

***Reproduced from Planets and Satellites, G. P. Kuiper and B. M. Middlehurst, Eds., University of Chicago Press, Chicago, Ill., 1961; copyright 1961 by the University of Chicago.

TERRESTRIAL ATMOSPHERIC RADIATION

The noise contribution of the atmospheric radiation is significant where the atmosphere attenuates the microwave energy.

The earth's atmosphere radiates thermal noise as a result of absorption of incident radiation. The effect of ionospheric radiation can be approximated by assuming that each 0.1 db of absorption is equivalent to 7°K antenna noise temperature. Since the ionospheric absorption is less than 0.1 db for frequencies greater than 0.3 GHz ionospheric absorption noise can be neglected in this regime.[1]

Tropospheric noise is primarily due to absorption by oxygen and water vapor. Thus the antenna is immersed in an atmosphere that emits black body radiation. The tropospheric contribution to noise temperature, T_s, of a narrow beam antenna having a radiation pattern which admits no side or back lobes is

$$T_s = \int_0^\infty \alpha T \exp\left[-\int_0^r \alpha dr\right] dr \qquad (1)$$

where and T are respectively the absorption coefficient and temperature at a distance r from the antenna. Calculated curves of T_s versus frequency are shown in the figure[2] for various values of antenna beam zenith angle. As expected, the temperature curves show maxima at the absorption peaks of water vapor and oxygen. Also, at any frequency the sky noise varies inversely with the elevation angle (90° corresponds to looking horizontal). This is due to the longer path length required to fully penetrate the atmosphere at low elevation angle.

---

[1] Millman, G.H., "Atmospheric Effects on VHF and UHF Propagation," Proceedings of the IRE, 48, No. 8, pp. 1492-1501, August 1958.

[2] Blake, L.V., "Tropospheric Absorption and Noise Temperature for a Standard Atmosphere," Summary of a Paper Presented at the 1963 PT-GAP International Symposium, NBS, Boulder Colorado, July 9-11, 1963.

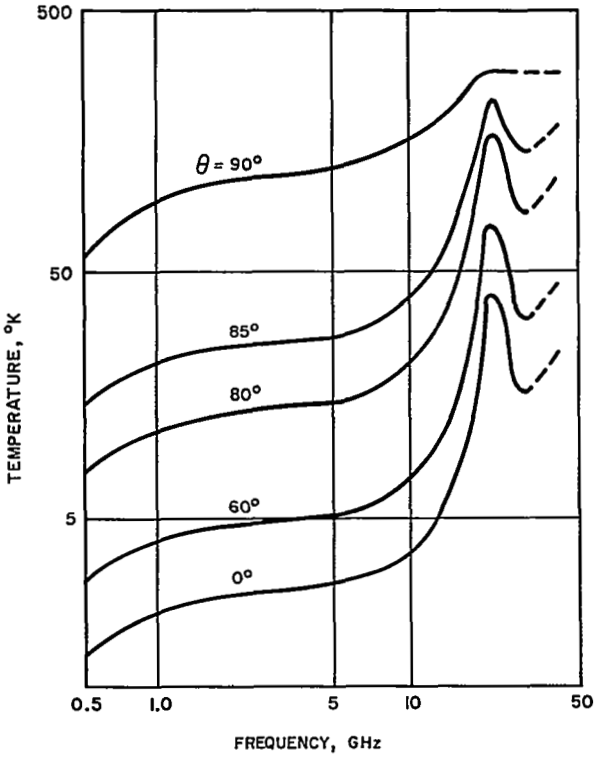

Sky Noise Temperature due to
Oxygen and Water Vapor

RADIO FREQUENCY EFFECTIVE TEMPERATURE - SUMMARY

The composite of the various contributions to antenna temperature have a minimum in the frequency range 1.5 - 8 GHz. For this reason this band is highly desirable for high performance deep space missions.

The previous topics have documented the variations of noise contributions to the receiver (antenna) effective noise temperature. These are plotted in a composite form in the figure[1]. As is seen there is a minimum temperature range in the approximate band of 1.5 to 8 GHz. The relatively low noise contribution from sources external to the receiver in this band makes it desirable for high performance deep space to earth communication links. A refined study of this type has led to the selection of the 2290 to 2300 MHz for the DSIF receiving frequency.

---

[1] Grimm, H. H. "Fundamental Limitations of External Noise", IRE Trans. Instrumentation pp 97-103, December, 1959.

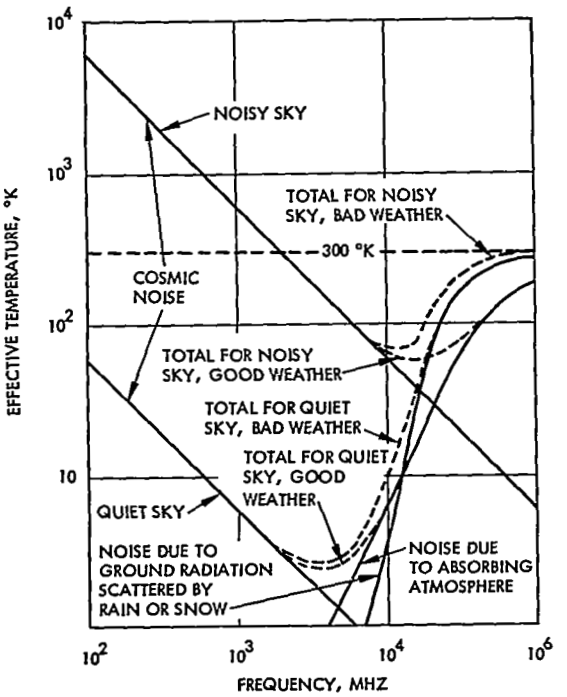

Radio Frequency Noise Summary

Optical Frequency Background

COSMIC BACKGROUND RADIATION

The spectral radiant emittance of the brightest stars is given.

Cosmic radiation is largely from the brighter stars. Ramsey[1] has prepared charts giving spectral radiant emittance outside the earth's atmosphere of the brightest stars. In making these calculations it was assumed that the stellar spectra follow Planck's law. The figure depicts spectral radiant emittance reaching the top of the earth's atmosphere from the stars which exhibit the greatest irradiance in the visible region. Variable stars such as Betelguex, Mira, and R. Hydrae are presented at their maximum emittance.

(The table lists several radiometric quantities which are useful in characterizing optical background.)

The background constitutes an interfering signal in a communicating system. It is therefore required to determine the power of the interfering signal in order to compare it to the desired signal. This may be done by noting the dimensions of the background spectral emittance and the physical description of the optical receiver.

As an example consider, from the figure, the spectral radiance of the star Achernar at a wavelength of 0.5 microns. This value is 10^{-11} watts/cm^2-micron. For a receiving aperture of 50 cm followed by a one micron optical filter the total received power of the background is:

$$P_B = (10^{-11}) \left(\frac{\pi 50^2}{4}\right)(1) = 1.97 \times 10^{-8} \text{ watts.}$$

This power will then interfere with the desired signal strength when Achernar is in the field of view and when the receiving aperture is outside the earth's atmosphere.

---

[1] Ramsey, R. C., "Spectral Irradiance from Stars and Planets, above the Atmosphere, from 0.1 to 100 microns," Applied Optics, I, No. 4, July 1962.

Background Radiation Measurement Quantities

Title	Description	Typical Units
Spectral radiant emittance	Radiant power into a hemisphere per unit area of source in hemisphere	$\frac{\text{watts}}{\text{cm}^2}$
Spectral radiance	Radiant power into a unit solid angle per unit projected area of source in hemisphere	$\frac{\text{watts}}{\text{cm}^2\text{-ster-micron}}$
Spectral irradiance	Radiant power incident upon a surface per unit surface area	$\frac{\text{watts}}{\text{cm}^2}$

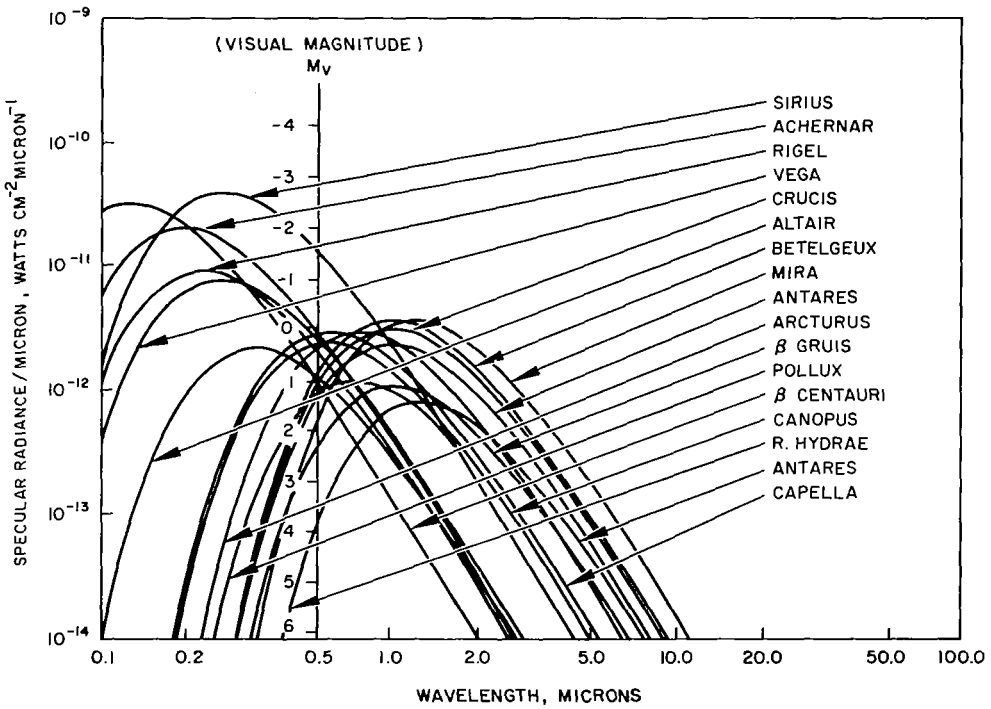

Spectral Irradiance of Brightest Stars Outside the Terrestrial Atmosphere

SOLAR BACKGROUND RADIATION

The solar irradiance corresponds to that of a 6000°K black body. The spectral distribution is given over a wavelength range of 1 Å to 10 meters.

The mean solar irradiance over all wavelengths outside the earth's atmosphere at the mean solar distance is called the solar constant and is approximately 140 mw/cm^2 or 130 watts/ft^2. Over 98 percent of this solar irradiance is contained in the wavelength region 0.3 to 4.0 microns. Variation in solar distance throughout the year causes this irradiance to vary as much as 3.5 percent from the mean; solar activity can produce fluctuations of 1.5 percent in the solar constant. In addition to these relatively small variations, the amount of solar irradiation that reaches a particular portion of the earth's surface varies with solar elevation angle and atmospheric conditions.

The spectral distribution of solar radiation in the visible and near infrared resembles that of a black body at 6000°K. H. Malitson[1] has compiled a chart of measurements of solar spectral irradiance in the wavelength range 1 Å to 10 m. The figure shows the spectral distribution of solar radiation outside the atmosphere at the earth's mean solar distance.

---

[1] Malitson, H.H., "The Solar Energy Spectrum," Sky and Telescope, pp. 162-165, March 1965.

THE SOLAR SPECTRUM

Displayed here is the entire radiation pattern of the sun, from X-rays through visible light to radio waves. The solar energy received at the top of the earth's atmosphere can be read from the vertical scales. Wavelengths to which these energies apply are indicated at the bottom, frequencies at the top.

The units of spectral irradiance read, in unabbreviated form, "ergs per square centimeter per second in a wavelength interval of one micron." Because of the enormous range of energies charted here, it was necessary to fold this logarithmic scale thrice in the infrared and radio regions. The folded sections are accompanied by the appropriate numerical labels.

Along the scale at the top, frequencies in cycles per second (c/s) increase toward the right. One gigacycle per second (Gc/s) is equivalent to 10^9 (one billion) cycles per second; therefore, 1,000 gigacycles equals 10^{12} cycles. Farther to the right, one megacycle per second (Mc/s) is 10^6 (one million) cycles per second.

The wavelengths, given along the bottom scale, become longer toward the right; they are indicated successively in angstroms (A), microns (μ), millimeters (mm), centimeters (cm), and meters (m). One micron is 10,000 angstroms, and one millimeter is 1,000 microns.

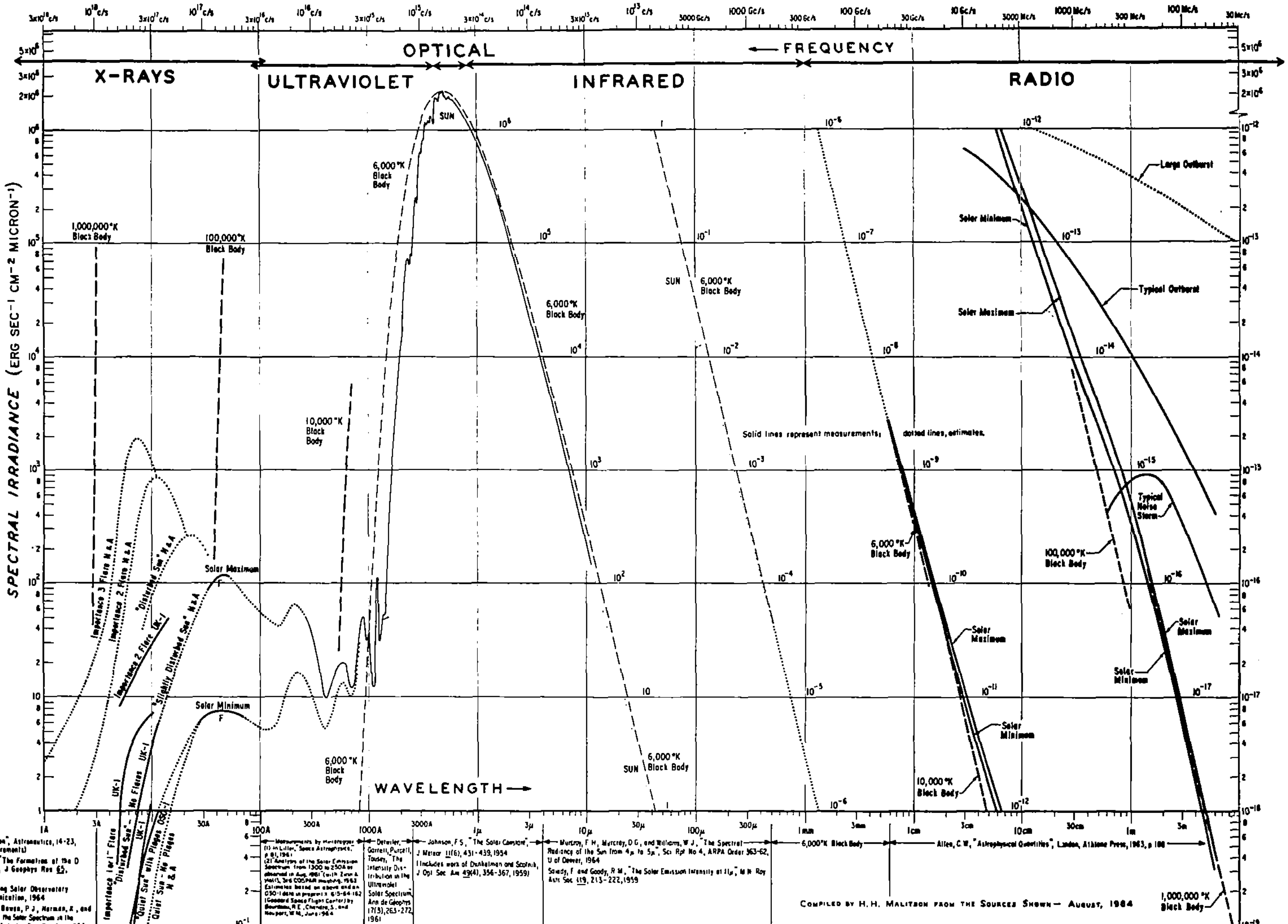

F = Friedman, H., "Solar Radiation", Astronautics, 14-23, August 1962 (rocket measurements)

N & A = Nicolet, M and Aikin, A C., "The Formation of the D Region in the Ionosphere", J Geophys Res 65, 1469-1483, 1960

OSO-I = Data from the First Orbiting Solar Observatory W A White, private communication, 1964

UK-I = Pounds, K A., Willmore, A P, Bowen, P J, Norman, K, and Sanford, P W, "Measurements of the Solar Spectrum in the Wavelength Band 4-14A" Published in Proc. Roy Soc., 1964. Ariel I satellite data

Solar Spectral Irradiance Outside the Earth's Atmosphere

PLANETARY AND LUNAR RADIATION

Radiation from the planets and the moon is given for reflected sunlight and for the self emittance of the planets due to their ambient temperature.

The steady state background irradiance from the planets and the moon results from two processes: reflection of incident solar energy and self-emission as a result of the planets non-zero temperatures. Figures A and B show the background spectral irradiance outside the terrestrial atmosphere due to reflected and self-emitted energy for the planets and the moon respectively. These curves assume constant the albedo at peak power wavelength. The planetary irradiances at other than peak power wavelengths may be determined from these curves and the spectral albedo which is plotted in Figure C[1]. The peak spectral irradiances per micron due to self-emitted radiation were calculated from

$$H_{peak} = W_{max} \frac{(1-A)}{\pi} \frac{\pi d^2}{4R^2}$$

where

H_{peak} = peak spectral irradiance per micron (watts cm^{-2} μ^{-1})

A = bond albedo

d = planet diameter

R = planet's range to the earth

W_{max} = peak spectral radiant emittance per micron at wavelength λ_{max}

where λ_{max} is given by Wien's law

$$\lambda_{max} = \frac{2898}{T}$$

T = Temperature °K

These data are summarized on the Table. The values of temperature for each planet were obtained from Kuiper[1]. The peak irradiances per micron from reflected solar radiation are based on the solar illumination curves for a 6000°K black body and the planetary albedo at the peak power wavelength. The superior planets (those outside the earth's orbit) are assumed to be at opposition, the inferior planets (those within the earth's orbit) are assumed to be at greatest elongation. These astronomical terms are explained by Figure D.

---

[1] Kuiper, G. E., "The Solar System," III, Planets and Satellites, University of Chicago Press, 1961.

Summary of Peak Spectral Irradiance Data

Planets	Distance to Earth (times 1×10^{16} km)	Diameter (times 1000 km)	Bond Albedo	Temperature (°K)	Peak Wavelength (μ)	Max Emission at Peak Wavelength watt $cm^2 \mu$	Visual Magnitude	Angle to Eliptic Plane (Degrees)
Mercury	137.8	4.8	0.056	613	4.65	3.36×10^{-11}	+ 0.11	7
Venus	103.3	12.4	0.76	235	12.2	8×10^{-13}	- 4.23	3.3
Moon (satellite)	0.384	3.45	0.067	373	7.7	3×10^{-7}	-12.54	-
Mars	78.3*	6.8	0.16	217	10	1.02×10^{-12}	- 2.01	1.8°
Jupiter	628.3	142.8	0.73	138	20.7	2.24×10^{-13}	- 2.55	1.3°
Saturn	1277	120.8	0.76	123	23.3	1.85×10^{-14}	+ 0.67	2.5°
Uranus	2720	47.6	0.93	90	32μ	4.8×10^{-17}	+ 5.8	0.66°
Neptune	4330	44.6	0.84	-	-	-	+ 7.6	1.7°
Pluto	11,200	14.4**	0.14	-	-	-	+14.7	17.1°***

*Distance between Mars and Earth varies because of the orbit of Mars. At favorable opposition which occurs every 15 or 17 years during Aug - Sept., the distance can be as small as 55×10^6 km whereas at unfavorable opposition the distance is 105×10^6 km.

**The value measured by Kuiper[1] is believed to be much too small. When this value of diameter is used, the density of Pluto comes out to be unrealistically high.

***Pluto's orbit is quite eliptical and a portion lies inside the orbit of Neptune however they do not intersect.

The Bond albedos and planet temperatures were taken from References 2-6. Visual magnitudes were calculated with the absolute visibility V(1, 0) taken from the same references. There is a wide variation in reported planetary temperatures in the literature. Variations can be as large as 60°K in the case of Venus.

[1] Kuiper, G. E., "The Solar System" III, Planets and Satellites, University of Chicago Press, 1961.

[2] Ko, H. C., "The Distribution of Cosmic Radio Background Radiation," Proceedings of the IRC, 46, No. 1, pp. 218-215, January 1958.

[3] Brown, R., Hanbury and Hazard, C. "A Model of Radio-Frequency Radiation from the Galaxy," Philosophical Magazine, 44, No. 7, pp. 939-936, September 1953.

[4] Stephenson, R. G., "External Noise," Space Communications, Edited by A. V. Balikrishnan, McGraw-Hill Book Company, Inc.

[5] Cottony, H. V., and Johler, J. R., "Cosmic Radio Noise Intensities in the UHF Band," Proceedings of the IRE, 40, pp. 1487-1489, 1946.

[6] Piddington, J. H., and Trent, G. H., "A Survey of Cosmic Radio Emission at 600 mc," Australian Journal of Physics, 9, pp. 481-493, December 1956.

PLANETARY AND LUNAR RADIATION

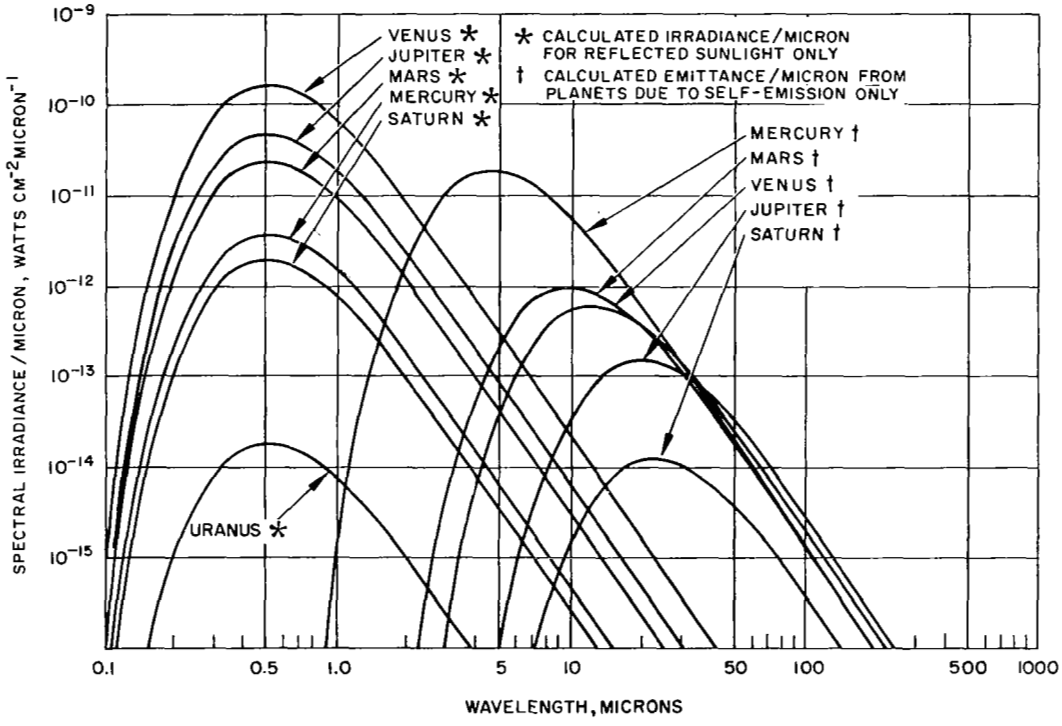

Figure A. Calculated Planetary Special Irradiance/Micron Outside Terrestrial Atmosphere

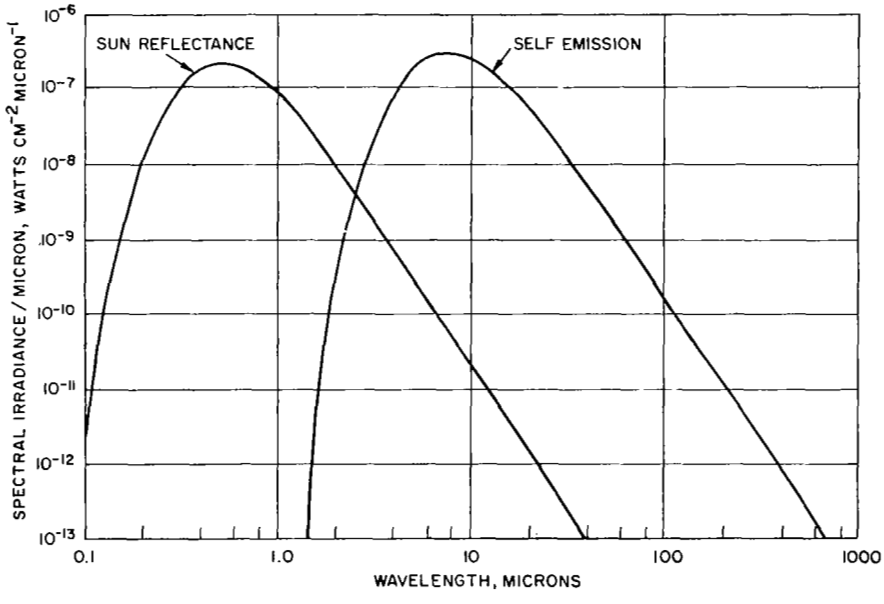

Figure B. Full Moon Spectral Irradiance Outside Terrestrial Atmosphere

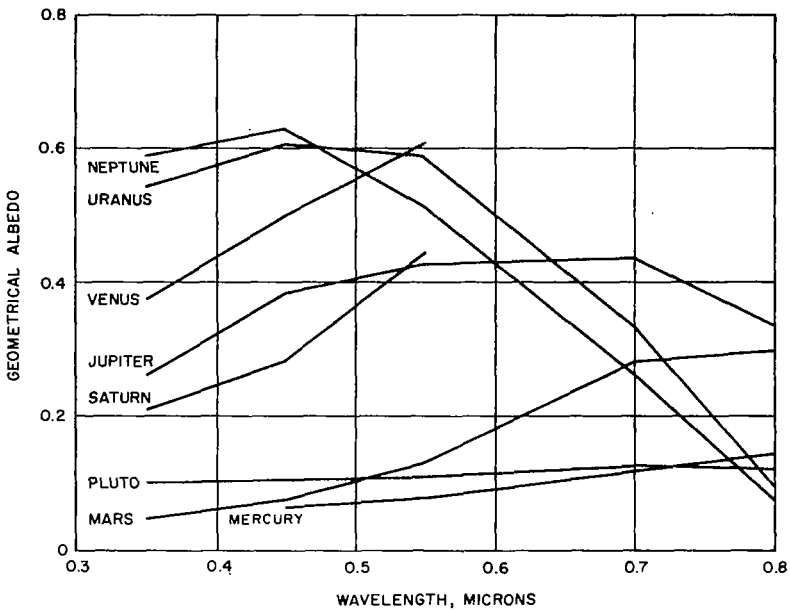

Figure C. Spectral Albedo versus Wavelength

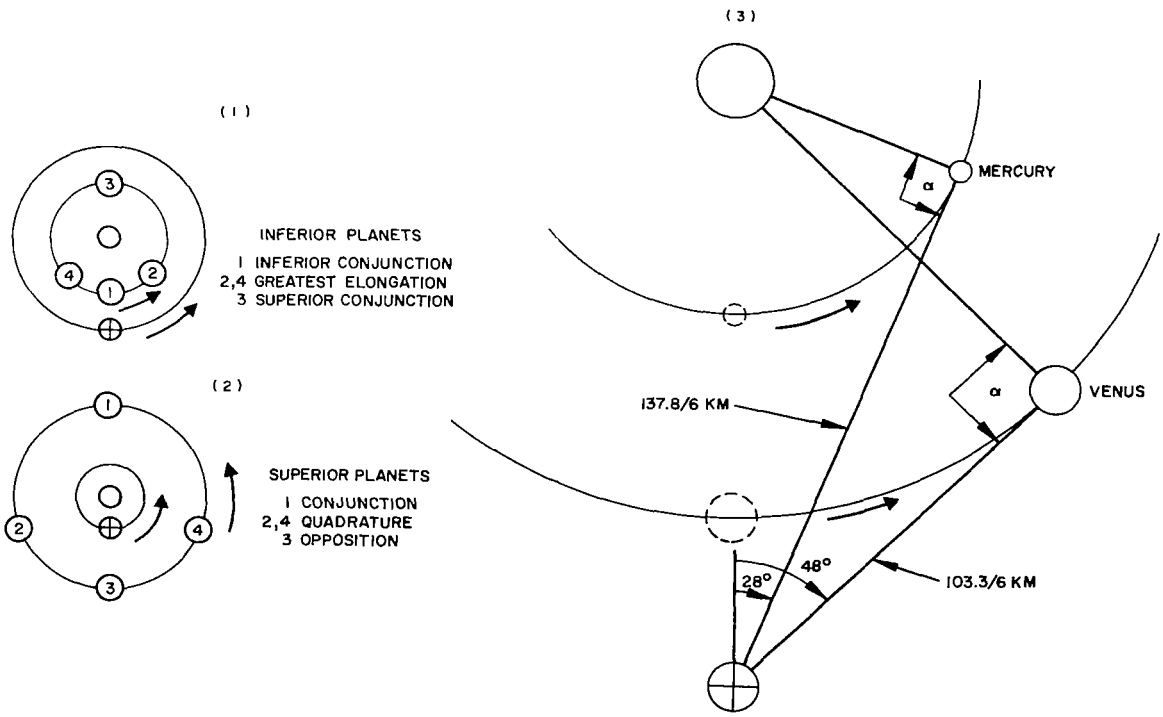

Figure D. Position of Mercury and Venus at Greatest Elongation ($\alpha = 90^{o}$)

EARTH RADIATION

Radiation from the Earth is given for reflected energy from the sun and for self emission.

Earth radiation to space consists of reflected solar energy and self-emitted energy. Spherical albedos of the earth in the wavelength regions of interest are as follows:[1]

Wavelength	Spherical Albedo
Ultraviolet	0.50
Visible	0.40
Infrared	0.28

The mean albedo over the solar spectrum is approximately 0.35. In addition, the earth radiates by self-emission as a black body at a temperature of 220°K to 320°K, depending on latitude. When the albedo and black body radiation from the earth's surface is combined with the effect of selective atmospheric absorption, the spectral radiant emittance of Figure A results.

For distances sufficiently great that the earth may be treated as a point source, the spectral irradiance may be calculated by assuming that the earth is a Lambertian radiator and using spectral radiant emittance of Figure A. Alternately the total irradiance over the solar spectrum may be calculated by using the solar constant and the average albedo. The spectral irradiance at a distance R from the center of the earth under the point source assumption is

$$H_\lambda = \frac{W_\lambda}{\pi} \frac{\pi d^2}{4R^2}$$

where

W_λ = spectral radiant emittance $\left(\frac{\text{watts}}{\text{cm}^2 \text{ micron}}\right)$ of Figure A

d = diameter of the earth 12.73×10^3 km

R = distance from the earth's center (km)

In the case of reflected radiation, the above expression represents a maximum H_λ corresponding to the fully illuminated earth being viewed by the receiving surface. The problem of determining the irradiance of a body near the earth (or any other planet) is more difficult since the view factor must be taken into account. This problem has been

---

[1] Goldberg, I. L., "Radiation from Planet Earth," U. S. Army Research and Development Laboratory, Fort Monmouth, New Jersey, September 1961.

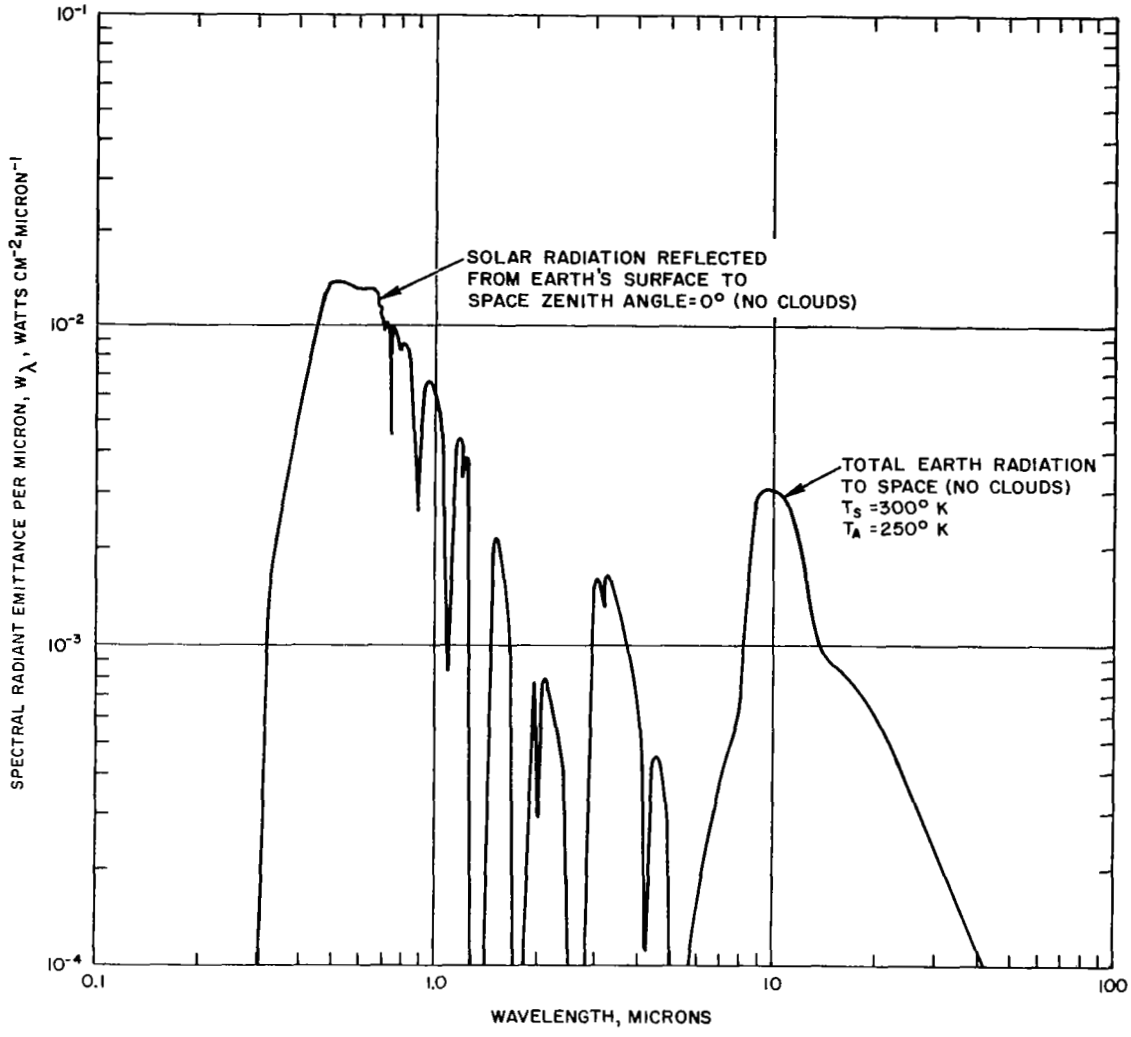

Figure A. Solar and Terrestrial Radiation

Reflected solar and total earth radiation to space values should be divided by π to obtain the radiance for each case. T_S is the surface temperature and T_A is the effective radiating air temperature.

EARTH RADIATION

exhaustively treated by Dennison[2, 3]. The reflected solar irradiance H_λ incident on a unit surface of a body near a planet is given by

$$H_\lambda = W_\lambda F$$

where W_λ is the radiant emittance of the reflected solar energy and F is a purely geometrical factor which is a function of the altitude of the body and its orientation relative to the planet-sun axis. The factor F is plotted in Figure B as a function of altitude for various values of the bistatic angle σ. The bistatic angle is formed by the planet-sun line and the position vector of the satellite. F has been computed by Dennison for numerous orbit parameters.

---

[2] Dennison, A. J., "Illumination of a Space Vehicle Surface Due to Sunlight Reflected from Earth," Journal of the American Rocket Society, 32, pp. 635-637, April 1962.

[3] Dennison, A. J., "Illumination of a Cell Surface in Space Due to Sunlight Reflected from Earth," Report No. T1S61SD101, General Electric Co., June 1961.

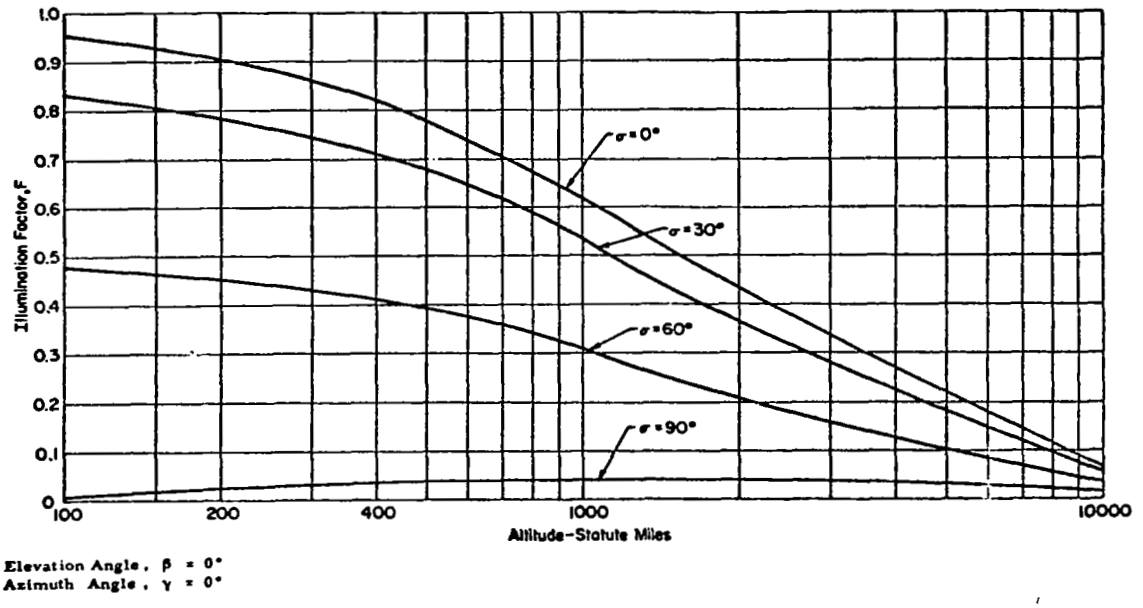

Figure B. Illumination Factor as a Function of Altitude for Parametric Values of Bistatic Angle, σ.

TERRESTRIAL ATMOSPHERIC BACKGROUND – DAYTIME SKY

The daytime sky radiance of the earth is given for a clear sky; sunlit clouds have a value about an order of magnitude larger.

The radiance of the sky in the optical wavelengths is the result of two mechanisms: molecular scattering of incident radiation and emission by atmospheric constituents as a result of absorption of incident radiation. Atmospheric emission is significant only at wavelengths longer than 2μ. Scattering of solar radiation is the overwhelming contribution to daytime sky radiance in the visible and near visible wavelengths. Daytime spectral sky radiance versus wavelength is plotted in the figure. The figure assumes clear sky conditions; radiances of sunlit clouds are typically an order of magnitude greater.

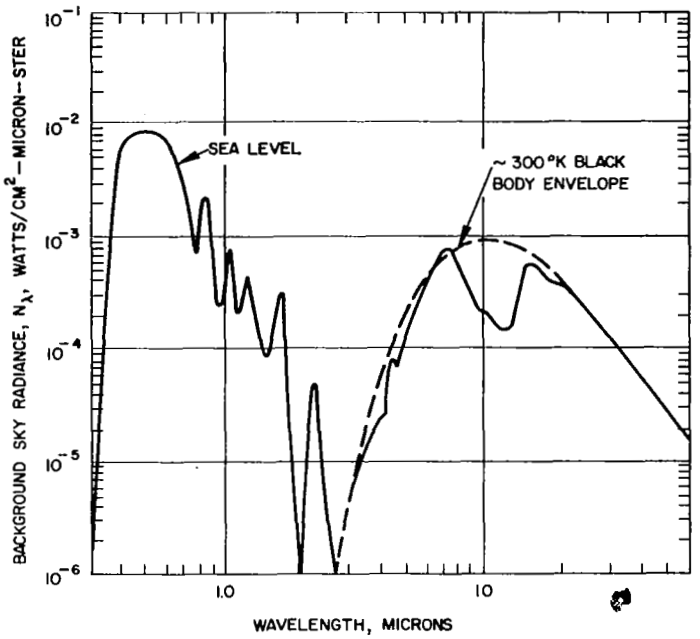

Diffuse Day Sky Component of Typical Background Radiance from Sea Level, Zenith Angle = 45 Degrees, Excellent Visibility

TERRESTRIAL ATMOSPHERIC BACKGROUND - NIGHT-TIME SKY

Night-time sky radiance is given for a variety of conditions.

S. K. Mitra estimates the contributions of various sources of night sky radiance as follows:

Starlight	30%
Zodiacal light	15%
Galactic light	5%
Airglow	40%
Scattered light from last 3 sources	10%

These estimates are for visible wavelengths and for conditions several hours after sunset with no moon. All these components of night emission vary with direction, time, atmospheric and meteorological conditions. Values of night sky radiance presented here are typical.

According to Mitra, peak sky radiance due to stellar sources is of the order of 10^{-1} watts/cm^2-steradian-μ at 0.55μ and follows approximately a Planckian spectral distribution. The effective irradiance produced at ground level is 3.34×10^{-10} watts/cm^2 at 0.55μ. These figures are 1/4 to 1/6 the actual visible light observed from the night sky at a dark location on a clear night. The remaining contributions come from diffuse sources. The principal noise interference problem due to stars is the result of the relatively small number of very bright stars.

Measurements of the spectrum of diffuse night sky radiance have been made by F. E. Roach.[2] The results shown in Figure A are averaged over times, seasons, and direction of view in the celestial sphere. Figure B shows clear sky radiance in the infrared for various zenith angles.

Except for the narrow intense N_a and H atomic lines, relatively light sky emissions appear between 0.1 and 1.0 microns. Beginning at 1.0 microns intense OH molecular bands appear as "air glow." Above 2 microns thermal emission from the dense lower atmosphere obscures the air glow. Twilight zenith sky radiance in the 0.4 to 0.7 micron band is illustrated in Figure C[3] as an implicit function of the depression of the sun below the horizon. Zenith sky radiance in the 0.4 to 0.7 micron band from the full moon versus lunar elevation angle is illustrated in Figure D[3]. Variation in lunar sky radiance at zenith with lunar phase is illustrated in Figure E[3].

---

[1] Mitra, S. K., "The Upper Atmosphere," Asiatic Society, Calcutta, India, 1962.

[2] Roach, F. E., "Manual of Photometric Observations of the Airglow During the IGY," National Bureau of Standards Report No. 5006.

[3] Geo-Science Inc. Final Report: "Twilight and Airflow Study," Air Force Contract AF19(122)-433, January 1953.

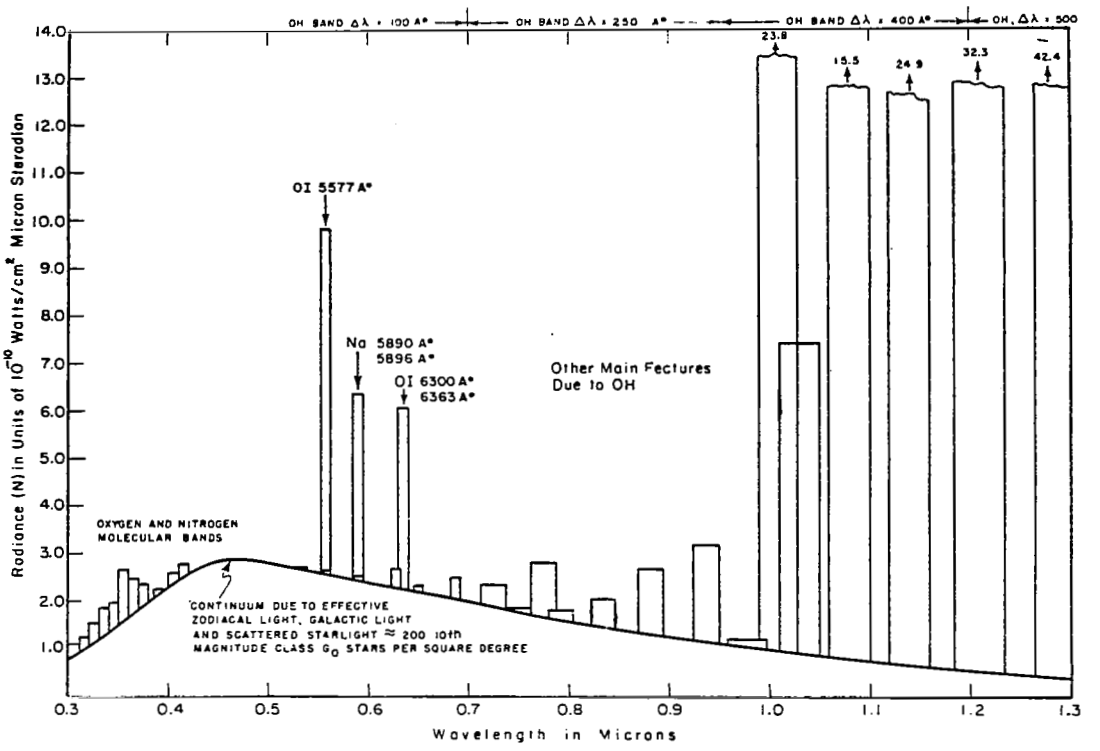

ESTIMATED AVERAGE DIFFUSE RADIATION FROM ZENITH NIGHT SKY

Figure A. Estimated Average Diffuse Radiation from Zenith Night Sky

Average diffuse radiation from zenith, 0.3 to 1.3 microns.

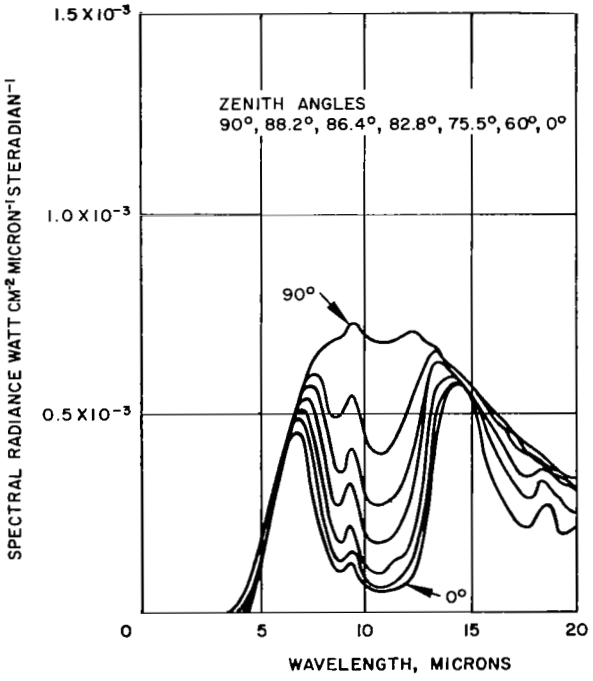

Figure B. Spectral Radiance in the Infrared of a Clear Sky for Several Elevation Angles Above the Horizon

These spectra were measured at an elevation of 11,750 feet, at night, with an ambient temperature of 8°C.

TERRESTRIAL ATMOSPHERIC BACKGROUND - NIGHT-TIME SKY

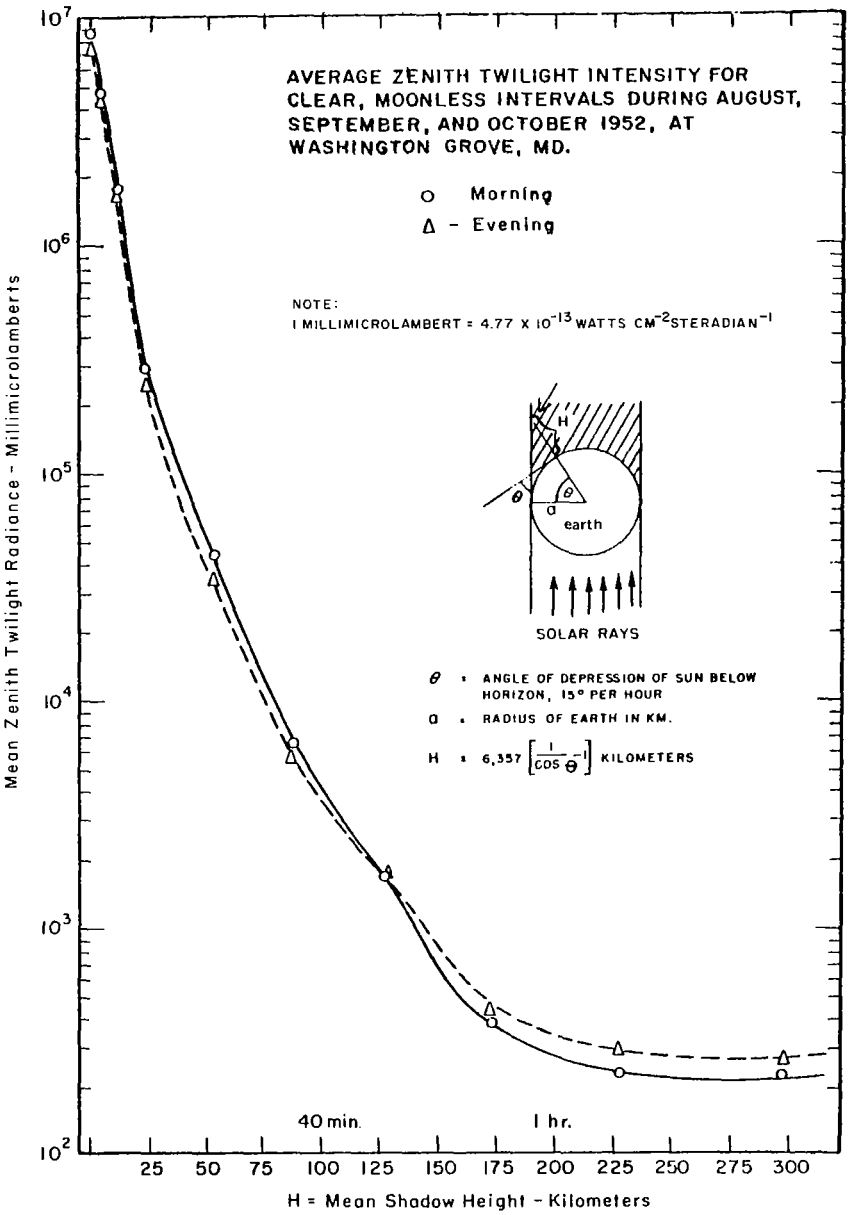

Figure C. Zenith Twilight Intensity

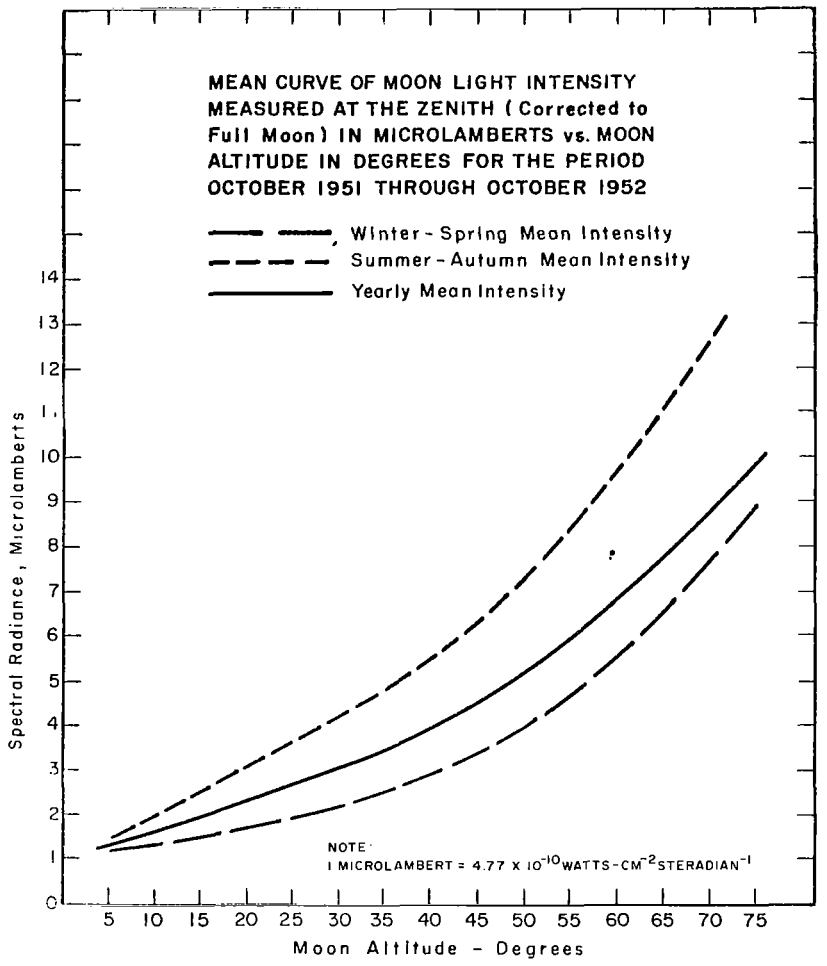

Figure D. Zenith Moonlight Intensity

TERRESTRIAL ATMOSPHERIC BACKGROUND - NIGHT-TIME SKY

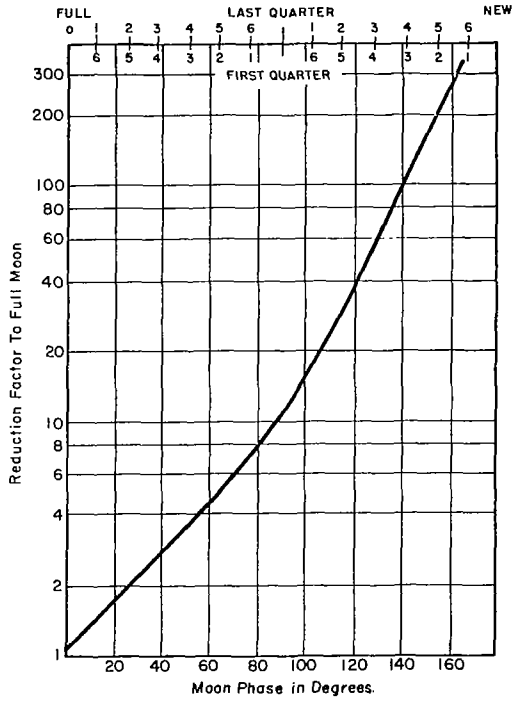

Figure E. Correction Factor for Moon Phase

BACKGROUND RADIATION AND ATMOSPHERIC PROPAGATION

Radio Propagation Through the Terrestrial Atmosphere

RADIO FREQUENCY ATTENUATION

Radio frequency attenuation in the atmosphere is due to water, water vapor, and oxygen. Plots are given showing values of attenuation over a frequency range of 50 MHz to 400 GHz.

Absorption in the ionosphere, as illustrated in Figure A,[1] is very small for microwave frequencies. The effect of ionospheric attenuation can be approximated by assuming that each 0.1 db of attenuation is equivalent to 7°K antenna noise temperature. Ionospheric absorption is negligible for frequencies greater than 0.3 GHz.

Tropospheric absorption is due almost entirely to water vapor and oxygen. Calculated attenuation curves for the frequency range 1.1 GHz to 100 GHz are shown in Figure B[2] for various values of zenith angle. The curves are in satisfactory agreement with experimental attenuation data, shown in Figure C[3]. A summary propagation data for a horizontal path, including rain and fog is given in Figure D.

[1] Millman, G.H., "Atmospheric Effects on VHF and UHF Propagation," Proceedings of the IRE, 48, No. 8, pp. 1492-1501, August 1958.

[2] Blake, L.V., "Tropospheric Absorption and Noise Temperature for a Standard Atmosphere," summary of a paper presented at the 1963 PT-GAP International Symposium, NBS Boulder, Colorado, July, 1963.

[3] Meyer, James W., "Radar Astronomy at Millimeter and Submillimeter Wavelengths," Proceedings of the IEEE, 54, Number 4, p. 488, April 1966.

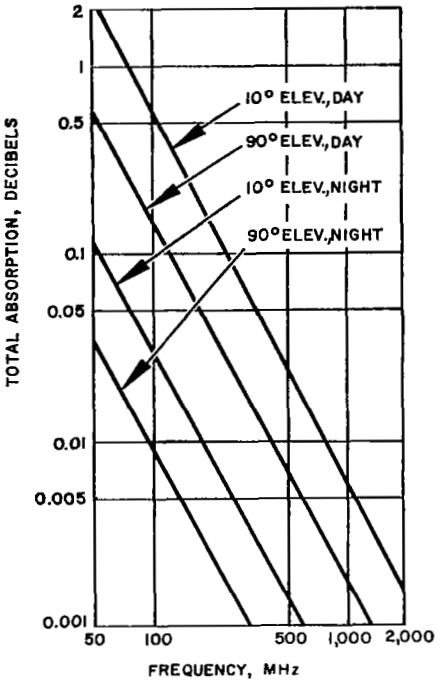

Figure A. Ionospheric Attenuation for a Source at 1,000-km Height

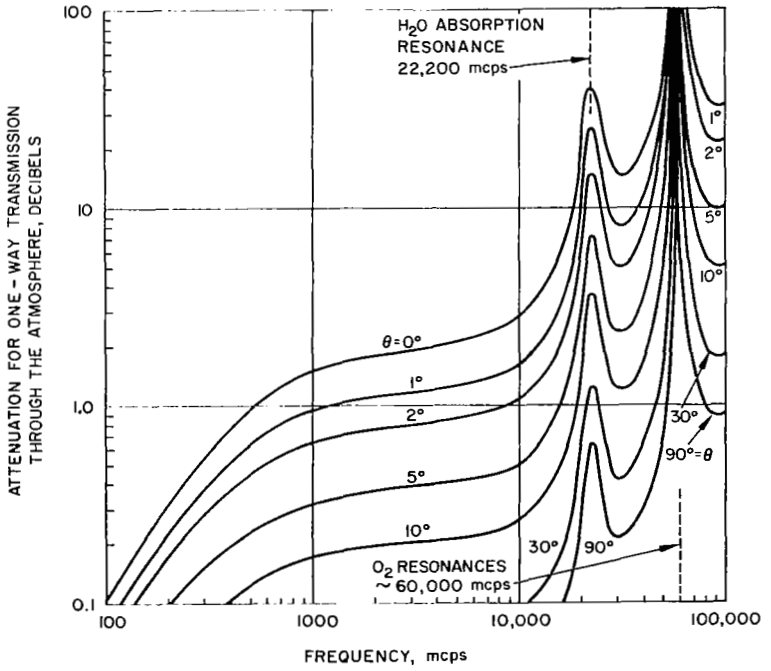

Figure B. One-Way Attenuation Through Standard Summer Atmosphere Due to Oxygen and Water Vapor

RADIO FREQUENCY ATTENUATION

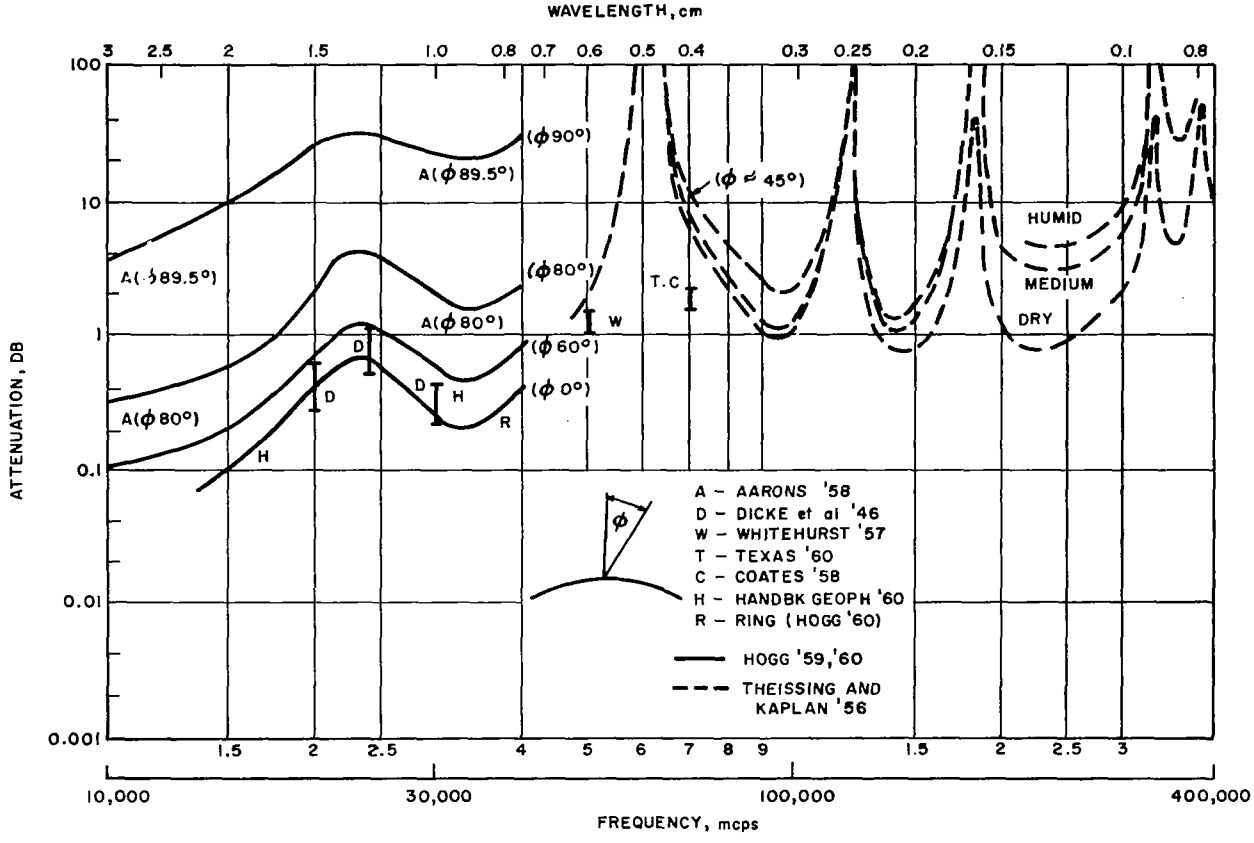

Figure C. Total Attenuation for One-Way Transmission Through Atmosphere

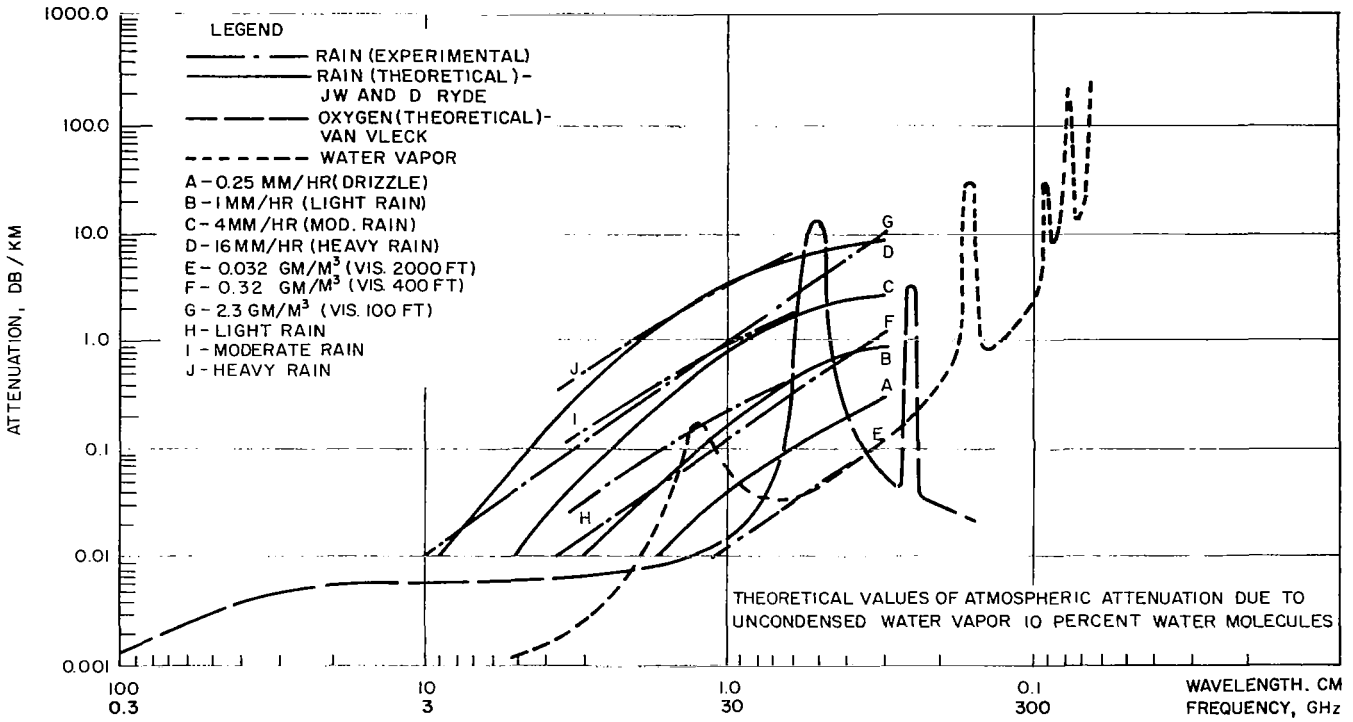

Figure D. Atmospheric Attenuation Summary

RADIO FREQUENCY ATTENUATION FROM 52 TO 68 GHz

Oxygen absorption in the region of 52 to 68 GHz causes this region to be essentially opaque to radio energy, especially at sea level.

The attenuation curves given in the previous topic indicated the large attenuation to microwave frequencies in the 50 to 70 GHz region. At sea level this region is almost opaque to radio propagation. Oxygen absorption of microwave energy causes this large attenuation. At high altitudes the resonants components of this absorption are more easily seen, specifically there are 45 resonant lines between 45 and 72 GHz.

While long range propagation through the atmosphere is not practical between 50 and 70 GHz, communication between spacecraft can be accomplished and will not cause interference to ground stations.

Recent experimentation and calculation by Reber, Mitchell and Carter at the Aerospace Corporation[1] have produced detailed plots of the total attenuation through the atmosphere caused by oxygen.

These plots are given in Figures A and B. Figure A is the zenith attenuation through the entire atmosphere. Figure B is the tangential attenuation through the entire Earth's atmosphere. (Note that this is the one way attenuation from a point on the earth through the atmosphere.)

---

[1] Reber, E. E., Mitchell, R. L., and Carter, C. J., "Oxygen Absorption in the Earth's Atmosphere," Aerospace Report No. TR-0200(4230-46)-3, November 1968.

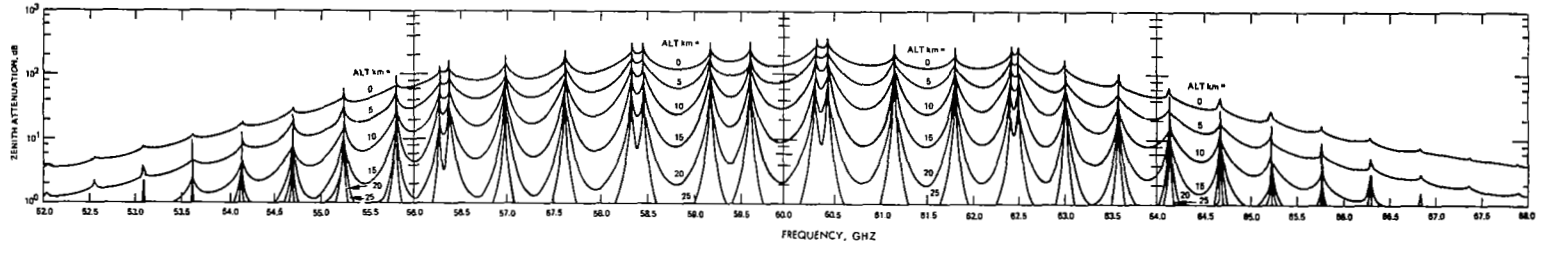

Figure A. Zenith Attenuation, 52 to 68 GHz

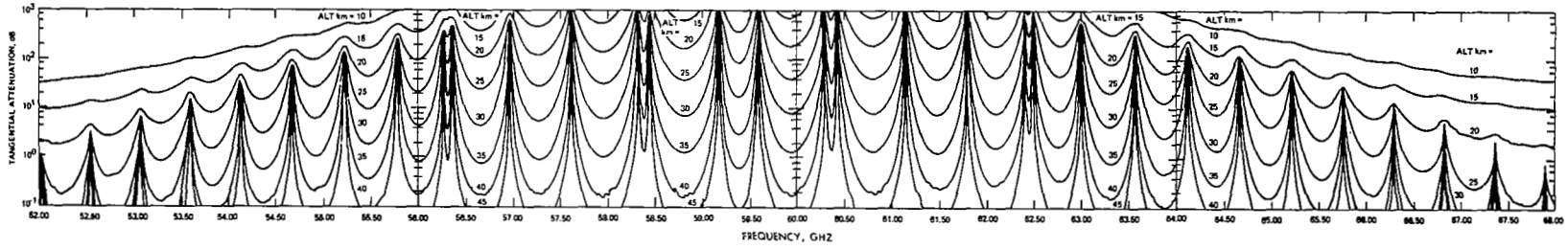

Figure B. Tangential Attenuation, 52 to 68 GHz

BACKGROUND RADIATION AND ATMOSPHERIC PROPAGATION

Radio Propagation Through the Atmosphere

Optical Transmission Through the Atmosphere

RADIO TURBULENCE EFFECTS

Turbulence effects are given in terms of rms wave front deviation.

For rf propagation through the troposphere, variations in the index of refraction are principally due to water vapor irregularities. These irregularities can be attributed to atmospheric turbulence. In the stratosphere, which contains a negligible amount of water vapor as compared to the troposphere, variations in the refractive index are less and can be assumed to be primarily a function of thermodynamic variations in pressure and temperature. Models have been developed, describing the atmospheric structure in statistical terms, as a basis for the application of scattering theories[1, 2]. Some correlation has been achieved between these theories and a number of experimental measurements[3, 4] taken over various path lengths under different and incompletely defined meteorological conditions.

An indication of expected deviations of an incoming wavefront over an antenna aperture can be gained from the phase measurements obtained in the NBS Maui experiment[5]. Here phase deviations in transmission over a 15-mile path, which dropped from 10,000 feet to 100 feet, were measured by two receivers for several baseline lengths up to 4,800 feet. The measurements were made at a frequency of 9,414 MHz, but the deviations in terms of path length can be expected to be relatively independent of frequency. Since the measurements at the various antenna locations were made during different recording periods and therefore under different meteorological conditions, the sample points are not strictly correlated over the baseline range. The trend of these samples, however, is remarkably consistent and is shown in the figure, where phase deviations have been converted to linear deviations in the wavefront.

---

[1] Booker, H. S., and Gordon, W. E., "A Theory of Radio Scattering in the Troposphere," Proceedings of the IRE, 38, Number 4, pp 401-412, April 1950.

[2] Wheelon, A. D., "Radio-Wave Scattering by Tropospheric Irregularities," Journal of Research of the NBS, 63D, Number 2, pp 205-233, 1959.

[3] Herbstreit, J. W., and Thompson, M. C., "Measurements of the Phase of Radio Waves Received over Transmission Paths with Electrical Lengths Varying as a Result of Atmospheric Turbulence," Proceedings of the IRE, 43, Number 10, pp 1391-1401, October 1955.

[4] Smith, P. L., "Scattering of Microwaves by Cloud Droplets," Proc. World Conference on Radio Meteorology, Boulder, Colorado, pp 202-207, 1964.

[5] Norton, K. A., et al., "An Experimental Study of Phase Variations in Line-of-Sight Microwave Transmissions," NBS Monograph 33, November 1961.

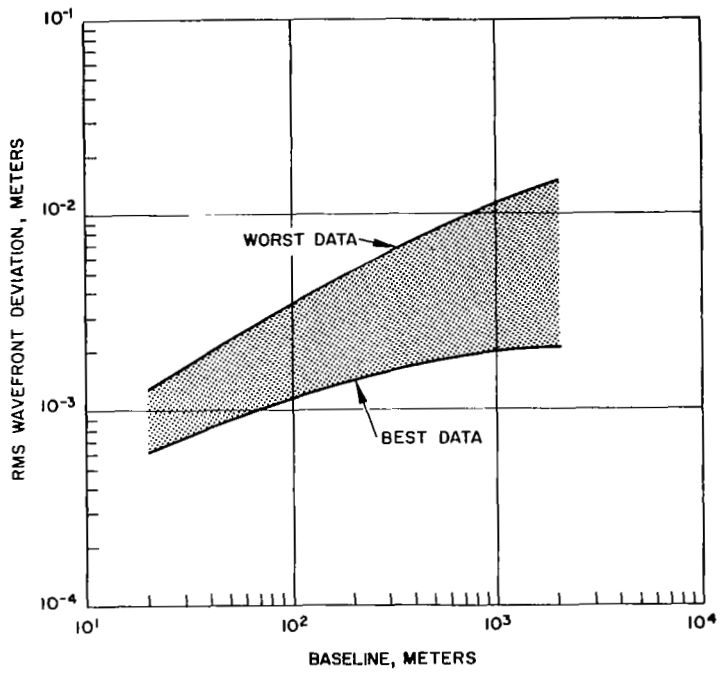

Atmospheric Distortion of r-f
Wavefront Based on NBS Data

ATMOSPHERIC ATTENUATION AT OPTICAL FREQUENCIES

The visible and IR "windows" are given. However, it is important to realize that individual laser frequencies must be checked against the known absorption lines of the atmosphere to assure a clear "window."

There are several transmission windows in the infrared as indicated in Figures A and B[1] but roughly half of the spectrum is still blocked by molecular absorption bands. The density of absorption bands decreases in the near infrared and visible regions as shown in Figure C[1]. The curves, given for several values of zenith angle, are for very clear atmospheric conditions.

It is important to note that the atmospheric absorption bands comprise a large number of sharp absorption lines not resolved on the scale of the curves shown. For the essentially monochromatic radiation generated by lasers, windows may exist within these bands or conversely, relatively isolated absorption lines may exist in apparent windows. Thus high-resolution spectral measurements are necessary in the vicinity of laser lines of interest.

High-resolution solar spectra,[2, 3, 4, 5, 6, 7] which have been taken for many years, represent the best source of information on atmospheric absorption lines. While these measurements have generally been made at high altitudes in order to minimize atmospheric effects and do not provide absolute data on transmission through a standard atmosphere, the measured lines at which attenuation occurs are still strong and serve to identify those wavelengths which must be avoided in the design of a ground-based laser communication link. A detailed study of the absorption spectrum in the vicinity of a number of laser lines has been

---

[1] Chapman, R. M., and Carpenter, R., "Effect of Night Sky Backgrounds on Optical Measurements," Tech. Rpt. 61-23-A, Geophysics Corp. of America, May 1961.

[2] Minnaert, M., Mulders, G. F. W., and Houtgart, J., Photometric Atlas of the Solar Spectrum from λ3612 to λ8771, Schnabel, Kampert and Helm, Amsterdam, The Netherlands, 1940.

[3] Babcock, H. D., and Moore, C. E., The Solar Spectrum, 6600 to 13495, Carnegie Institution of Washington, Publication 579, 1947.

[4] Migeotte, M., "The Solar Spectrum Observed at the Junglraujoch (Switzerland) 7500 to 9070 Angstrams," Tech. Status Rpt. No. 16, Contract AF 61(514) -962, July-September 1960.

[5] Migeotte, M., Annex to Technical Status Report Number 18, Contract AF 61(514)-962, January-March 1961.

[6] Mohler, O. C., Pierce, A. K., McMath, R. R., and Goldberg, L., Photometric Atlas of the Near Infrared Solar Spectrum λ8465 to λ25242, University of Michigan Press, Ann Arbor, Mich., 1950.

[7] Migeotte, M., Neven, L., and Swensson, J., "The Solar Spectrum from 2.8 to 23.7 Microns," Part I, Photometric Atlas, Tech. Final Rpt., Phase A, Part I, Contract AF 61(514)-432, 1957.

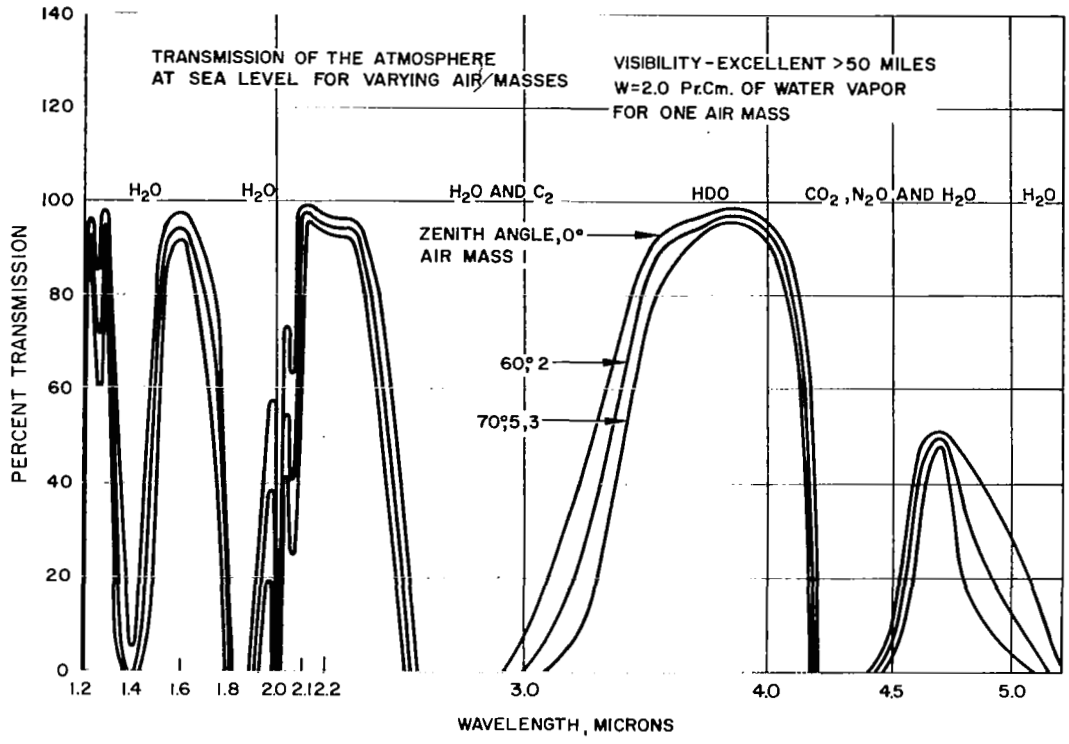

Figure A. Atmospheric Transmission, 1.2 to 5.0 Microns

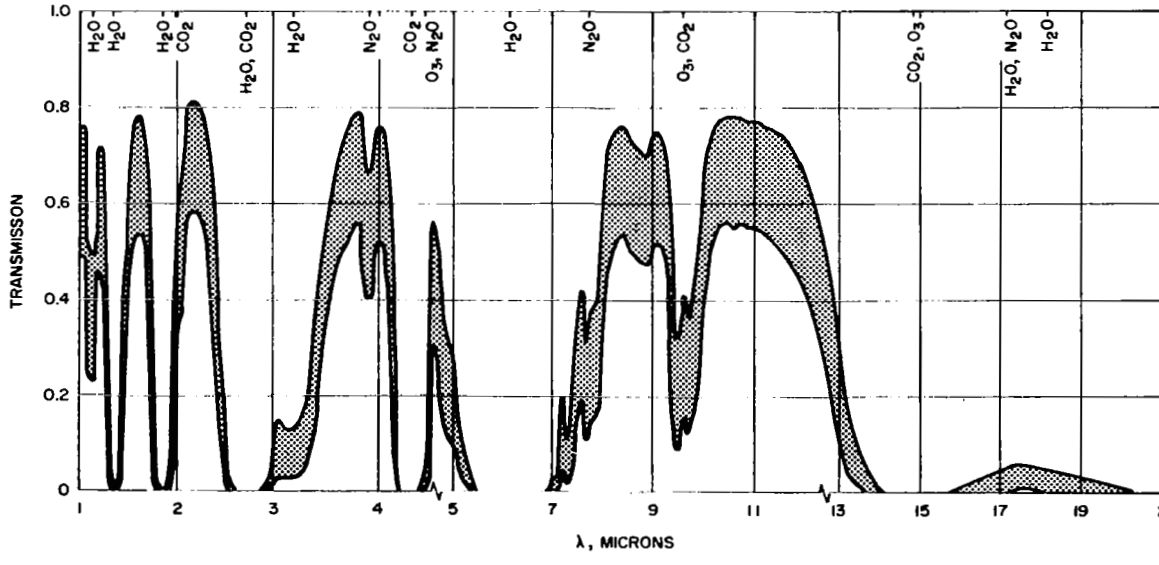

Figure B. Transmission of the Atmosphere in the Infrared at Sea Level for Zenith Angles from 20 to 70 Degrees

Absorbing factors: CO_2, N_2O, CH_4, CO, O_3, and haze (visibility = 32 km).

ATMOSPHERIC ATTENUATION AT OPTICAL FREQUENCIES

made[8,9,10] and indicates, for example, that the output of a ruby laser operated at room temperature lies between water vapor absorption lines situated about a half an angstrom unit above and below the 6943 Å operating point. While similar windows exist above and below this wavelength, the allowable operating temperature range for the laser rod to maintain the radiation within any one of these windows is of the order of 15°C. This emphasizes the importance of detailed spectral measurements of atmospheric absorption about each specific wavelength of interest.

Provided the laser wavelength does not coincide with an absorption line, attenuation in the atmosphere will be due to scattering effects. The attenuation at short wavelengths is due to molecular (Rayleigh) scattering of the radiation for which the scattering coefficient varies as $1/\lambda^4$. This together with absorption by ozone in the upper atmosphere accounts for the sharp cutoff of transmission in the ultraviolet as shown in Figure C. Scattering from aerosol particles and droplets in the first few kilometers of the lower atmosphere also plays a major part in attenuation of electromagnetic radiation in the visible and near-infrared regions.[11,12] For this type of (Mie) scattering (where particle dimensions are comparable with wavelength) the wavelength dependence of the scattering coefficient is a function of particle size and type, but for typical aerosol distributions encountered, experimental measurements[13] suggest that the dependence is about $1/\lambda$.

---

[8] Long, R. K., "Absorption of Laser Radiation in the Atmosphere," Rept. No. 1579-3, The Ohio State University Research Foundation, Contract AF 33(657)-10824, 196

[9] Long, R. K., Atmospheric Attenuation of Ruby Lasers, Proc. IEEE, 51, 5, pp 859-860, 1963.

[10] Long, R. K., and Boehnker, C. H., "Measured Atmospheric Absorption at Ruby Optical Maser Wavelengths," Report 1641-10, Ohio State University Research Foundation, Contract No. AF 33(657)-11195, 1965.

[11] Middleton, W. E. K., Vision Through the Atmosphere, University of Toronto Press, 1958.

[12] Elterman, L., "A Model of a Clear Standard Atmosphere for Attenuation in the Visible Region and Infrared Windows," Research Report, Optical Physics Laboratory Project 7670, AFCRL, 1963.

[13] Knestrick, G. L., Corden, T. H., and Curcio, J. A., "Atmospheric Scattering Coefficients in the Visible and Infrared Regions," J. Opt. Soc. Am. 52, 9, pp 1010-1016, 1962.

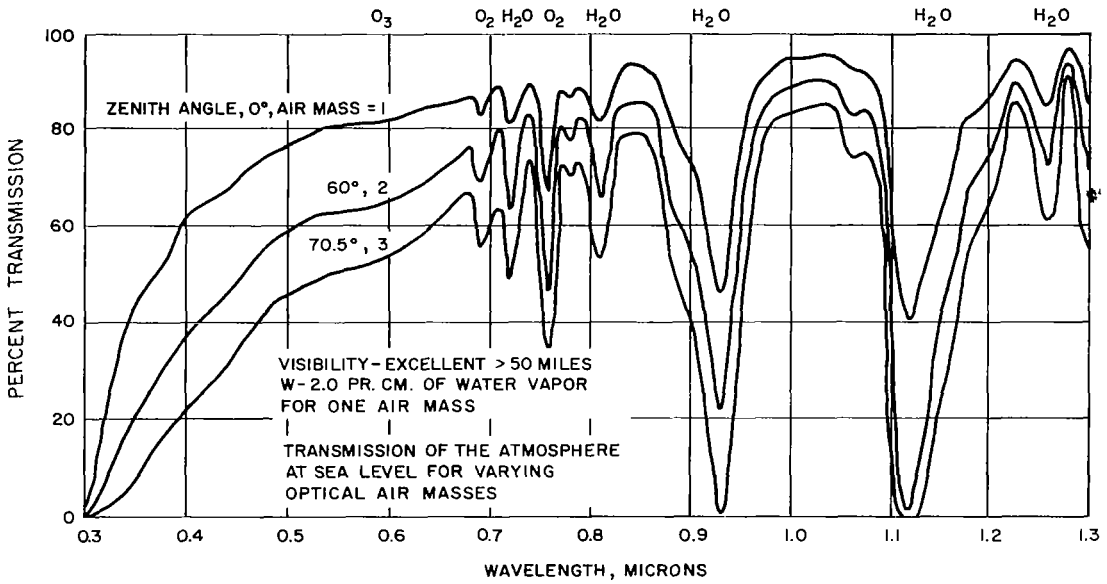

Figure C. Atmospheric Transmission, 0.3 to 1.3 Microns

RAIN AND FOG ATTENUATION AT OPTICAL FREQUENCIES

Both rain and fog are capable of causing very high attenuations (30-60 db) to laser frequencies ranging from 0.63μ to 10.6μ.

Measurements of laser propagation through the atmosphere in the presence of fog or rain indicate that very large attenuations may be expected under such conditions. Measurements taken to date have not provided detailed correlation of particle size and measured attenuation or a detailed contour of the rain fall rate or fog density over the range used. However, data taken has been measured in weather conditions which are typically encountered and as such must certainly be a consideration in laser communications.

Figure A[1] indicates rain and fog attenuation while Figure B[2] indicates rain fall attenuation for three laser frequencies of interest, 0.63, 3.55 and 10.6μ. The rain attenuation for these 3 frequencies is in the range of 2 to 10 db/km/inch/hr.

---

[1] Hogg, D. C., "Effect of the Troposphere on the Propagation of Coherent Optical Waves," Proc. PTGAP IEEE International Symposium, pp 102-108, 1965.

[2] Chu, T. S., "Attenuation by Precipitation of Laser Beams at 0.63μ, 3.5μ and 10.6μ," IEEE Jour. of Quantum Elect.

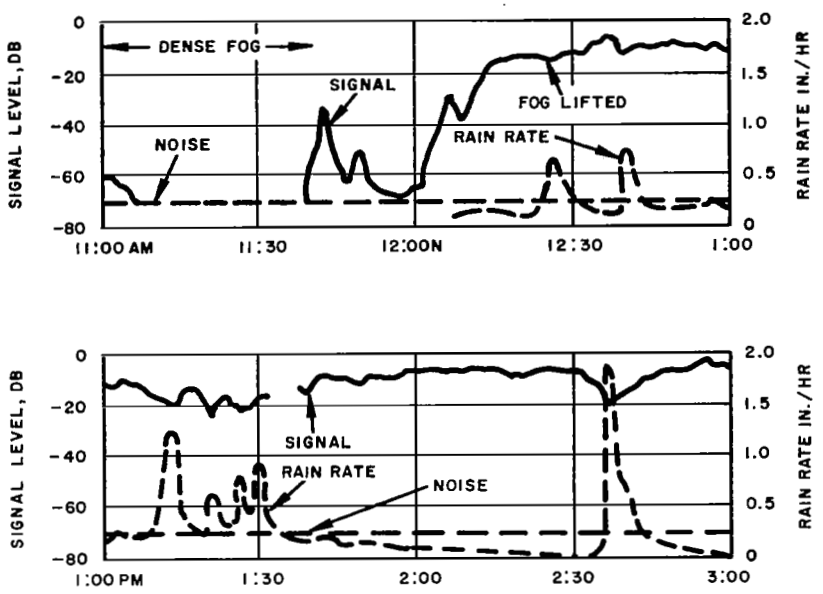

Figure A. Fog-Rain Attenuation, $\lambda = 0.63\mu$ for a 2.6 Km Path

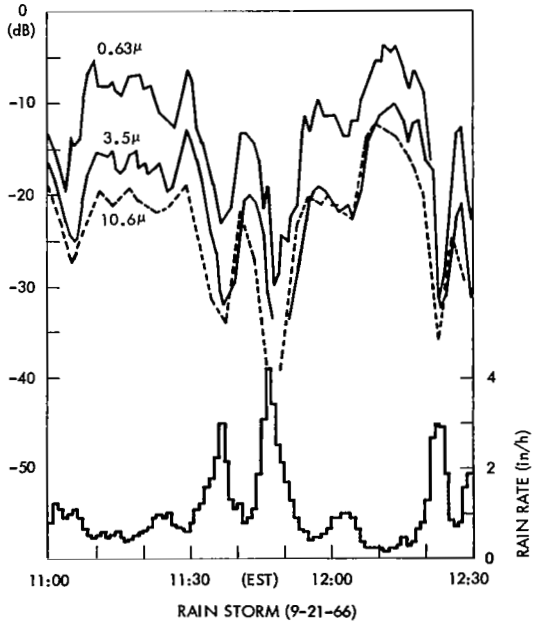

Figure B. Measurement of 2.6 Km Transmission Loss

0 dB signal level in clear weather.

BACKGROUND RADIATION AND ATMOSPHERIC PROPAGATION

Optical Turbulence Effects

Background Radiation and Atmospheric Propagation
Optical Turbulence Effects

INTRODUCTION

Optical turbulence may be caused by: loss of spatial coherence, scintillation, image dancing, beam steering, random polarization fluctuation.

Communications and tracking by coherent light through the atmosphere results in system limitations in addition to those imposed by attenuation and scattering associated with incoherent waves. Laser beam directivity and coherence are degraded by the presence of atmospheric turbulence. The turbulent atmosphere is inhomogeneous and its index of refraction is a function of position and time. As a result of this variation, the character of the beam is altered by the following phenomena:

1. Loss of spatial coherence: destruction of the phase coherence across the beam, the phase changing rapidly with position, leads to blurring of the image.

2. Scintillation: Variations in intensity due to atmospheric turbulence result from random changes in beam cross section.

3. Image dancing: variations in the angle of arrival of the received wavefront will cause the image to be focused at different points in the focal plane of the receiving optics.

4. Beam steering: the entire beam may be deviated from the line of sight, giving rise to a loss of power at the receiving aperture.

5. Random polarization fluctuation.

Any quantitative treatment of the effect of atmospheric turbulence must account for the finite beam diameter, D, which may vary from several millimeters up to several meters, and the important parameter is the ratio of D to inhomogeneity dimensions ℓ.

First, if $D/\ell \ll 1$, the major effect of the turbulence will be to refract the beam as a whole, so that over ranges large compared to ℓ, the projected location of the center of the beam will execute a two-dimensional random walk in the receiver plane. Hence, if the turbulence is isotropic, the displacement of the beam from the line of sight will be Rayleigh distributed. Second, if $D/\ell \approx 1$, the inhomogeneities will, in a first approximation, act as lenses which focus and defocus all or parts of the beam, causing a granular structure of the wavefronts. The steering and spreading of the beam will both be small in this case; and unless the transmission range is larger than the far-field range, scintillation will also be small. Last, if $D/\ell > 1$, small portions of the beam will be independently diffracted and scattered (focused and defocused). Thus, for ranges large compared to ℓ^2/λ, along with spreading of the beam, a badly distorted wavefront may be expected in which intensity fluctuations are strong.[1] For an earth-based receiver and a deep space transmitter, $D/\ell \gg 1$ is always the case so that the principal

---

[1] J. I. Davis, "Consideration of Atmospheric Turbulence in Laser Systems Design," Applied Optics, 5, Number 1, pp. 139-47, January 1966.

effects are loss of coherence, scintillation and image dancing. For an earth based transmitter and spaceborne receiver, $D/\ell \ll 1$ is the case and image dancing and scintillation result.

SCINTILLATION

Scintillation data through the atmosphere has been recorded for visible light using stars.

Scintillation or fluctuations in intensity of signals received from a far exoatmospheric optical transmitter are analogous to the twinkling of stars for which considerable empirical data at visible wavelengths is available. The magnitude of the fluctuations depends on the dimensions of the receiving optics aperture, the zenith angle of the light source, and meteorological conditions. The receiving aperture diameter also significantly effects the dependence of fluctuation magnitude on source zenith angle. Figure A shows the empirical dependence of scintillation amplitude on receiving aperture diameter. Figures B and C show, for two receiver aperture sizes, variation of the quantity log σ_p with zenith angle ϕ. Here $\sigma_p = [(P - \bar{P})/\bar{P}^2]^{1/2}$, P is the actual light flux through the receiver aperture, and $\bar{P}$ is the time average light flux through the aperture.[1]

[1] V. I. Tatarski, Wave Propagation in a Turbulent Medium, McGraw-Hill Book Company, Inc., New York, 1961.

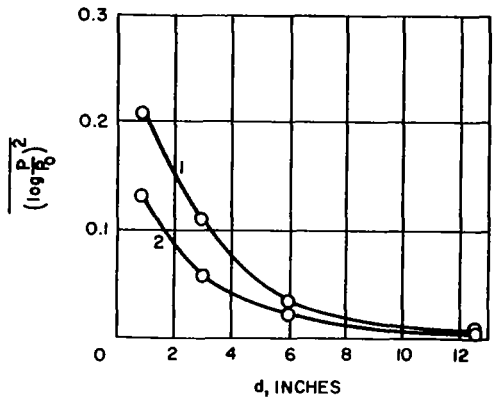

Figure A. Empirical Dependence of Amount of Star Twinkling on Diameter of Telescope Diaphragm (1, winter; 2, summer)

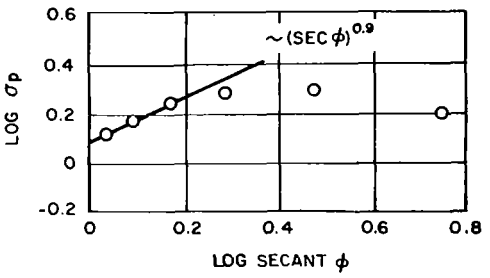

Figure B. Dependence of Amount of Star Twinkling on Zenith Distance When Telescope Diaphragm Has a Diameter of Three Inches

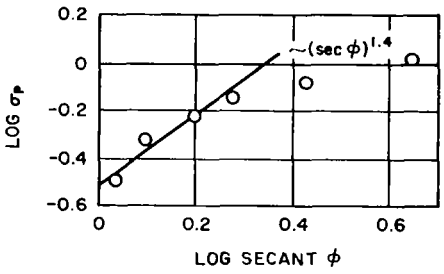

Figure C. Dependence of Amount of Star Twinkling on Zenith Distance When Telescope Diaphragm Has a Diameter of 12.5 Inches

LOSS OF SPATIAL COHERENCE[1]

Coherence length is a function of atmospheric path length, wavelength, and atmospheric conditions.

Spatial coherence is degraded by phase changes in a direction perpendicular to the propagation direction. Due to local refractive index variations in the path of the rays collected by the aperture the initially plane wavefront becomes distorted so that the aperture is no longer an equiphase surface.

In order to illustrate the effects of loss of spatial coherence at the aperture plane of an optical heterodyne receiver, a power reduction factor ρ will be defined as the ratio of the power received when the wave is partially coherent to that received when it is totally coherent. ρ may be expressed for optical heterodyne detection systems as

$$\rho = \frac{1}{z^2}\psi(z)$$

where $\psi(z)$, plotted in Figure A (Fried) contains the dependence of signal-to-noise ratio on receiver diameter and z is the receiver aperture diameter in units of coherence length D_o, given approximately by

$$D_o(\lambda,\phi) = D_o(\lambda_o, 0)\left(\frac{\lambda}{\lambda_o}\right)^{6/5}[\cos\theta]^{3/5}$$

where

λ = wavelength

θ = zenith angle

$D_o(x_o, 0)$ = coherence length for wavelength λ_o and zenith angle 0.

Physically, D_o is a measure of the spatial coherence in a plane perpendicular to the propagation direction. The power reduction factor ρ decreases as z^2 for $z > 1$. The power reduction factor is plotted in Figure A as a function of normalized receiver aperture diameter. The coherence length D_o is plotted in Figure B as a function of wavelength for various receiver altitudes and transmission path zenith angles (as indicated geometrically in Figure C).

It can be seen that the useful collector diameter may be quite small for wavelengths in the visible and near infrared. The advantage of using longer wavelengths can be seen from the $\lambda^{6/5}$ dependence of the coherence length. Since this is approximately a linear relationship, a factor of 10 or more increase in effective collecting aperture diameter is possible in going from 1.06μ to 10.6μ.

[1] Davis, J. I., High Energy Laser Systems Analysis, Semi-annual Report, Hughes Aircraft Company Reference Number A7910, 31 December 1965.

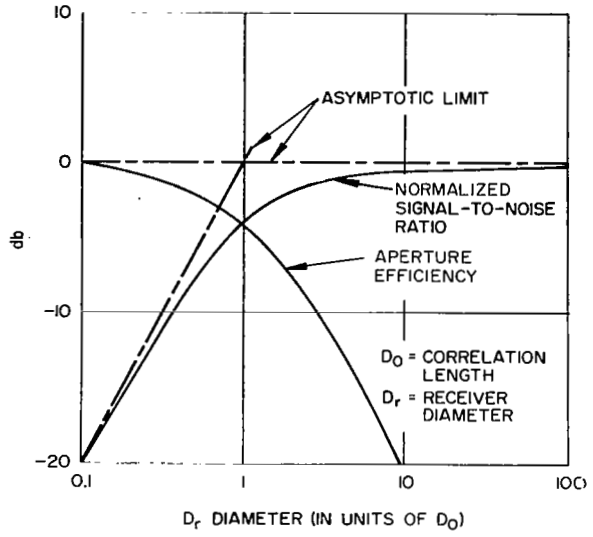

Figure A. Signal Loss for Coherent Detection Caused by Atmospheric Turbulence

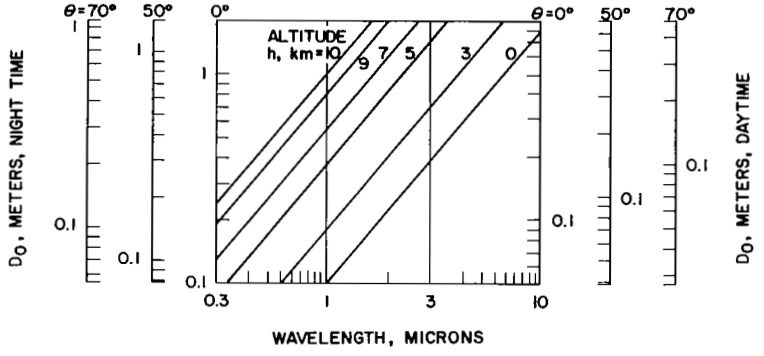

Figure B. Dependence of Correlation Length, D_o, on Zenith Angle, θ, Altitude, h, and Wavelength, λ

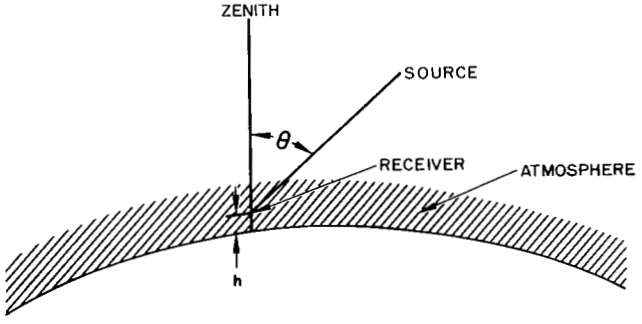

Figure C. Geometry for Optical Heterodyne Receiver in Atmosphere (After Fried)

IMAGE DANCING[1]

Image dancing is generally an insignificant effect.

Image dancing is the variation in the angle of arrival of the received wavefront causing the image to be focused at different points in the focal plane of the receiving optics.

Since the rms angular deviation, σ_θ, is generally small (see the Figure), the rms displacement of the image from the focal point of the lens will almost always be negligible. The displacement of the image will, in fact, always be less than $3f\sigma_\theta$, where f is the lens focal length, and the Figure shows that this displacement will usually be negligible.

Hufnagel and Stanley[2] have derived an expression for image blurring, and their results show that, with the limitation to small scattering angles, diffraction and scintillation cancel each other in the far field, so that the problem may be treated according to ray tracing. Consequently, using the above arguments based on geometrical optics, it may be concluded that the angular blur of a point source is approximately Gaussian with mean zero and fluctuation σ_θ^2.

---

[1] Davis, J. J., "Consideration of Atmospheric Turbulence in Lasar Systems," Applied Optics, 5, pp. 139-147, January 1966.

[2] Hufnagel, R. E., and Stanley, N. R., J. Opt. Soc. Am., 54, 52, 1964.

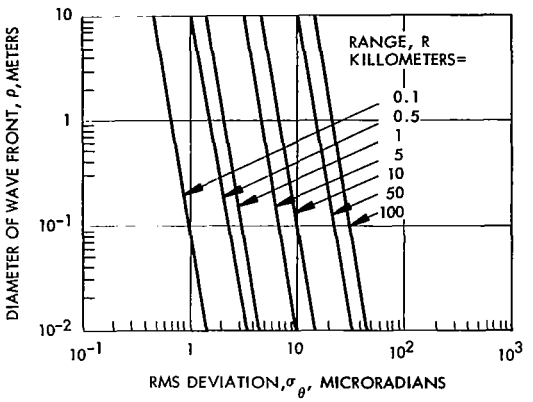

Diameter of Wavefront, ρ, versus
Standard Deviation in Angle of Arrival, σ_θ,
for Intermediate Turbulence

BEAM STEERING

Beam steering is a random phenomena which is generally smaller than 10 microradians.

The net effect of numerous deflections of the beam over its path is to produce an angular deviation, $\Delta\alpha$, of the beam from its line of sight path, causing part or all of the beam to miss the receiver. This effect is referred to as beam steering. Essentially the projected location of the center of the beam executes a two-dimensional random walk in the receiver plane. If the turbulence is isotropic, the displacement of the beam from the line of sight will be Rayleigh distributed. Making the assumption that the correlation distance for the derivative of the angular deviation with respect to distance along the path is small compared to the total range, R, it can be shown that the net lateral displacement of a ray has an rms deviation

$$R\Delta\alpha_{rms} = \frac{R\Delta\theta_{rms}}{\sqrt{2}}$$

where $\Delta\theta_{rms}$ = rms value of the deflection on the image plane of the receiver.

Hence it may be inferred that the beam is deviated by

$$\Delta\alpha_{rms} = \frac{\Delta\theta_{rms}}{\sqrt{2}}$$

When the receiver is in the far field of the transmitter, the effect of beam steering will be negligible if the rms angular deviation of the beam $\Delta\alpha_{rms}$ is small (1/3 or less) compared to the half angular divergence of the beam.

The figure is a plot of the rms beam deviation angle, δ_θ, as a function of the propagation wavelength and range[1]. Compensation for beam steering may be effected simply by increasing the beam divergence angle so that even if the beam is deviated by turbulence, the receiver will still be illuminated. The penalty paid, of course, is a reduction in spatial power density in the receiver plane.

---

[1] Davis, J. I., "Consideration of Atmosphere Turbulence in Laser Systems Design," Applied Optics, 5, 1, 139-147, January 1966.

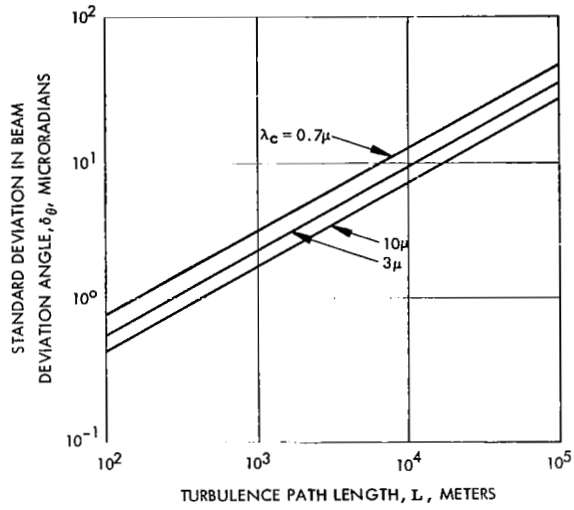

Standard Deviation in Beam Deviation Angle of a Phase Coherent Portion of a Laser Beam due to Intermediate Atmospheric Turbulence

POLARIZATION FLUCTUATIONS

Polarization fluctuations do not appear to be a problem for laser communications.

The electric field of a wave entering a region of turbulence can be broken up into components E_{X1} and E_{Y1} in the plane of incidence. The polarization angle of the incident wave is

$$Z = \tan^{-1} \frac{E_{Y1}}{E_{X1}}$$

After leaving the turbulence region the electric field components are changed to E_{X2} and E_{Y2} due to a change in the index of refraction of the medium. The polarization angle is then

$$Z + \Delta Z = \tan^{-1} \frac{E_{Y2}}{E_{X2}}$$

Saleh[1] has developed an expression for the mean square change in the polarization angle. For an isotropic atmosphere the rms polarization change is

$$\sqrt{\overline{[\Delta Z]^2}} = 2\pi \overline{[\Delta n]^2} \frac{L}{L_0}$$

where $\overline{[\Delta n]^2}$ is the mean square change in index of refraction due to thermal variations. The index of refraction change has been empirically determined to be related to the altitude of observation, h_0, in meters by the relation

$$\overline{[\Delta n]^2} = 10^{-12} \exp\left\{-\frac{h_0}{1600}\right\}$$

As an example of transmission over a low-altitude ($h_0 \approx 0$), horizontal path of 10^4m with a turbulence dimension of $L_0 = 1$ m, the rms change in polarization angle, $\sqrt{\overline{[\Delta Z]^2}}$, in on the order of 10^{-8} rad. Experiments verify that polarization fluctuations do not appear to be a problem for laser propagation.[1]

---

[1] Saleh, A. A. M., "An Investigation of Laser Wave Depolarization due to Atmospheric Transmission." IEEE Journal of Quantum Electronics, QE-3, 11, 540-543, November 1967.

PART 2 EARTH RECEIVING FACILITIES

SUMMARY OF EARTH RECEIVING NETWORKS

Several radio networks have been developed for space communication; DSN, MSFN and STADAN. However there is no optical network to utilize the superior performance promised by optical communications for certain missions.

There are three major ground networks for spacecraft radio communications. These are the Deep Space Network, DSN; the manned Space Flight Network, MSFN; and the Satellite Tracking and Data Acquisition Network, STADAN. These three networks are briefly described below.

DSN

The Deep Space Network (DSN) is a precision tracking and communications system capable of providing command, tracking, and data acquisition from spacecraft designed for deep space exploration. Although it is designed for use in deep space exploration, the DSN may be used with other types of missions, e.g., manned missions, where its capabilities can be used to advantage.

The DSN is comprised of nine Deep Space Stations (DSS) clustered in three Deep Space communication complexes (DSCC) and called the Deep Space Instrumentation Facility (DSIF), an intersite communications network called the Ground Communications Facility (GCF), and a Space Flight Operations Facility (SFOF) located in Pasadena, California.

MSFN

The Manned Space Flight Network (MSFN) provides tracking, communication, telemetry, and voice transmission in real time between the manned spacecraft and the Mission Control Center. This capability is provided to MSFN stations by: the Unified S-Band System (USBS), a VHF telemetry and voice system, a UHF command system, and by C-Band and S-Band tracking radars. The performance of a typical MSFN station is influenced by the strategic location of the station for mission coverage and the communication between the station and the mission control center.

STADAN

The primary purpose of the STADAN is to receive data from scientific satellites and to produce tracking information for orbit computation. Most of the equipment in the STADAN has been designed for use by many programs, with emphasis on quick adaptability to the differing requirements of several simultaneously-orbiting spacecraft. Most programs do not require data from all STADAN stations, so the specific capabilities of each station have been tailored to differing levels of performance.

The STADAN consists of three major systems: the Data Acquisition Facilities, Minitrack, and the Goddard Range and Range Rate System. The Data Acquisition Facilities (DAF) is equipped with multi-frequency, high gain antennas and its capability of handling large quantities of data at high rates exceeds that of the standard Minitrack systems.

The second major functional system, Minitrack, has been used to track all U.S. satellites which have suitable beacons, since the beginning of the space program. In addition to its tracking functions, the Minitrack system has the facilities for receiving telemetry data in the 136- to 137-MHz and 400-to 401-MHz bands.

The third major system of the STADAN is the Goddard Range and Range Rate Tracking System which complements the Minitrack network by providing improved tracking data for space probes, launch vehicles, and satellites in highly elliptical orbits.

A particular STADAN station may have any combination of the above systems, and the specific configuration of the system will vary depending on the cumulate requirements placed on the station.

Optical Ground Sites

At present there are no ground networks for optical communications. There are, however, a few facilities which are being used for laser earth to space transmission and for making measurements needed to design such links. These facilities include 1) a telescope facility and Goddard Space Flight Center which has successfully performed laser ranging experiments to a low altitude satellite; 2) a lunar ranging site in the Catalina Mountains of Arizona which has measured range to the moon using a retroreflector placed on the moon by the Apollo astronauts; and 3) atmospheric experiments being conducted by the Smithsonian Astrophysical Observatory for NASA at Mount Hopkins.

Clearly the radio receiving facilities are well developed, are performing with manned and unmanned spacecraft, and are being developed as required. Conversely, optical communications facilities are in an early experimental phase. Since optical communications do show clear advantages over radio communications for some missions (missions requiring exceptionally high data flow, e.g., a planetary orbiter mission). There is therefore a need for implementing an optical communication network. This is discussed further in subsequent topics.

Earth Receiving Facilities

INTRODUCTION

Radio and optical facilities will be surveyed. Three radio networks for space communication are presently in operation

---

The general requirements to be met by ground facilities are:

a. Tracking of spacecraft to determine their precise location and trajectory in space.

b. Acquisition of scientific and engineering data transmitted from spacecraft via telemetry.

c. Transmission of commands from ground stations to direct the performance of specific missions by the spacecraft.

d. Communication of voice information between ground stations and manned spacecraft.

e. Communicating data from remote receiving and transmitting sites to a central control facility.

Ground facility considerations will be discussed separately for optical frequencies and radio frequencies. Very extensive radio frequency facilities are already in being. However, optical facilities are still in the conceptual design stage. The existing radio frequency facilities and their capabilities will be surveyed. The constraints affecting the selection of optical facility locations will be discussed and existing astronomical observatories which might be applicable to incoherent optical reception will be described.

To provide effective ground instrumentation support of flight projects, NASA has established a worldwide network of tracking and data acquisition stations which, at the present time, contains ground stations which are operational or under construction at 26 locations. These stations are located in the United States and 16 foreign countries and territories.

The network consists of three functionally oriented types of facilities to support three generic types of missions. These are the Manned Space Flight Network (MSFN) for support of manned missions, the Deep Space Network (DSN) for support of unmanned lunar and planetary missions, and the Satellite Tracking and Data Acquisition Network (STADAN) for support of unmanned Earth-orbiting scientific and applications satellites.

The three types of facilities are interconnected through control centers and a versatile communications system (NASCOM) which permits the facilities of one network to supplement those of another as required. For example, Manned Space Flight Network facilities are frequently used in support of both unmanned earth satellite missions and the early phases of lunar and planetary missions. Similarly, the Deep Space Network will be used as backup for the facilities of the Manned Space Flight Network during the critical lunar approach and landing and return phases of the Apollo mission when continuous communications is vital.

EARTH RECEIVING FACILITIES

Deep Space Network

Earth Receiving Facilities
Deep Space Network[1]

INTRODUCTION TO THE DEEP SPACE NETWORK[2]

The Deep Space Network consists of the 1) deep space stations, 2) the intercommunications network, and 3) the central control facility. The deep space stations are of primary concern in the study and will be described further in subsequent topics.

The Deep Space Network (DSN) is a precision tracking and communications system capable of providing command, control, tracking, and data acquisition from spacecraft designed for deep space exploration. Although it is designed for use in deep space exploration, the DSN may be used with other types of missions wherein its capabilities can be used to advantage.

The DSN is comprised of nine Deep Space Stations (DSS) clustered in three Deep Space communication complexes (DSCC) and called the Deep Space Instrumentation Facility (DSIF), an intersite communications network called the Ground Communications Facility (GCF), and a Space Flight Operations Facility (SFOF) located in Pasadena, California.

The design philosophy of the DSN is to provide a precision radio tracking system which measures two angles, radial velocity and range providing two way communications with spacecraft in an efficient and reliable manner. The DSN will be improved and modernized to remain consistent with the state of the art and project requirements. In addition to their participation in the DSN, the Goldstone stations are utilized for extensive investigation into space tracking and communications techniques and for the development of new equipment. In most cases, new equipment is installed and tested at Goldstone before it is integrated into the DSN. Once this equipment has been accepted for general use, it is classed as Goldstone Duplicate Standard (GSDS) equipment.

Operational control of the DSN during a mission is provided by the Space Flight Operations Facility at JPL. The SFOF furnishes trajectory information to the DSIF, reduces the data which the DSIF acquires from the spacecraft, and furnishes facilities for the operations control of the spacecraft.

The DSIF consists of stations situated so that a spacecraft in or near the ecliptic plane at ranges greater than 10,000 miles is always within the field-of-view of at least one of the selected ground antennas. The primary DSIF complex is at Goldstone, California. Other stations are located at Johannesburg, Republic of South Africa; Canberra, Australia; and Madrid, Spain. The exact geographic locations of DSIF stations are listed in the table.

The DSS parameters are of primary importance in this study since these stations interface with the spacecraft communications systems. The DSS parameters will be discussed in subsequent topics.

---

[1] Description of the Deep Space Network Operational Capabilities as of January 1, 1966, W. H. Bayley, et al., JPL Technical Memorandum 33-255, July 1, 1966.

[2] JPL Space Programs Summary 37-54, Vol. II.

Tracking and Data Acquisition Stations of the DSIF

DSCC	Location	DSS	Antenna		Year of initial operation
			Diameter, ft	Type of mounting	
Goldstone	California	Pioneer	85	Polar	1958
		Echo[a]	85	Polar	1962
		(Venus)[b]	(85)	(Az-El)	(1962)
		Mars	210	Az-El	1966
Canberra	Australia	Woomera[c]	85	Polar	1960
		Tidbinbilla[c]	85	Polar	1965
	South Africa	Johannesburg[c]	85	Polar	1961[d]
Madrid	Spain	Robledo[c]	85	Polar	1965
		Cebreros[c]	85	Polar	1967

[a] Established in 1959 to support NASA's Echo Project to explore the feasibility of transcontinental two-way communications using a passive satellite, the Echo DSS was originally configured with an 85-ft-diam Az-El-mounted antenna. In 1962, when the need arose for a second 85-ft-diam polar-mounted antenna at the Goldstone site, the 85-ft-diam Az-El-mounted antenna was moved to the Venus DSS, and an 85-ft-diam polar-mounted antenna was constructed at the Echo DSS.

[b] A research-and-development facility used to demonstrate the feasibility of new equipment and methods to be integrated into the operational network. Besides the 85-ft-diam Az-El-mounted antenna, the Venus DSS has a 30-ft-diam Az-El-mounted antenna that is used for testing the design and operation of the feed system for the Mars DSS 210-ft-diam antenna.

[c] Normally staffed and operated by government agencies of the respective countries (except for a temporary staff at the Madrid DSCC), with some assistance of U.S. support personnel.

[d] Between 1958 and 1962, a temporary mobile tracking station was located near Johannesburg to provide L-band communications required by the Ranger and Mariner Venus 1962 spacecraft.

DSS TRACKING CAPABILITY

The angle and range tracking accuracies for the Deep Space Stations are given, both for the 85 and 210 foot antennas.

Angle Tracking. The automatic angle tracking systems used in the DSIF are of the simultaneous-lobing type. The 85 ft polar mounted antennas have two maximum tracking rate capabilities, 0.7 deg/sec and 0.03 deg/sec about each axis, depending on tracking system bandwidth requirements. For strong signal levels, the root-mean-square angle tracking error is 0.01 to 0.02 degree. The rms tracking error at receiver threshold increases to approximately 0.05 degree. Bias errors lie in the range of -0.1 to +0.1 degree. However, optical calibration techniques such as star tracking have led to the accurate determination of certain bias errors, and these are removed from the observed data at the computational facility. Resolution of angle encoders is 0.002 degree.

The 210 ft antenna has an angular accuracy of 0.01 degree, a maximum angular velocity of 0.5 deg/sec and a maximum angular velocity of 0.2 deg/sec^2.

Angle data from all the DSIF antennas are digitally encoded by angle sensors on the antenna, and the coded signals are recorded in teletype code on punched paper tape by the data handling equipment.

Range Rate Measurement Capability. Provisions for one-way, two-way, three-way non-coherent doppler or three-way coherent doppler are available at the DSIF.

In the one-way mode, the DSIF is in a receive-only condition and the spacecraft is not interrogated by the ground transmitter. Due to the relatively poor frequency stability of spacecraft oscillators and increasingly precise trajectory determination requirements, the one-way technique is now used only as a backup measure. One-way doppler velocity determination accuracy is approximately 30 meters/sec.

In the two-way mode, a stable carrier signal in the 2110-2120 MHz band is transmitted to the spacecraft. There it is received phase tracked and used to control the spacecraft transmitter with a transmit to receive frequency ratio of 240/221. It is then transmitted to the ground station where it is compared with the ground transmitter signal to determine the doppler frequency shift. The resultant accuracy in velocity determination both present and projected (using the 210-foot dish) is shown in the table.[1]

When one ground station is in a transmit-receive mode and a second ground station is simultaneously in a receive-only mode, the resultant mode of the second ground station is called three-way noncoherent doppler. Precision doppler may be extracted by the second ground station since the transmitting frequency of the two way ground station

---

[1] Projected NASA/JPL Deep Space Capabilities in the 1970's, AIAA/AAS Stepping Stones to Mars, Baltimore, Maryland, March 28-30, 1966.

DSIF Range and Range Rate Measurement Accuracy

Parameter	Two-Way Doppler Tracking, Mariner Mars, 85 ft Antenna	Two-Way Doppler Tracking, 1970's, 210 ft Antenna	Ranging 1970's, 210 ft Antenna
Resolution at 1 A.U.			
1. Guaranteed accuracy at 1 A.U. equivalent uncorrelated RMS error at 1 sample/min	0.5 cps (0.030 meters/sec)	0.015 cps (0.001 meters/sec)	
2. Probable accuracy under same conditions	0.010 cps (0.0006 meters/sec)	0.003 cps (0.0002 meters/sec)	
1. Near Earth - at sample spacing of 5 minutes or more			2.0 meters accuracy 0.1 meters resolution
2. 1 A.U. - At sample spacing of 1 hour or more			10 meters accuracy 2.0 meters resolution

is known. The three-way noncoherent doppler mode provides for the reception of additional high accuracy doppler information. The three-way coherent mode is identical to the three-way noncoherent mode except that the transmitter frequency of the two-way ground station is relayed to the receive-only ground station. The receive-only station uses this additional information in its doppler loop to provide greater precision, resulting in doppler data of quality nearly equal to that of the two-way station.

A summary of these doppler tracking capabilities is shown in the figure.

Range Measurement Capability. Range determination is an extension of two-way doppler tracking technique. A ground transmitter signal is phase modulated by long pseudorandom binary waveforms. At the spacecraft it is detected, reconstructed and remodulated or merely detected and remodulated before being transponded back to the ground station. There it is cross-correlated in the tracking receiver with a local model of the original signal. When maximum correlation is achieved, the phase difference between the transmitter code and the receiver code is a measure of the spacecraft range. Present and projected (using the 210-foot dish) range determination accuracy is also shown in the table. The ranging system is operable as long as carrier phase coherence is maintained in the two-way system.

a. ONE-WAY DOPPLER (f_1):
SPACECRAFT (S/C) TRANSMITS TO THE DSIF STATION WHICH OPERATES ONLY IN THE RECEIVE MODE.

b. COHERENT THREE-WAY DOPPLER (f_{c3}):
$f_r(t_r)$ AND $f_x(t_x)$ ARE COHERENTLY DIFFERENCED AT THE RECEIVING STATION; THIS CONFIGURATION WAS USED DURING THE Ma II (VENUS) MISSION BY UTILIZING THE MICROWAVE LINK BETWEEN TWO OF THE GOLDSTONE STATIONS; i.e., DSIF 12 TRANSMITTED, AND DSIF 11 RECEIVED; THE S/C TRANSPONDER RECEIVES THE INCOMING SIGNAL, MULTIPLIES IT BY 240/221, AND RETRANSMITS IT TO THE GROUND STATION FOR f_{c3}, f_2, AND f_3.

c. TWO-WAY DOPPLER (f_2):
A SPECIAL CASE OF COHERENT THREE-WAY DOPPLER, WHERE THE SAME DSIF STATION IS THE TRANSMITTING AND RECEIVING STATION.

d. THREE-WAY DOPPLER (f_3):
NORMALLY THE TRANSMITTING AND RECEIVING STATIONS ARE LOCATED ON DIFFERENT CONTINENTS, AND NO MICROWAVE LINK IS AVAILABLE TO ALLOW THE COHERENT DIFFERENCING OF $f_r(t_r)$ AND $f_x(t_x)$.

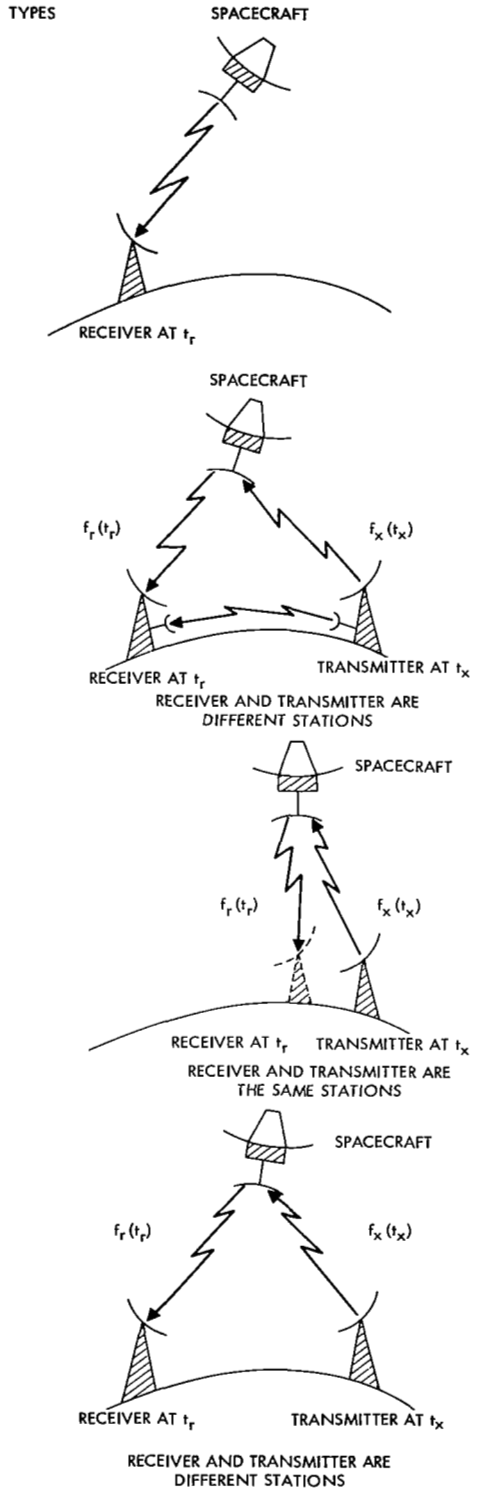

Types of Doppler Provided by DSIF Network

COMMUNICATION FREQUENCIES AND BANDWIDTHS

Deep Space Station transmit and receive frequencies are given as are nominal if bandwidths at the earth station.

Allocated DSIF Frequencies. All JPL projects and non-JPL projects, except Apollo, which will use the DSIF for tracking and data acquisition, will use S-band frequencies, i.e., 2110 to 2120 MHz from Earth to spacecraft and 2290 to 2300 MHz from spacecraft to Earth with frequencies being in the exact ratio of 221/240 for two way doppler tracking. This frequency band has been divided into transmitting and receiving channels in accordance with the table. The channels operate in pairs to maintain the 221/240 ratio. These channel assignments permit communications to and from different spacecraft which may be operational in the same time period.

Telemetry Assembly of Receiver Subsystem. The S-band phase lock loop receiver is a double conversion superheterodyne with a 50-MHz first i-f and a 10-MHz second i-f. The output of the 10-MHz i-f passes through a bandpass filter which can be selected to have any one of four different bandwidths: 3.3 MHz, 420 kHz, 20 kHz, and 4.5 kHz. When required, this filter may be replaced with one designed to meet particular characteristics. Some stations are equipped with standard phase-lock IRIG discriminators and channel selectors for channels 1 through 8. If necessary, arrangements can be made to furnish an output from the 50 MHz IF amplifier with a bandwidth of 10 MHz.

Television. The capability of recording television pictures is provided in the receiver at two points. For very wideband signals an output 10 MHz wide is available from the 50-MHz first i-f. A detection bandwidth of 300 Hz to 1.65 MHz is also available from the output of the video amplifier which follows the wideband phase detector.

Ground Command and Control. All presently planned JPL projects use a digital command and control system with a transmission rate of one bit per second. Three successive identical commands are sent by teleprinter circuits to the station and received on punched paper tape. This tape is placed in the tape reader of the ground command subsystem; then it is read into the system where the command is verified, displayed, and recorded on punched paper tape. Initiation of actual command-modulated RF transmission can be done manually or automatically by insertion of a given time of day. During transmission to the spacecraft the RF signal is detected and compared bit by bit with the stored command. Transmission is inhibited when an error is detected by this monitor.

In the event that the communications design of a particular spacecraft is incompatible with the existing ground command subsystem, it will be necessary for the project to furnish sufficient mission-peculiar equipment to replace the functions of the present system. This equipment should (1) accept commands from punched paper tape received on teleprinter circuits, (2) be self checking, and (3) deliver a voltage from 0 to 2.5 volts peak into 20 ohms.

Frequency and Timing Standards. The basic frequency standards at the stations consist of two stable crystal oscillators (one for redundancy). These oscillators will be supplemented with two atomic standard (rubidium vapor) oscillators per station. Using the crystal oscillators for the timing standard, the drift is stable to 2 parts in 10^{10} over 24 hours, and the initial frequency setting error is less than 5 parts in 10^{9}. Local time readout can be synchronized to WWV or WWVH to at least 10 milliseconds. Using the atomic standard oscillators, the drift error is not greater than 2 parts in 10^{11}. Using VLF receivers and WWVH it is anticipated that local time settings can be made to 3 milliseconds or less.

COMMUNICATION FREQUENCIES AND BANDWIDTHS

DSIF Frequencies

Channel	Ground Receiver Frequency, Channel A	Ground Transmitter Frequency, Channel B
1	2290.185185	—
2[a]	0.555556	—
3	0.925926	—
4	1.296296	—
5[a, b]	1.666667	2110.243056
6	2.037037	0.584105
7	2.407407	0.925154
8[a]	2.777778	1.266204
9	3.148148	1.607253
10	3.518519	1.948303
11*	3.888889	2.289352
12	4.259259	2.630401
13	4.629630	2.971451
14[a, b]	5.000000	3.312500
15	5.370370	3.653549
16	5.740741	3.994599
17[a]	6.111111	4.335648
18	6.481481	4.676697
19	6.851852	5.017747
20[a]	7.222222	5.358796
21	7.592593	5.699846
22	7.962963	6.040895
23[a, b]	8.333333	6.381944
24	8.703704	6.722994
25	9.074074	7.064043
26[a]	9.444444	7.405092
27	9.814815	7.746142
28	—	8.087191

DSIF Frequencies (continued)

Channel	Ground Receiver Frequency, Channel A	Ground Transmitter Frequency, Channel B
29	—	2118.428241
30	—	8.769290
31	—	9.110339
32	—	9.451389
33	—	9.792438

[a]Recommended center frequencies for channels requiring 1-MHz bandwidths.
[b]Recommended center frequencies for channels requiring 3-1/3-MHz bandwidths.

DSIF COMPONENT PERFORMANCE CHARACTERISTICS

Performance is given for the Deep Space Station receivers, transmitters and antennas.

DSS Receiver. The DSIF stations incorporate S-band receivers able to detect both amplitude and phase modulation and to provide an accurate received power measurement. The receivers have the following general capabilities:

1. Accepting RF signals which contain angle-of-arrival error, carrier frequency and phase, range code modulation, and telemetry modulation information.

2. Coherently detecting frequency and phase of the received signal carrier. Continuously providing the two-way doppler frequency information due to the relative motion of the spacecraft and the earth.

3. Detecting angle-error RF signals to provide d-c error signals which are unambiguous in polarity and approximately linearly related in magnitude to the angular error between the angle of arrival of the received RF signal and the RF axis of the antenna.

4. Demodulating the range code and clock and, in conjunction with the ranging subsystem, continuously providing the two-way phase (time) delay experienced by the range code during round-trip transmission to and from the spacecraft.

5. Demodulating telemetry modulation and providing telemetry subcarrier or telemetry modulation spectrum information.

6. Providing an absolute level measurement of the received signal carrier power.

System noise temperature of the 85-foot antenna receiver system is $55^{\circ}K$. System noise temperature of the 210-foot antenna receiver system is $27^{\circ}K$.[1] These temperatures include the maser preamplifier, receiver, transmission line, and listening feed and presume the antenna is pointed at a "quiet" region of the sky. A summary of receiver characteristics is given in Table 1.

DSIF Antennas. The 85-foot DSIF antenna is a fully steerable polar-mounted paraboloid reflector. It has a gain of 53 db at 2300 MHz. Each axis of the antenna has a two-speed drive. Maximum and minimum angular velocities about the hour angle and declination axes are 0.85 deg/sec and 0.02 deg/sec, respectively. Maximum angular acceleration for the 85-foot dish is 2 deg/sec^2 about either axis.

---

[1] Manned Space Flight Network Augmentation Study for the Apollo Extension System, Part 1, Goddard Space Flight Center, Greenbelt, Maryland.

Table 1. DSIF Receiver Capabilities

	S-band
Nominal center frequency, MHz	2295 ±5
Automatic frequency tracking range	
Strong signal levels, kHz	±67
Threshold signal levels (6-deg phase error), kHz	±2.3
Automatic-phase-control effective noise bandwidth at threshold, Hz	12, 48, or 152 $^{+0}_{-10}$ %
Automatic-phase-control effective noise bandwidth strong signals, Hz	120, 255, or 500 $^{+0}_{-10}$ %
Effective system noise temperature[a]	
Parametric preamplifier, °K	270 ±50
Maser, °K	55 ±10
Threshold carrier level (level below which phase lock cannot be maintained)	
BW = 12 Hz	
Parametric amplifier, dbm	-163.5
Maser amplifier, dbm	-170.4
Maximum frequency tracking rate	
BW = 12 Hz	
Strong signal level (30 deg phase error), cpsps	150
Threshold signal level (6 deg phase error), cpsps	4
Dynamic signal level range, from threshold to:	
Receiver, dbm	-60
Maser or parametric, dbm	-80
Intermediate frequencies	
First, MHz	50
Second, MHz	10
Intermediate frequency amplifier half power bandwidths	
First, MHz	10
Second, MHz	3.33

*Includes receiver, transmission line, feed and antenna pointing at quiet sky.

DSIF COMPONENT PERFORMANCE CHARACTERISTICS

The 210-foot DSIF antenna is a fully steerable altitude/azimuth-mounted paraboloid reflector. It has a gain of 61 db at 2300 MHz. Each axis of the antenna has a two-speed drive. At 0.01 degree angular tracking accuracy, maximum velocity is 0.5 deg/sec and maximum acceleration is 0.2 deg/sec^2. At 0.02 degree angular tracking accuracy, maximum velocity is 0.2 deg/sec and maximum acceleration is 0.1 deg/sec^2.

The performance of the 210-foot altitude/azimuth-mount DSIF antennas (constructed at Goldstone; proposed for Madrid and Canberra) is shown in Table 2. Tracking errors and bias data will be determined upon completion of the antenna installation.

DSIF Transmitter. The DSIF transmitter has a phase modulation capability and transmits range code modulation and command information to the spacecraft. Each transmitter subsystem contains a transmitter synthesizer exciter and a final amplifier. The synthesizer accepts a stable reference signal from a 1-MHz atomic frequency standard and synthesizes RF frequencies.

Output carrier frequency tuning range is approximately ±100 kHz. The transmitter will accept command modulation and/or range code signals and provide the required modulation spectrum at the S-band transmit frequency. Normal power output is presently 10 kw (+70 dbm) at the input to the antenna, continuously variable from +50 dbm to +10 dbm. Transmitter power for the 210-foot antenna system is expected to be increased to 400 kw in the future.

Table 2. 210-Foot Altitude/Azimuth Antenna Performance

Azimuth coverage, degree	± 300 (from SE at Goldstone)
Elevation coverage, degree	5 to 88 (tracking sidereal target) 4.5 to 90.5 (final limits)
Pointing accuracy, degree	0.01 Precision I 0.02 Precision II
Maximum angular rate, degree/second	0.5 (wind ≤ 30 mph)
Maximum acceleration, degree/second	0.2 (wind ≤ 30 mph) Precision I 0.1 Precision II
Servo bandwidth adjustment, Hz	0.01 to 0.2
Gain at 2300 MHz, db	61
Beamwidth at 2300 MHz, deg	≈ 0.1
System temperature, °K*	27 (receive mode)
Antenna temperature, °K	≈ 10
Reflector diameter, ft	210
Reflector F/D ratio	0.4235

*Includes maser amplifier, receiver, transmission line, listening feed, and the antenna pointing at a quiet sky.

EARTH RECEIVING FACILITIES

Manned Space Flight Network

STATION LOCATIONS AND GENERAL CAPABILITIES

Earth Receiving Facilities
Manned Space Flight Network[1]

STATION LOCATIONS AND GENERAL CAPABILITIES

The Manned Space Flight Network supports all manned flights. Its communication format is similar to the DSN.

The Manned Space Flight Network (MSFN) provides tracking, communication, telemetry, and voice transmission in real time between the manned spacecraft and the Mission Control Center. This capability is provided to MSFN stations by: The Unified S-Band System (USBS), a VHF telemetry and voice system, a UHF command system, and by C-Band and S-Band tracking radars. The performance of a typical MSFN station is influenced by the strategic location of the station for mission coverage and the communication between the station and the mission control center.

The present MSFN ground station locations and the facilities at each are shown in Table 1. For the forthcoming Apollo Applications program, these will be augmented by installation of an additional USBS station at Fairbanks, Alaska and the conversion of four presently single USBS stations to dual USBS (Bermuda, Antigua, Corpus Christi, and Guaymus). Data received from spacecraft can be processed, recorded, and transmitted to control centers.

Data processing rates of the USBS stations are 200K bits/sec per USBS receiver, considerably in excess of the 51.2K bits/sec transmission capability of the present Apollo spacecraft. USBS ground station data handling capabilities are shown in Table 2.

The Unified S-Band System. The major system located at MSFN remote sites is the Unified S-Band System (USBS). The USBS was designed to provide doppler extraction, two-way communications, angle tracking and ranging, for the Apollo manned lunar mission. There are several variations in station equipment for the basic USBS system. This includes the single installation (1 transmitter, 3 receivers) and dual installation (2 transmitters, 4 receivers), 30-foot antenna systems, the primary and backup 85-foot antenna systems and the single and dual instrumentation ships. The ranging, doppler extraction and angle tracking functions are similar to those of the Deep Space Network.

---

[1] Manned Space Flight Network Augmentation Study for the Apollo Exterior System, Part 1, Goddard Space Flight Center, Greenbelt, Maryland.

Table 1. MSFN Ground Station System Equipment

EQUIPMENT / STATIONS		CAPE KENNEDY	GRAND BAHAMA	BERMUDA	ANTIGUA	ATLANTIC SHIP	CANARY ISLAND	ASCENSION ISLAND	MADRID	TANANARIVE	INDIAN OCEAN SHIP	CARNARVON	GUAM	CANBERRA	HAWAII	KWAJALEIN	GUAYMAS	CORPUS CHRISTI	ENTRY SHIP 1
UNIFIED S-BAND SYSTEM		D 30'	S 30'	S/D 30'	S/D 30'	D 30'	S 30'	D 30'	D 85'		S 30'	D 30'	D 30'	D 85'	D 30'	D 85'	S 30'	S 30'	S 12'
TRACKING	FPQ-6	X		X	X			X				X							
	FPS-16	X	X	X		X		X			X				X				X
	MPS-26						X												
	TMQ-18							X											
	MISTRAM	X																	
	AZUSA	X																	
	GLOTRAC				X														
	VERLORT			X			X					X			X		X	X	
	USB-RANGING & DOPPLER	X	X		X	X		X	X		X		X	X		X	X	X	
	CAPRI									X									
TELEMETRY	VHF ANTENNA																		
	TLM-18	X																	
	AGAVE			X		X	X			X	X				X		X		
	TEL TRAC	X	X		X		X	X				X	X		X		X	X	
	VHF RECEIVERS	X	X	X	X	X	X	X		X	X	X	X		X		X	X	X
	UNIFIED S-BAND	X	X	X	X	X	X	X	X		X	X	X	X	X	X	X	X	X
ACQUISITION	TEL TRAC	X	X				X					X	X		X		X	X	
	TLM-18	X																	
	AGAVE			X		X	X			X	X				X		X		
	ACQUISITION BUS	X		X	X	X	X	X			X	X			X		X	X	X
	USB ANTENNA	X	X	X	X	X	X	X	X			X	X	X	X	X	X	X	X
A/G VOICE	HF XMTR RCVR	X	X	X	X	X	X	X		X	X	X	X		X		X	X	X
	VHF XMTR/RCVR	X	X	X	X	X	X	X		X	X	X	X		X		X	X	X
	UNIFIED S-BAND	X	X	X	X	X	X	X	X		X	X	X	X	X	X	X	X	X
COMMAND	UHF COMMAND	X		X	X	X	X	X			X	X	X		X		X	X	X
	DIGITAL COMMAND	X		X	X	X	X	X	X		X	X	X	X	X	X	X	X	X
	DRED	X																	
	DRUL		X	X	X										X			X	
	UNIFIED S-BAND	X	X	X	X	X	X	X	X		X	X	X	X	X	X	X	X	X
DATA DECOM	PCM DECOM	X	X	X	X		X	X	X			X	X	X	X	X	X	X	X
	PCM SIMULATOR	X	X	X	X		X	X	X			X	X	X	X	X	X	X	X
	PAM-PDM DECOM	X		X								X			X		X	X	
	FM FM DECOM	X	X	X			X					X			X		X	X	
ON-SITE DATA PROCESSORS	TELEMETRY	X	X	X	X		X	X	X		X	X	X	X	X	X	X	X	
	COMMAND	X	X	X	X		X	X	X		X	X	X	X	X	X	X	X	
RECORDERS	MAG TAPE - DATA	X	X	X	X	X	X	X	X	X	X	X	X	X	X	X	X	X	X
	MAG TAPE - VOICE	X	X	X	X	X	X	X	X		X	X	X	X	X	X	X	X	
	OSCILLOGRAPHIC	X	X	X	X		X	X	X	X	X	X	X	X	X	X	X	X	X
	EVENT	X	X	X	X		X	X	X		X	X	X	X	X		X	X	
	VIDEO	X	X	X	X		X	X	X		X	X	X	X	X	X	X	X	X
CONSOLES AND DISPLAYS	CONSOLES																		
	USB SYSTEM	X	X	X	X	X	X	X	X		X	X	X	X	X	X	X	X	X
	CAPCOM					X	X	X			X	X					X		
	M&O	X	X	X	X	X	X	X	X		X	X	X	X			X		
	FLT DYNAMICS					X					X								
	GROUP DISPLAYS						X	X				X					X		
TELEVISION	MONITOR	X	X	X	X		X	X	X			X	X	X	X	X	X	X	X
	SCAN CONVERTER	X							X					X		X		X	
	USB TELEVISION (GRD XMSN TO MCC-H)	X														X		X	
SPAN	SOLAR RADIO TELESCOPE						X					X				X			
	SOLAR OPTICAL TELESCOPE						X					X							

NOTE:
S = 1 XMTR/2 RCVR
D = 2 XMTR/4 RCVR
S/D = S (uplink) / D (downlink)

In addition to the above listed MSFN Stations, DOD Stations provide some C-band radar tracking support capability for manned and un-manned missions. These stations are: Patrick AFB, GBI, Eleuthera, Pretoria, White Sands, Pt. Arguello, and Eglin AFB.

Table 2. MSFN USBS-Equipped Ground Station Data Handling Capability

Stations	USBS Downlink Receiver/Demod	PCM Demod	Data Processing	Wide-Band Data and TV Tape Recording	**Ground Data Transmission	USBS Uplink
Cape Kennedy (D) 4 Downlink Carriers	200 Kb/Link x 4 = 800 Kb	1 Meg B/System x 3 = 3 Meg B	Word Storage 32 K x 2 = 64 K Transfer Rate 500 K (30 Bit Words) Per Second	1.5 MHz/Chan/System 3 Systems	(1) Chan at 40.8 Kb (1) TV	200 Bps - Info Bit Rate 1000 Bps - Sub Bit Rate
Grand Bahama (S) 3 Downlink Carriers	200 Kb/Link x 3 = 600 Kb	1 Meg B/System x 3 = 3 Meg B			(1) Chan at 40.8 Kb	
Bermuda (S) 3 Downlink Carriers	200 Kb/Link x 3 = 600 Kb	1 Meg B/System x 4 = 4 Meg B			(3) Chan at 2.4 Kb	
Antigua (S) 3 Downlink Carriers	200 Kb/Link x 3 = 600 Kb	1 Meg B/System x 3 = 3 Meg B		1.5 MHz/Chan/System 2 Systems	(3) Chan at 2.4 Kb	
Atlantic Ship (D) 4 Downlink Carriers	200 Kb/Link x 4 = 800 Kb					
Canary Island (S) 3 Downlink Carriers	200 Kb/Link x 3 = 600 Kb				(2) Chan at 2.4 Kb	
Ascension (D) 4 Downlink Carriers	200 Kb/Link x 4 = 800 Kb				(2) Chan at 2.4 Kb	
Madrid (D) 4 Downlink Carriers				1.5 MHz/Chan/System 2 Systems	(3) Chan at 2.4 Kb	
Carnavon (D) 4 Downlink Carriers				1.5 MHz/Chan/System 3 Systems	(2) Chan at 2.4 Kb	
Guam (D) 4 Downlink Carriers				1.5 MHz/Chan/System 2 Systems	(3) Chan at 2.4 Kb	
Pacific Ship (D) 4 Downlink Carriers				1.5 MHz/Chan/System 2 Systems	-	
Canberra (D) 4 Downlink Carriers				1.5 MHz/Chan/System 2 Systems	(3) Chan at 2.4 Kb	
Hawaii (D) 4 Downlink Carriers				1.5 MHz/Chan/System 3 Systems	(3) Chan at 2.4 Kb	
Goldstone (D) 4 Downlink Carriers	200 Kb/Link x 4 = 800 Kb			1.5 MHz/Chan/System 2 Systems	(3) Chan at 2.4 Kb (1) TV	
Guaymas (S) 3 Downlink Carriers	200 Kb/Link x 4 = 800 Kb			1.5 MHz/Chan/System 3 Systems	(2) Chan at 2.4 Kb	
Corpus Christi (S) 3 Downlink Carriers	200 Kb/Link x 3 = 600 Kb			1.5 MHz/Chan/System 3 Systems	(3) Chan at 2.4 Kb	
Entry Ship #1 (S) 3 Downlink Carriers	200 Kb/Link x 3 = 600 Kb			1.5 MHz/Chan/System 2 Systems	-	
Entry Ship #2 (S) 3 Downlink Carriers	200 Kb/Link x 3 = 600 Kb	1 Meg B/System x 3 = 3 Meg B	Word Storage 32 K x 2 = 64 K Transfer Rate 500 K (30 Bit Words) Per Second	1.5 MHz/Chan/System 2 Systems	-	200 Bps - Info Bit Rate 1000 Bps - Sub Bit Rate

*Limiting data transfer from spacecraft to ground station.
**Limiting real-time data transfer to the mission control center.

ANTENNAS, TRANSMITTERS AND RECEIVERS

Parameter values associated with the antennas, transmitters and receivers of the MSFN are given with particular emphasis on the Apollo program.

The antennas, transmitters, and receivers of the Manned Space Flight Network located at the station sites are comprised of the Unified S-Band System (USBS). These components are described below.

Antennas

The 30-foot antenna system receives in the 2270 to 2300 MHz band with a minimum gain of 44.0 db, corresponding to an overall efficiency of 53 percent, including losses of less than 0.5 db. Monopulse sum and error signals of comparable gain are provided to the tracking receiver in this band as well. The feed system receives and transmits only circular polarization with remote switching capability. Receiving and transmitting circuits are switched simultaneously, with the primary data as well as the monopulse tracking signals, having the same polarization sense as the transmitted signals.

The 85-foot antenna systems are electrically similar to those of the 30-foot antenna. The primary difference between the two systems is that the 85-foot antenna developes gains of 50.5 db receiving and 50.0 db transmitting and better sidelobe control is possible.

Acquisition aid antennas are mounted on both the 30-foot and the 85-foot antennas. For the 30-foot antenna the acquisition aid antenna is a 42-inch diameter paraboloidal dish having a beamwidth of approximately 10 degrees and a minimum gain of 22 db over the receiving band of 2270-2300 MHz.

Transmitter

The MSFN transmitter provides a maximum power of 20 kilowatts.

Parametric Amplifiers and System Noise Temperature

Parametric amplifiers are used to provide a low system noise temperature for both the main tracking and acquisition antennas. Identical units are used to simplify maintenance and allow substitution in case of an emergency. A noise temperature of 170°K is achieved without cooling.

Receiver Exciter

The receiver portion of the USB system has the ability to process either 4 (dual configuration) or 3 (single configuration) rf carriers simultaneously. These are:

1) 2272.5 MHz from the CSM (command and service module of Apollo Spacecraft).

2) 2277.5 MHz from the S-IVB (third stage engine).

Table 1. LEM Down-Link MSFN S-Band Transmission Summary

2282.5 MHz Carrier Combination	Information	Modulation Techniques	Subcarrier Frequency	Carrier Phase Deviation
1	Carrier Voice 51.2 kbps TM	 FM/PM PCM/PM/PM	 1.25 MHz 1.024 MHz	 0.7 Radians 1.3 Radians
2	Carrier PRN Voice 51.2 kbps TM	 PM on Carrier FM/PM PCM/PM/PM	 1.25 MHz 1.024 MHz	 0.2 Radians* 0.7 Radians 1.3 Radians
3	Carrier 1.6 kbps TM	 PCM/PM/PM	 1.024 MHz	 1.3 Radians
4	Carrier BU Voice 1.6 kbps TM	 PM on Carrier PCM/PM/PM	 1.024 MHz	 0.8 Radians 1.3 Radians
5	Carrier Backup Voice	 PM (24 db clipping)		 0.8 Radians
6	Carrier Key	 AM/PM	 512 KHz	 1.4 Radians
7 (Lunar Stay Mode)	Carrier Voice/Biomed 1.6 kbps TM	 FM/PM PCM/PM/PM	 1.25 MHz 1.024 MHz	 1.3 Radians 0.7 Radians
8	Carrier Voice/EMU/ Biomed 51.2 kbps TM	 PM on Carrier (no clipping) PCM/PM/PM		 TBD
				Carrier Deviation Ratio
9	Voice/EMU/ Biomed TM	FM/FM PCM/PM/FM	1.25 MHz 1.024 MHz	0.17 0.37
10	TV Voice/EMU/ Biomed 1.6 or 51.2	FM at Baseband FM/FM/FM PCM/PM/FM	 1.25 MHz 1.024 MHz	2.0 0.17 0.37

*Down PRN ranging phase deviation is to be set with up-voice and up ranging modulation and with a high signal-to-noise ratio in the turn around channel.

ANTENNAS, TRANSMITTERS AND RECEIVERS

3) 2282.5 MHz from the LEM (lunar excursion module of the Apollo Spacecraft) or the S-IVB.

4) 2287.5 MHz from the CSM.

The RF carriers are modulated in the spacecraft in accordance with Tables 1, 2, and 3. The USBS demodulates these carriers.

The transmitter section of the USBS has the ability to transmit two RF carriers, one at 2106.4 MHz to the CSM and the other at 2101.8 MHz to the LEM. The information channels and coding schemes for each of these links is shown in Tables 4 and 5.

Table 2. CMS to MSFN S-Band Transmission Combination Summary (FM Modes)

2272.5 MHz Carrier Combination	Information	Modulation Technique	Subcarrier Frequency
1	Playback Voice at 1:1	FM at Baseband	
	Playback CSM		
	51.2 kbps TM at 1:1	PCM/PM/FM	1024 KHz
	Scientific Data		
	Playback at 1:1	FM/FM	95 KHz
		FM/FM	125 KHz
		FM/FM	165 KHz
2	Playback Voice at 32:1	FM at Baseband	
	Playback CSM		
	1.6 kbps TM at 32:1	PCM/PM/FM	1024 KHz
	Scientific Data		
	Playback at 32:1	FM/FM	95 KHz
		FM/FM	125 KHz
		FM/FM	165 KHz
3	Playback LEM	FM at Baseband	
	1.6 kbps		
	Split Phase TM at 32:1		
4	Television	FM at Baseband	
5	Real-Time		
	Scientific Data	FM/FM	95 KHz
		FM/FM	125 KHz
		FM/FM	165 KHz

ANTENNAS, TRANSMITTERS AND RECEIVERS

Table 3. CSM to MSFN S-Band Transmission Combination Summary (PM Mode)

2287.5 MHz Carrier Combination	Information	Modulation Technique	Subcarrier Frequency
1	Carrier		
	Voice	FM/PM	1.25 MHz
	51.2 kbps TM	PCM/PM/PM	1.024 MHz
2	Carrier		
	PRN	PM On Carrier	
	Voice	FM/PM	1.25 MHz
	51.2 kbps	PCM/PM/PM	1.024 MHz
3	Carrier		
	PRN	PM On Carrier	
	Voice	FM/PM	1.25 MHz
	1.6 kbps	PCM/PM/PM	1.024 MHz
4	Carrier		
	Voice	FM/PM	1.25 MHz
	1.6 kbps	PCM/PM/PM	1.024 MHz
5	Carrier		
	1.6 kbps	PCM/PM/PM	1.024 MHz
6	Carrier		
	Key	AM/PM	512 KHz
7	Carrier		
	PRN	PM On Carrier	
8	Carrier		
	Backup Voice	PM On Carrier	
	1.6 kbps TM	PCM/PM/PM	1.024 MHz
9	Carrier		
	PRN	PM On Carrier	
	1.6 kbps TM	PCM/PM/PM	1.024 MHz

Table 4. LEM Up-Link S-Band Transmission Combinations Summary

Combination	Information	Modulation Technique	Subcarrier Frequency	Carrier Phase Deviation
1	Carrier, PRN	PM on Carrier	-	0.37 Radians
2	Carrier, Voice	FM/PM	30 KHz	1.4 Radians
3	Carrier			
	PRN	PM on Carrier	-	0.37 Radians
	Voice	FM/PM	30 KHz	1.4 Radians

Table 5. MSFN to CSM S-Band Transmission Combinations Summary

2106.4 MHz Carrier Combination	Information	Modulation Technique	Subcarrier Frequency
1	Carrier, PRN	PM On Carrier	-
2	Carrier, Voice	FM/PM	30 KHz
3	Carrier, Up-Data	FM/PM	70 KHz
4	Carrier		
	PRN	PM On Carrier	-
	Voice	FM/PM	30 KHz
5	Carrier		
	PRN	PM On Carrier	-
	Up-Data	FM/PM	70 KHz
6	Carrier		
	PRN	PM On Carrier	-
	Voice	FM/PM	30 KHz
	Up-Data	FM/PM	70 KHz
7	Carrier		
	Voice	FM/PM	30 KHz
	Up-Data	FM/PM	70 KHz
8	Carrier		
	Voice Backup	FM/PM	70 KHz

OTHER MSFN FACILITIES

The UHF system available at some USBS stations is described and a block diagram of a typical MSFN station is given.

In addition to the USBS, 80 percent of the MSFN stations have VHF telemetry and voice capability. The VHF telemetry system supplements the USBS in monitoring spacecraft and astronaut performance. The transfer of commands from ground stations to spacecraft is accomplished by an USBS or an UHF digital command system. C-Band and S-Band radars are available at approximately 95 percent of all MSFN stations. A typical MSFN remote site systems block diagram is shown in the figure. Sites which do not have flight controllers will not have a memory character vector generator, a console computer, interface adapter, flight control consoles.

Air-to-ground voice capability is provided on both VHF and Unified S-Band. Magnetic recorders, voice, and chart recorders are available at each site to record PCM telemetry, TV, voice and analog event status information. TV monitors are available to display only slow scan TV from the spacecraft.

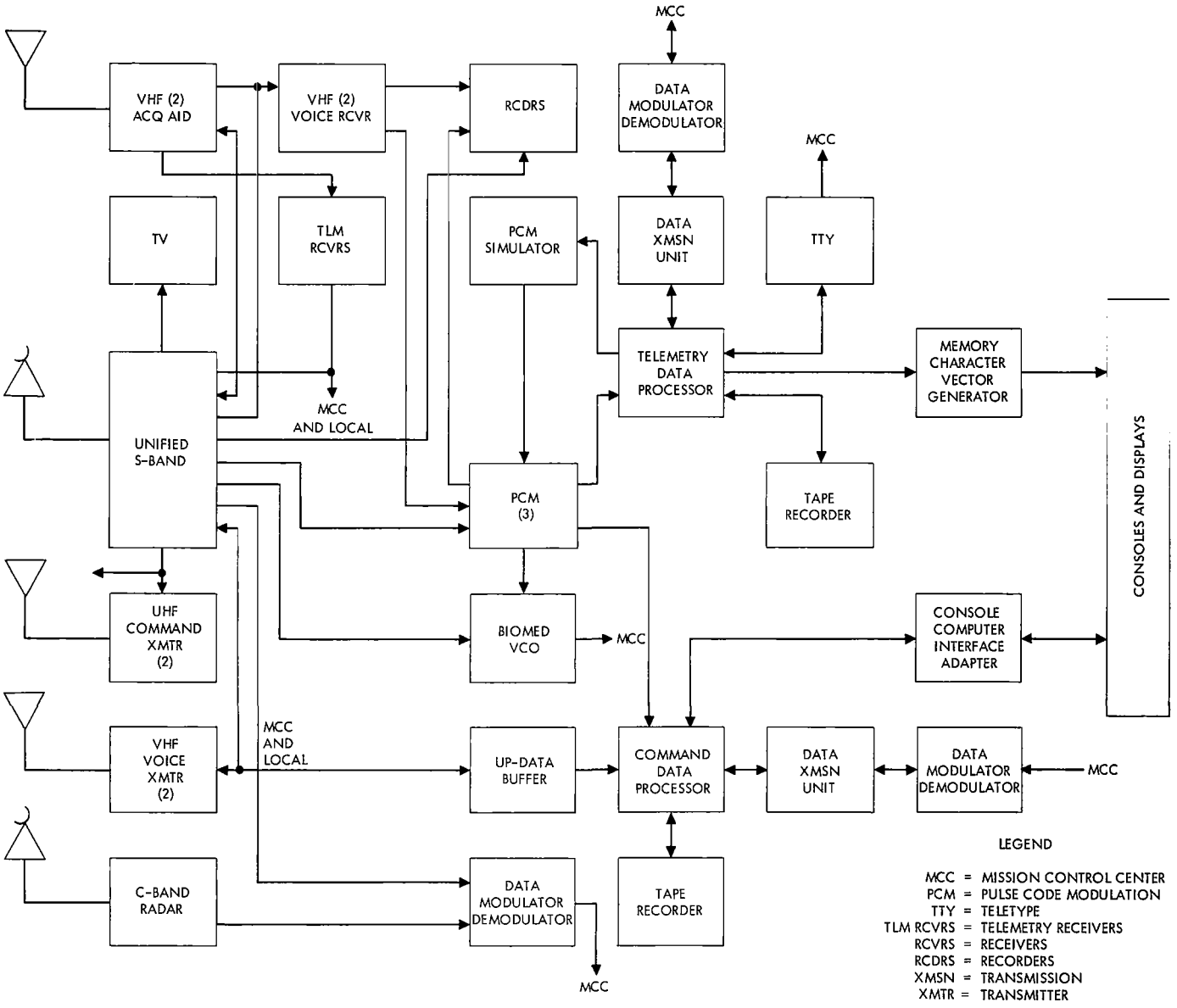

Typical MSFN Remote Site Block Diagram

EARTH RECEIVING FACILITIES

Satellite Tracking and Data Acquisition Network (STADAN)

Earth Receiving Facilities
The Satellite Tracking and Data Acquisition Network (STADAN)[1]

STADAN STATION LOCATION AND GENERAL CAPABILITIES

The STADAN Network is widely used for near earth unmanned satellites.

The primary purpose of the STADAN is to receive data from scientific satellites and to produce tracking information for orbit computation. The following material is presented to give an overall description of the existing network capabilities. Most of the equipment in the STADAN has been designed for use by many programs, with emphasis on quick adaptability to the differing requirements of several simultaneously-orbiting spacecraft. Most programs do not require data from all STADAN stations, so the specific capabilities of each station have been tailored to differing levels of performance. The result is that no two stations are identical in terms of either equipment or data handling capacity.

The STADAN consists of three major systems: the Data Acquisition Facilities, Minitrack, and the Goddard Range and Range Rate System. The first major functional system, the Data Acquisition Facilities (DAF), is equipped with multi-frequency, high gain antennas and its capability of handling large quantities of data at high rates exceeds that of the standard Minitrack systems.

The second major functional system, Minitrack, has been used to track all U.S. satellites which have suitable beacons, since the beginning of the space program. In addition to its tracking functions, the Minitrack system has the facilities for receiving telemetry data in the 136- to 137-MHz and 400- to 401-MHz bands.

The third major system of the STADAN is the transportable Range and Range Rate Tracking system which complements the Minitrack network by providing improved tracking data for space probes, launch vehicles, and satellites in highly elliptical orbits.

A particular station may have any combination of the above systems, and the specific configuration of the system will vary depending on the cumulate requirements placed on the station. STADAN sites are shown in the figure. The STADAN facilities are listed in the table and described in the following topics.

---

[1] Satellite Tracking and Data Acquisition Facilities Report (STADAN), NASA TMX 55026, Goddard Spaceflight Center, Greenbelt, Maryland, June 1964.

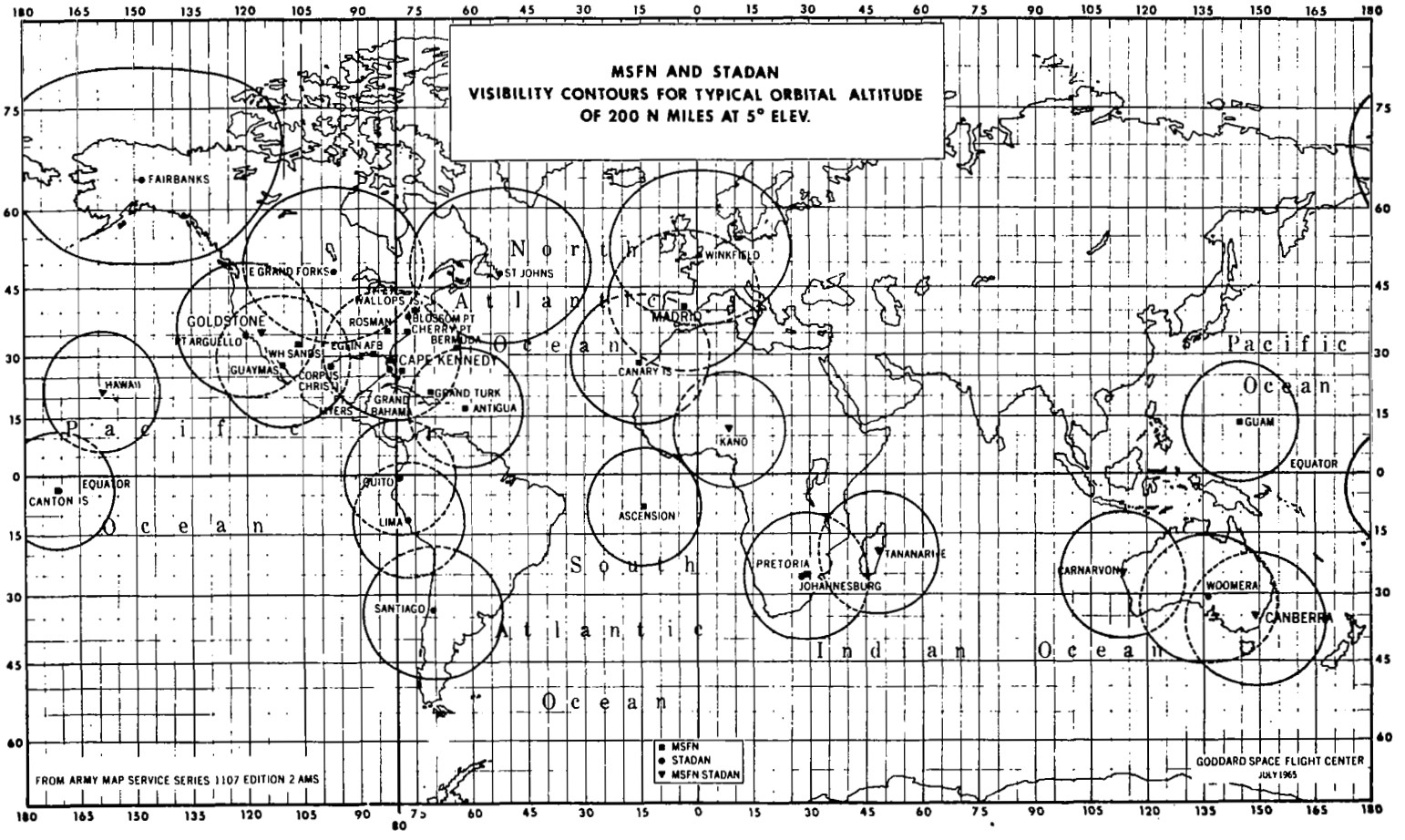

MSFN and STADAN Visibility Contours for Typical Orbital Altitude of 200 nm at 5° Elevation

STADAN Ground Stations System Equipment

		FAIRBANKS	GOLDSTONE (MOJAVE)	BLOSSOM PT.	CANBERRA	CARNARVON	COLLEGE	E. GRAND FORKS	FT. MYERS	JOHANNESBURG	LIMA	QUITO	ROSMAN	ST. JOHNS	SANTIAGO	TANANARIVE	WINKFIELD	WOOMERA	KANO	KAUAI
TRACKING SYSTEMS	MINITRACK	-	1	1	-	-	1	1	1	1	1	1	-	1	1	-	1	1	-	-
	GR&RR	1	-	-	-	1	-	-	-	-	-	-	1	-	1	1	-	-	-	-
TELEMETRY ANTENNAS	85 FT DISH AUTOTRACK	1	-	-	1	-	-	-	-	-	-	-	2	-	-	-	-	-	-	-
	40 FT DISH AUTOTRACK	1	1	-	-	-	-	-	-	1	-	1	-	-	1	1	-	-	-	-
	136 MHz SATAN AUTOTRACK	2	1	1	2	-	-	-	1	1	1	1	2	-	2	2	1	-	-	-
	136 MHz YAGI MANUAL	-	1	-	-	-	2	1	2	2	2	1	-	2	1	-	2	2	1	1
COMPUTERS	PB-250	1	1	-	1	-	-	-	-	1	-	1	1	-	1	-	-	-	-	-
TELEMETRY RECEIVERS	SPECIAL PURPOSE	2	-	-	-	-	2	-	2	-	-	-	2	-	-	2	-	-	2	2
	DIVERSITY TELEMETRY	10	7	2	8	-	-	-	4	7	3	7	12	-	7	7	4	2	-	-
	MOD I TELEMETRY	-	2	2	-	-	2	2	2	2	3	2	5	2	-	-	2	2	-	-
	PHASE DEMODULATOR	9	6	3	7	-	1	1	4	7	3	7	12	-	7	7	4	3	1	1
PCM DEMODULATORS	200 kbps CAPACITY	1	-	-	-	-	-	-	-	1	-	1	1	-	1	-	-	-	-	-
	320 kbps CAPACITY	-	1	1	-	-	1	1	1	1	1	1	-	1	1	-	1	1	-	-
	1 MEG bps CAPACITY	-	2	-	2	-	-	-	1	-	1	-	1	-	-	2	1	-	-	-
RECORDERS	8 CHANNEL TAPE	8	6	5	6	-	3	2	6	8	2	8	10	2	8	7	6	4	2	2
	8 CHANNEL PAPER	5	4	2	6	-	3	3	4	4	2	7	8	2	5	7	3	2	1	1
	6 CHANNEL OPTICAL	1	1	1	1	-	1	1	1	1	1	2	2	1	2	2	1	1	-	-
VHF COMMAND	ENCODER CONSOLE	1	1	1	1	-	1	1	1	1	1	1	1	1	1	1	1	1	1	1
	250 WATT AM	-	1	1	-	-	2	1	2	2	2	2	-	2	2	-	2	2	1	1
	2.5 KW AM	4	2	2	2	-	-	-	2	-	2	2	4	-	-	4	2	-	-	-
	5.0 KW AM	2	-	-	2	-	-	-	-	2	-	2	2	-	2	-	-	-	-	-
	148 MHz 23 DB ANTENNA	2	1	1	2	-	-	-	1	1	1	1	2	-	1	2	1	-	-	-
	148 MHz 10 DB ANTENNA	1	1	1	-	-	1	1	2	1	1	1	2	2	1	-	2	1	1	1

NOTES:

1. Autotrack receivers and programmers are provided as part of the basic telemetry antennas as appropriate.
2. Diversity telemetry receiver maximum bandwidth is 3 MHz i-f (1.5 MHz baseband).
3. MOD I telemetry receiver maximum bandwidth is 1 MHz i-f (500 KHz baseband).
4. Phase demodulator maximum bandwidth is 400 KHz i-f (200 KHz baseband). New units having a 3 MHz i-f bandwidth (1 MHz baseband) are being developed, but quantities per station are not finalized.
5. Tape recorder bandwidth - 250 KHz.
6. Paper recorder bandwidth - 100 Hz.
7. Optical recorder bandwidth - 4800 Hz.
8. Transmitter response - PCM/AM/AM to 120 Hz MOD rate.
9. Special purpose receivers have various plug-in bandwidth modules with a maximum bandwidth of 1 MHz.

MINITRACK FACILITIES

Parameter values for the Minitrack transmitters, receivers, and antennas are given.

The Minitrack facility comprises a system of ground stations, located throughout the world, which provides command and telemetry reception of satellites and space probes and tracking of satellites. The Minitrack system was designed to provide orbital information on satellites with a minimum lifetime of many days. Minitrack determines orbits by a series of angle and time observations. Spacecraft with highly eccentric orbits do not lend themselves well to tracking by this system since they have regions of slow angular motion.

Tracking Function. Each Minitrack station measures angular position versus time as the transmitting satellite passes through the beam of its receiving antennas. This is done by phase comparison of received signals from four antennas. One pair, separated a known distance, along an East-West base line and the other pair separated on a North-South base. Five other antennas are used to resolve angular measurement ambiguities.

The Minitrack tracking receiver is a seven-channel triple-conversion superheterodyne tunable over the 136- to 137-MHz range in one-kHz steps. Six channels carry satellite tracking information and one is used for aircraft calibration of the system.

Data Acquisition Function. Satellite telemetry is processed through a 136-MHz receiving system separate from that used for tracking. The data acquisition antenna consists of a Nine-Yagi antenna array having a gain of 19.2 db. Eight of the Yagis are used for telemetry reception and a centrally located Yagi is used to transmit command signals to the satellites.

The antenna scans through a 740-degree sector in azimuth and a ±80 degrees from vertical at 1 RPM. The polarization is either linear or circular.

Three stations in the southern hemisphere use sixteen Yagi arrays. These are similar to the eight-element system, but have a gain of 22.4 db.

The telemetry receiver provides AM and FM detection and has a total of five prediction bandwidths from 10 KHz to 1 MHz.

The receiver system noise figure at about 2.5 to 3.5 db.

A 200-watt AM modulated command transmitter is used. It may be operated over the frequency range from 108 to 152 MHz.

THE DATA ACQUISITION FACILITY (DAF)

The parameter values for the DAF transmitters, receivers and antennas are given.

For data rates in excess of the Minitrack capabilities, the Data Acquisition Facility (DAF) network utilizes 40-foot and 85-foot parabolic receiving antennas. Presently, 40-foot DAF antennas are colocated with Minitrack facilities at Santiago, Chile; Quito, Equador; and Johannesberg, South Africa. Two 85-foot DAF antennas are located at Fairbanks, Alaska; two at Rosman, North Carolina; and one at Canberra, Australia.

Eighty-Five Foot Antenna Installation

The 85-foot altitude azimuth-mounted parabolic antennas are capable of tracking at rates from 0 to 3 degrees/second and accelerations to 5 degrees/second/second. Pointing accuracy is ±2 minutes of arc. The antenna has five operational modes: it will automatically track on a satellite signal; it can be driven by teletype input, manually operated, slaved to an acquisition antenna, or it can be operated in various search modes for initial acquisition.

The antenna feed has been equipped to provide autotrack capability on 136, 400 and 1700 MHz and a telemetry feed for 235 MHz (in support of the TIROS weather satellite). It is a monopulse system employing three feeds. The polarization is either linear or circular.

The installation provides tracking receivers for the 1700 and 136 MHz bands. For tracking at 400 MHz, down conversion to 136 MHz is necessary. Telemetry reception is provided at 400 MHz, and 136 MHz.

Forty Foot Antenna Installation

The 40-foot altitude azimuth-mounted parabolic antennas are capable of tracking at rates from 0.005 degree/second to 5 degrees/second and at accelerations up to 5 degrees/second/second. The antenna pointing accuracy is ±60 seconds of arc. The antenna has five operational modes: automatic tracking, programmed drive, manually operated, slaved to an acquisition antenna, and various scan modes for initial acquisition.

The antenna feed system provides automatic tracking at 136 MHz and 400 MHz. Four polarizations are provided for auto tracking: two orthogonal linear and two orthogonal circular. For telemetry reception, two orthogonal polarizations are provided simultaneously, either linear or circular.

Tracking receivers are provided at 400 MHz and 136 MHz.

Telemetry receivers are provided at 136 MHz and 400 MHz.

All the 85-foot and 40-foot antenna DAF locations are equipped with 5 kw (3 kw at the 12-db antenna) command transmitters operating in the 120 to 155 MHz frequency range. The command antennas are selectable polarization disk-on-rod types, collimated with the main receiving antennas.

GODDARD RANGE AND RANGE-RATE SYSTEM

The parameters of the GR&RR system are given. The accuracy expected is ±15 meters in range and ±0.1 meter/second in range rate.

The range and range-rate system functions as a high-precision spacecraft tracking system capable of accurately determining the range and radial velocity of a spacecraft from near-Earth orbits out to cislunar distances. The necessity for such a system arises from the increasingly demanding requirements of spacecraft tracking.

This system measures the phase difference between the transmitted and received cw signal. A spacecraft transponder is necessary. This phase difference can be converted to the range and velocity of the satellite being tracked.

Each range and range rate station employs two distinct systems, an S-band system and a VHF system. For use with the S-band system, a three-channel ranging transponder is installed in the satellite. This permits tracking computations from data supplied by a single ranging station, or computations from data supplied simultaneously by a complex of two or three stations. The VHF system is used primarily for acquisition, but is also used for ranging when the spacecraft cannot carry the S-band transponder. In this case, a VHF transponder will be used which functions as a command receiver, telemetry transmitter, and single channel ranging transponder.

The systems are transportable. A typical range and range-rate station consists of one van containing receiving equipment, one van containing transmitting equipment, two transportable automatic tracking antenna systems, two transportable diesel generators, and simple fixed antennas as required for communications and WWV reception.

The S-band transmit receive system transmits ranging signals at one of three frequencies in the 2271-MHz range, and receives the resultant signals from the spacecraft at a frequency of 1705 MHz. The S-band antenna system is an automatic tracking type, with separate parabolic reflectors for transmitting and receiving. These antennas have gains of 35 and 33 db, respectively. The transmitted power is either one or ten kilowatts.

The VHF transmit-receive system transmits ranging signals to the spacecraft at a frequency of 148 MHz, and receives the resulting signals from the spacecraft at a frequency of 136 MHz. A single slotted antenna array is used for both transmitting and receiving. This antenna has a gain of 19 db. The transmitted power is either one kilowatt or ten kilowatts.

The range, range rate, and angular accuracies for the Goddard Range and Range Rate system are shown in the table.

Goddard Range and Range Rate Accuracies

	S-Band	VHF
Range	15 meters	50 meters
Range Rate	0.1 meter/sec	1.0 meter/sec
Angle	0.1 degree	1.0 degree

EARTH RECEIVING FACILITIES

Optical Receiving Site Considerations

Earth Receiving Facilities
Optical Receiving Site Considerations

INTRODUCTION

Basic considerations for optical sites are noted.

Since optical receiving facilities are still in the conceptual design stage, this section limits itself to exploring the natural constraints which determine their location and performance. A brief survey of the locations, elevations, and relevant characteristics of existing astronomical observatories which might be adaptable to noncoherent optical reception is also included.

The natural constraints which determine receiver site location and effectiveness fall into two categories: (1) Those associated with the geometric restrictions imposed by a maximum signal path zenith angle, and (2) those associated with weather conditions. Geometric constraints on geographic location are twofold. The first constraint determines the maximum separation of the sites on longitude (hence the minimum number of sites). The second sets limitations on their latitudes for communicating with a spacecraft in the ecliptic plane. A parameter that is not simply geometric in origin but which is fundamental to determining both these constraints is the maximum zenith angle of the transmission path through the atmosphere.

GEOMETRIC CONSIDERATIONS

A simplified atmospheric model and a geometric model level to the requirement of 3 or 4 stations required for a continuous communication network.

A first estimate of the number of earth stations needed for continuous communications with a deep space probe can be made by assuming: (1) perfect weather conditions, and (2) the maximum zenith angle at which observation is possible considering atmospheric losses. This maximum zenith angle is imposed by propagation effects other than steady atmospheric refraction (and this effect is relatively small and self-correcting as seen in Table 1).[1] One source has quoted 45 to 60 degrees as a limiting zenith angle, θ_{max}, for optical frequencies compared with 80 to 85 degrees for radar frequencies.[2] The value of the critical zenith angle depends on communication system parameters and the altitude of the receiving site. For a given wavelength, ϕ_{max} depends on the sensitivity of the communication system to progressively more severe propagation degradation of the signal incurred by increasing its pathlength through the atmosphere. The critical zenith angle is also a function of wavelength since the severity of propagation effects is wavelength dependent. These propagation effects, include random beam steering due to refractive description of the entire beam, random image dancing in the receiver image plane due to variations on wavefront angle of arrival, scintillation or random intensity variations, and random polarization changes.

For a ground-based station in a direct spacecraft-to-Earth link, angular coverage must include, in general, the ancient zodiac, a strip ±8-1/2 degrees about the ecliptic within which lie all of the major planets except Pluto. Since the earth is inclined at an angle of 23-1/2 degrees to the ecliptic, the total declination angle to be covered is ±32 degrees, and ground stations must be located within 50 degrees of the equator. The normal to the receiving aperture typically is normal to the axis of the earth. For M stations evenly spaced in longitude around the earth covering a declination band ±D and a longitudinal arc $2\pi/M$, the maximum beam excursion from the normal is ψ, where

$$\cos \psi = D \cos (\pi/M)$$

Values of ψ are given in Table 2 for the maximum declination angle, D = 32 degrees and for various M. The maximum zenith angle is then equal to the latitude plus ψ but not to exceed 90 degrees. From the table it is evident that three stations represents the practical minimum and there is little incremental improvement for additional stations above four. Four or more stations may be desirable, however, to limit atmospheric losses at minimum elevation angles. For the same reasons the stations should be located as near the equator as possible.

---

[1] Amateur Astronomer's Handbook, J.B. Sedgewick, London, Faber and Faber, Limited.

[2] Deep Space Laser Acquisition and Tracking Study, Northrop Space Laboratories, Report on NASA Contract NAS 9-2769, November 1964.

Table 1. Refraction Angle Versus Apparent Zenith Angle*

Apparent Zenith Angle (degrees)	Refraction Angle (minutes and seconds of arc)	Apparent Zenith Angle (degrees)	Refraction Angle (minutes and seconds of arc)
0	0 0.0	70	2 35.7
5	0 5.0	75	3 30.0
10	0 10.1	80	5 13.1
15	0 15.3	81	5 46.0
20	0 20.8	82	6 26.0
25	0 26.7	83	7 15.0
30	0 33.0	84	8 19.0
35	0 35.7	85	9 40.0
40	0 47.9	86	11 31.0
45	0 57.1	87	14 7.0
50	1 8.0	88	17 55.0
55	1 21.4	89	23 53.0
60	1 38.7	90	33 51.0
65	2 1.9		

Table 2. Maximum Angular Excursion of Beam from Normal for M Ground Stations

Number of Stations, M	Maximum Excursion Angle, ψ (degrees)
2	90
3	64.9
4	53.2
5	46.7
6	42.7
.	.
.	.
∞	32

*Apparent zenith angle of the beam traversing the atmosphere is its angle direction with respect to the zenith at its point of origin or termination within the atmosphere.

WORLD WIDE WEATHER CONSIDERATIONS

General conclusions on weather obscuration may be drawn from worldwide weather maps but specific sites must provide weather data before best sites may be selected for optical communications.

The vital weather condition for laser communication is cloud cover. It is justifiable to assume that obstruction of the line-of-sight signal path to a receiver by virtually any cloud precludes reception by the obscured site. Two types of receiver networks will be discussed.

In the first network to be considered, only one receiver is in the transmitted beam at any given time. Communication is passed to the next site in the network by a reorientation of the transmitted beam when the signal path zenith angle exceeds the aforementioned critical value. In this case the measure of effectiveness of the receiver site is the probability that the sky be essentially cloud free (fractional cloud cover* < 0.1 is the usual criterion). Significant fractional cloud cover would preclude continuous communication by intermittently obscuring the receiver site during its observation period. It is presumed that this erratic reception would not be acceptable in an operational communication system.

In the second type receiver network, more than one receiver may be in the transmitted beam at the same time. The receivers are therefore in the same general geographic area and possibly subject to similar cloud cover conditions. They are, however, separated (within the constraints of the transmitted beam diameter) sufficiently that a local pattern of cloud cover which obscures one receiver site will not necessarily obscure the other(s). Thus, reception may be continued even in the presence of broken clouds.

Cloud cover decreases in both extent and frequency with altitude. Hence, considerable benefits may be accrued by locating optical receiver sites at higher elevations whenever possible. In general, a specified extent and frequency of cloud cover occurs at higher altitudes nearer the equator. Both these general features are borne out in the charts of Figure A through D.[1] They show for the Northern Hemisphere altitudes for which the probabilities of a clear sky (less than 0.1 fractional cloud cover) are 0.95 and 0.60. Charts for the best and worst months are included to illustrate the strong seasonal variation. These charts are internally consistent and agree with the limited quantitative data available. It may be inferred from these charts that to assure greater than 0.95 probability of no cloud interference over the year for a single site within the critical latitude zone $L \leq 37$ degrees would require an airborne observer since altitudes required vary from 35 K to 45 K feet depending on season and site location. If one can be resigned

---

*Fractional cloud cover is the ratio of the solid angle subtended by cloud at an observer to 4π steradians, the angle subtended by the entire celestial dome.

[1]Estimates of Altitudes with Specified Probabilities of Being Above All Clouds, Irving Soloman, Technical Report 159, Air Weather Service, United States Air Force, 1961

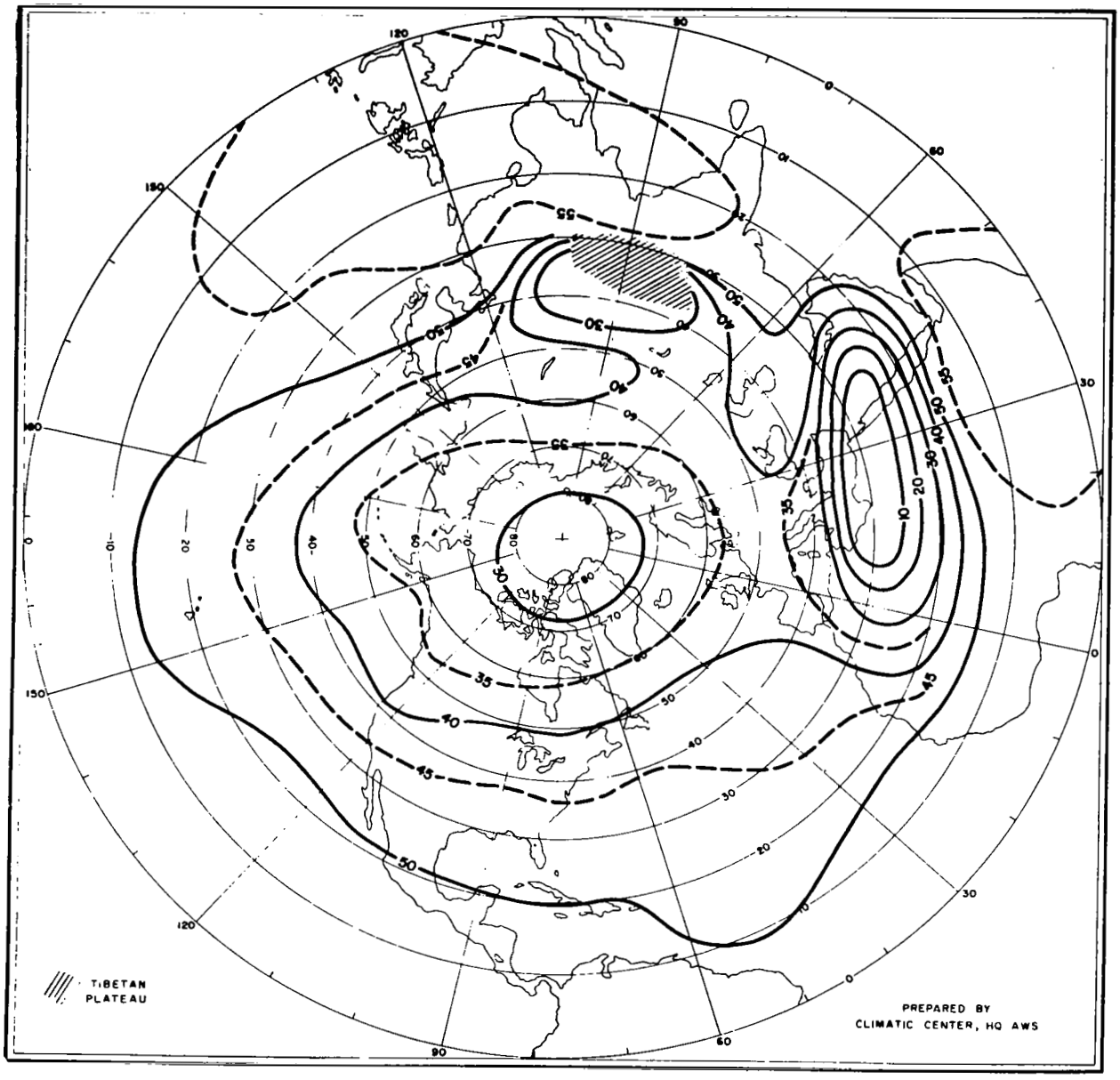

Figure A. Altitudes (in Thousands of Feet Above Mean Sea Level) Above Which There is 95 Percent Probability of Having 1/10 Sky Cover, July

WORLD WIDE WEATHER CONSIDERATIONS

to a clear sky probability of 0.60 for a single site and the use of redundant sites the prospects are brighter. The relative suitability of various ground level site locations is indicated by Figures E and F which show mean fractional cloud cover for best and worst months.[2]

Suppose instead of the minimum of three sites spaced 120 degrees apart in longitude there are six spaced 60 degrees apart. Then the spacecraft is always observable by at least two sites from a geometric standpoint. There is clearly a point of diminishing returns in this procedure since the utility of redundant sites depends on weather conditions at one site being independent from those at the adjacent sites and upon the transmitter beamwidth covering both sites. Assuming that this is the case, the probability of at least one of n sites being clear may be determined from specified minimum clear sky probabilities. Alternately, given a threshold probability for satisfactory operation and prespecified probabilities for a number of locations, the number of sites required to meet the threshold. If $P_i(C)$ is the clear sky probability at site i, the probability of obscuration is $P_i(O) = 1 - P_i(C)$. The probability that all n sites having independent probabilities of clear sky $P_i(C)$ will be obscured is

$$P(O) = \prod_n P_i(O)$$

Hence, the probability that all n will not be obscured, i.e., that at least one of the n will be clear, is

$$P(C) = 1 - \prod_n P_i(O)$$

If the sites are twofold redundant and the two sites in a geometric position to receive have $P_1(C) = 0.6$ and $P_2(C) = 0.7$, then the probability that at least one of the sites will be clear is $P_L = 0.88$. Figure G gives the probability of at least one clear site as a function of the number of sites in a geometric position to receive, with the geometric mean probability of a clear site $P_m(C) = \left[\prod_n P_i(C) \right]^{1/n}$ as a parameter.

In the foregoing discussion we have considered only the situation when there is virtually no cloud (i.e., < 0.1 fractional cloud cover) at the receiver. In the case where more than one ground receiver site is simultaneously in the transmitter field of view, it is possible to receive when there is partial cloud cover. In this case one or more of the receivers may be totally obscured. If the mean probability of a cloud free line of sight path over the range of zenith angles $\phi < \phi_{max}$ were known for each receiver, the effect of adding successive redundant receivers on the probability that at least one will be unobscured could be determined in an identical manner to the first case. Models have been constructed for determining the probability of a cloud free line of sight as a function of zenith angle from observations of cloud cover,

[2] Handbook of Meteorology, Berry, Bolling, and Beers, McGraw-Hill Book Company, Inc., New York 1945

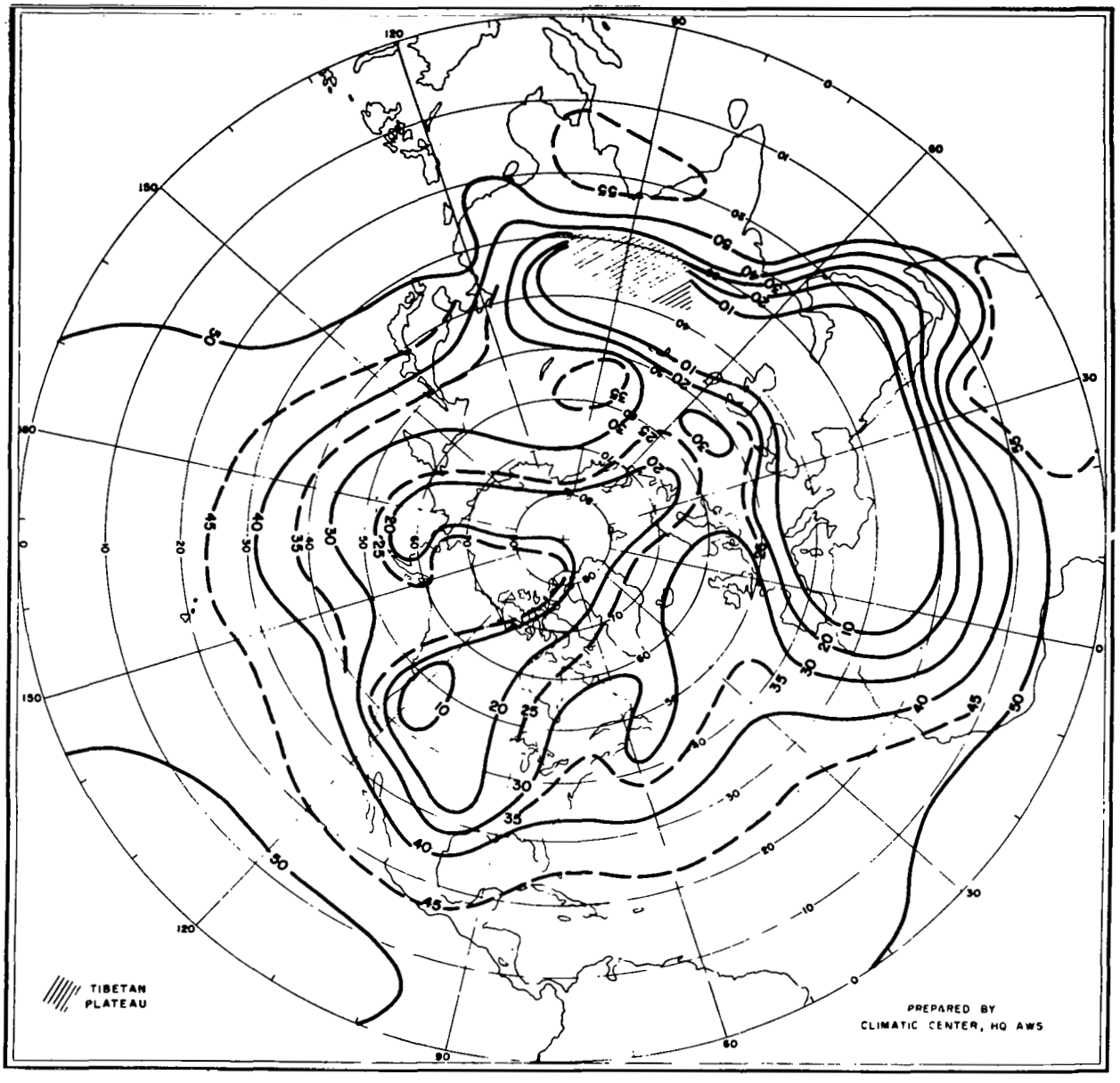

Figure B. Altitudes (in Thousands of Feet Above Mean Sea Level) Above Which There is 60 Percent Probability of Having 1/10 Sky Cover, July

WORLD WIDE WEATHER CONSIDERATIONS

percent of possible sunshine, and estimates of the width, thickness and spacing of clouds.[3,4] However, sufficiently extensive and accurate observations of these quantities are not available at the present time to permit accurate evaluation of the multiple receiver case.

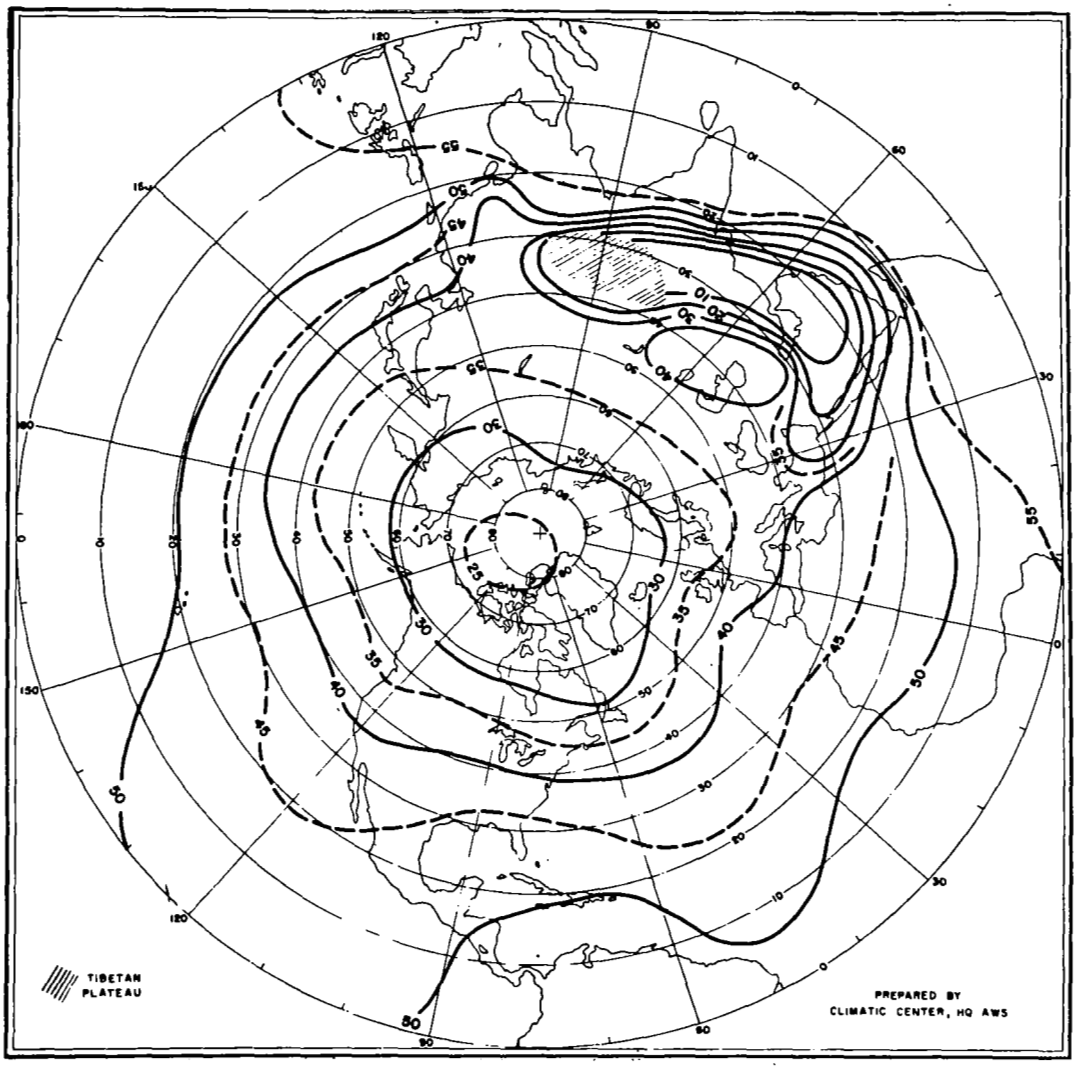

Figure C. Altitudes (in Thousands of Feet Above Mean Sea Level) Above which there is 95 Percent Probability of Having 1/10 Sky Cover, October

[3] Estimating Mean Cloud and Climatological Probability of Cloud-Free Line of Sight, Technical Report 186, Air Weather Service, United States Air Force, 1965.

[4] Estimating the Probability of Clear Lines of Sight from Sunshine and Cloud Cover Observations, Iver A. Lund, Journal of Applied Meteorology, Volume 4, Number 6, December 1965, pp. 714-722.

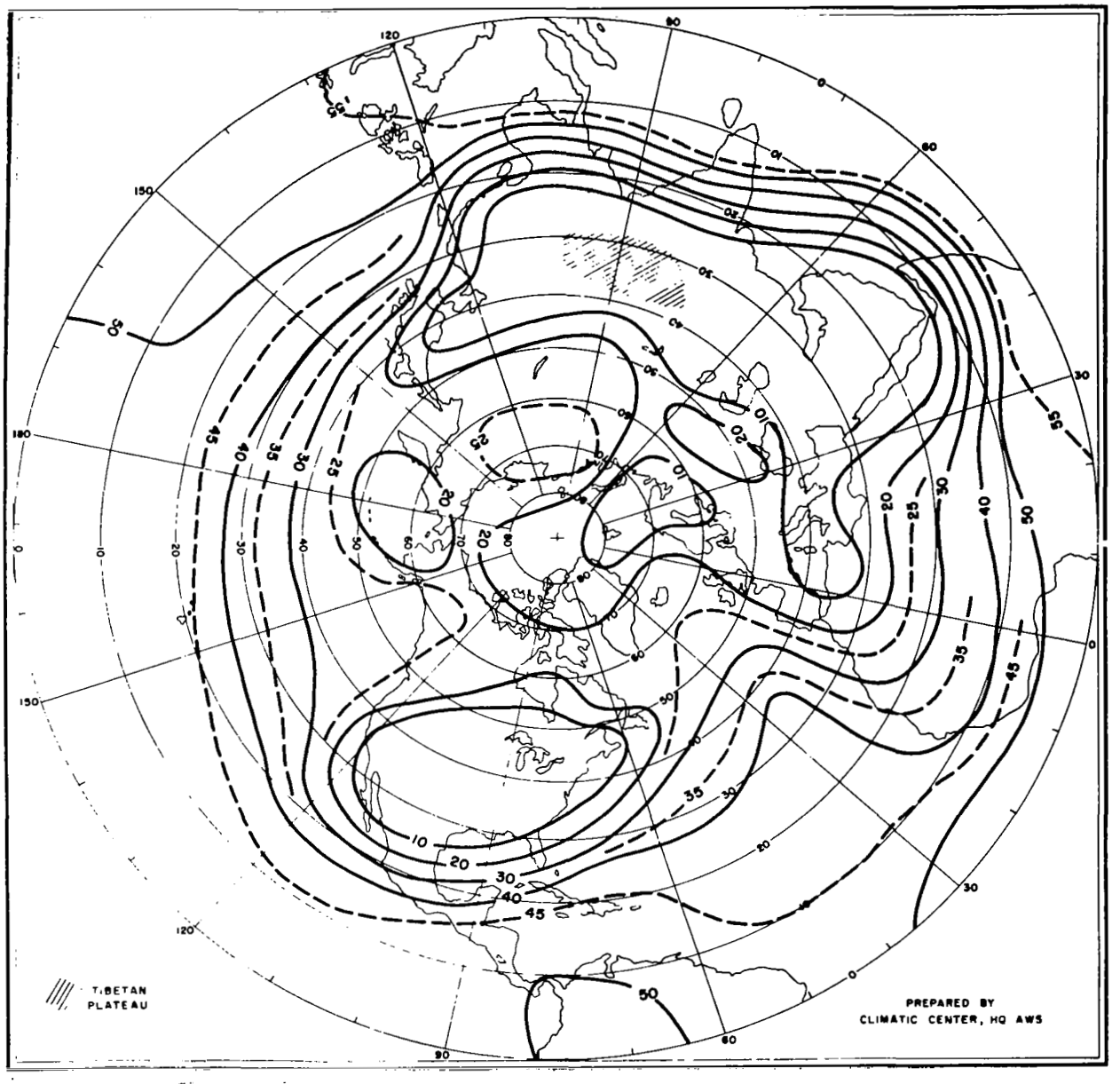

Figure D. Altitudes (in Thousands of Feet Above Mean Sea Level) Above Which There is 60 Percent Probability of Having 1/10 Sky Cover, October

WORLD WIDE WEATHER CONSIDERATIONS

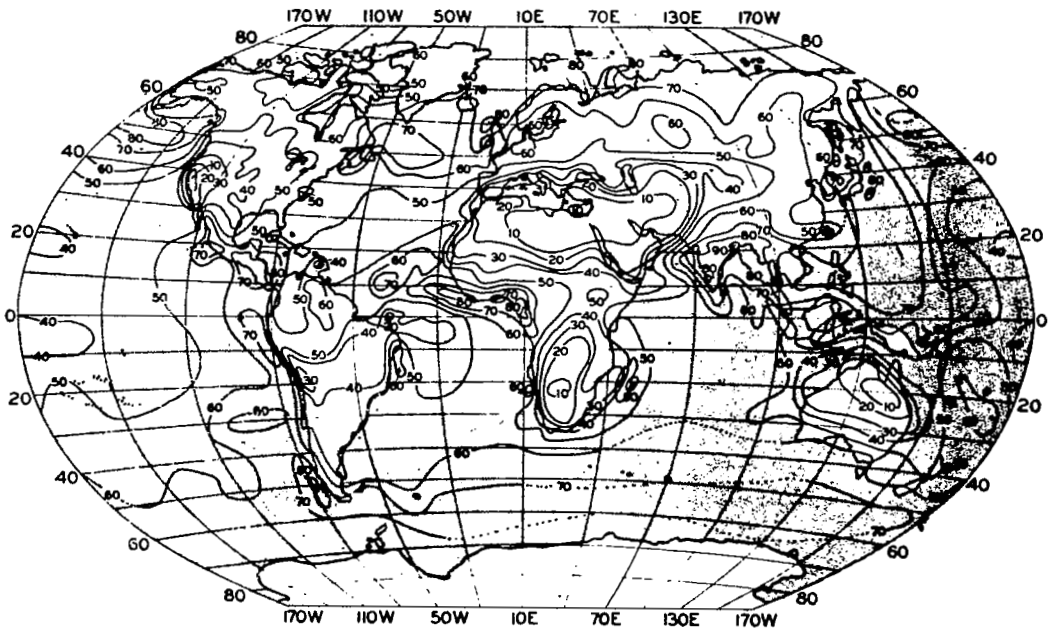

Figure E. Mean Cloudiness in Fractional Cloud Cover, July

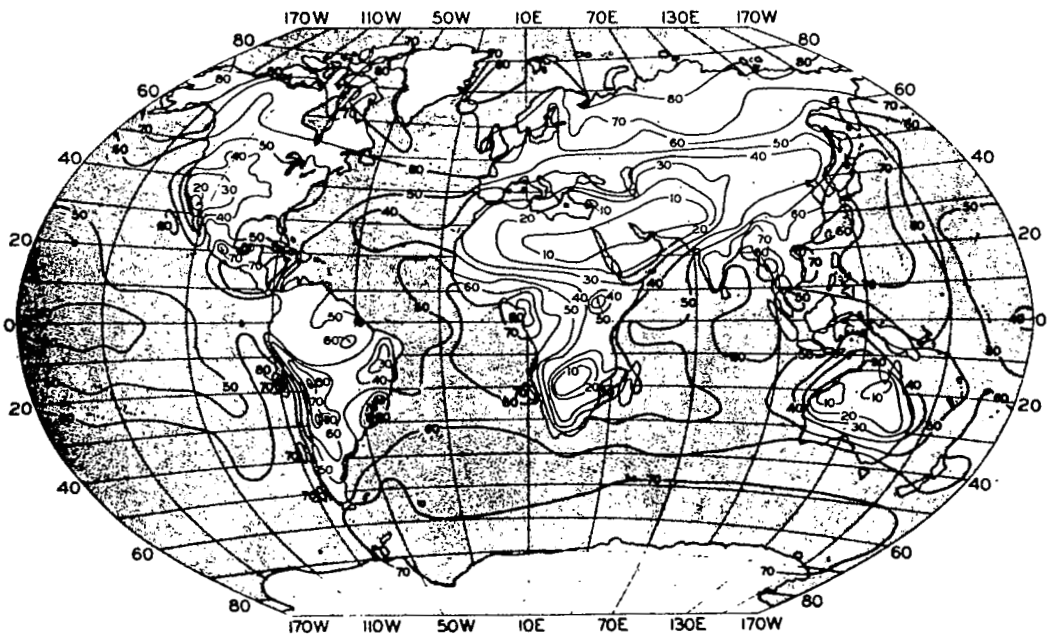

Figure F. Mean Cloudiness in Fractional Cloud Cover, September

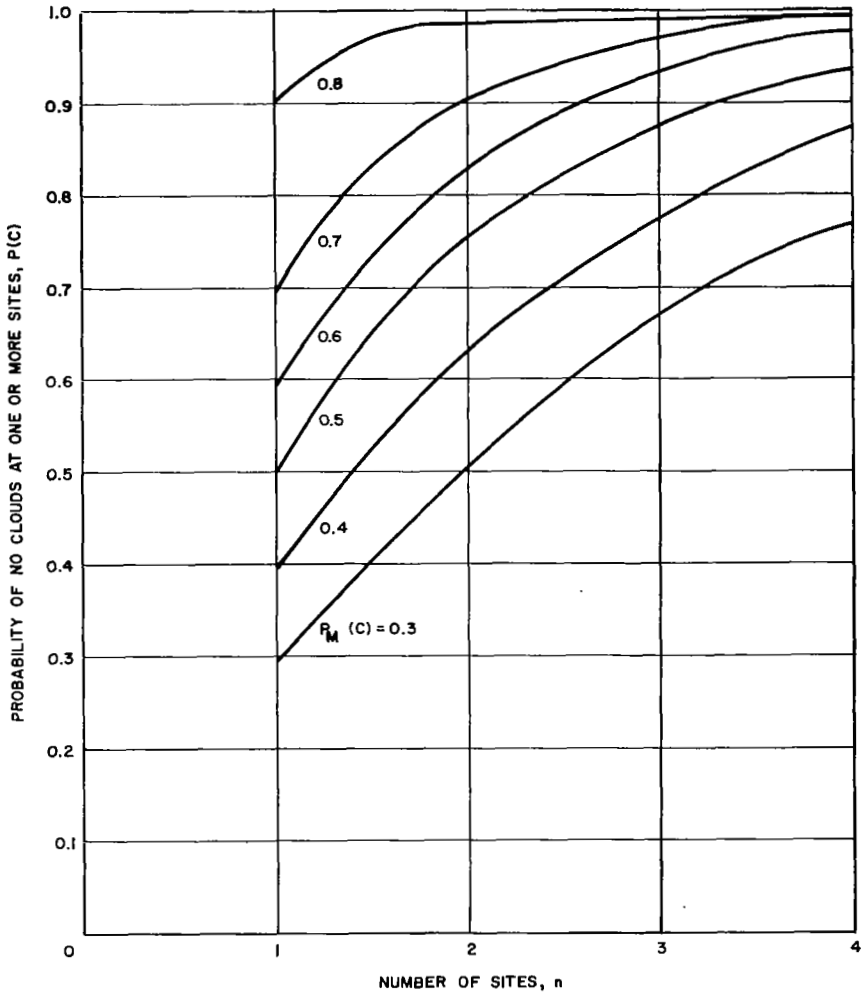

Figure G. Probability of No Clouds at One or More Sites P(C), Versus Number of Sites, n

EXISTING ASTRONOMICAL OBSERVATORIES

Six existing astronomical observatories are selected as potential sites for laser space communications.

Existing astronomical observatories could, in principle, be used for reception of optical communications. The major requirement is that the pointing accuracy of the telescope must be such that the spacecraft can be retained in the telescope field of view. The Palomar 200-inch telescope has a pointing accuracy of approximately 24 microradians; the Kett Peak 84-inch telescope has a pointing accuracy of approximately 300 microradians.[1] The telescope field of view is given by the ratio of detector radius to focal length. Using reasonably small detectors it can be made appreciably larger than the above pointing accuracies. A 2-inch diameter detector in the Palomar telescope which has a 660-inch focal length gives a 3 milliradian field of view. Smaller telescopes may have reduced tracking accuracies, but their focal lengths are correspondingly smaller. Hence, telescope pointing accuracy limitations do not appear to preclude the use of existing observatories.

Apart from the possibility of adapting the existing observatory telescopes to use as optical receivers, it would appear desirable in any case to consider existing observatory locations as optical receiver sites. Since observatories are subject to weather constraints similar to those for optical receivers, comparison of existing observatory records would indicate the relative suitability of that location as a receiver site. As an example of this, Table 1 lists cloud cover statistics for 10 selected stations. Furthermore, to reduce atmospheric degradation of the signal as well as minimize the probability of cloud interference, it is desirable to locate the receiver at a high elevation. This constraint also applies to astronomical observatories, many being located on mountain promontories.

Observatories having telescope aperture diameters larger than 20 inches which are located within the critical latitude range ±40 degrees are listed in Table 2[1] with their principal specifications, elevation above sea level, and geographic location. With the addition of one site in the Hawaiian Islands, a network of six high-altitude sites spaced approximately equal longitudes apart (to provide twofold redundancy) may be chosen from among these. They are shown in Table 3.

---

[1] Telescopes, Gerald P. Kniper and Barbara Mittlehurst, University of Chicago, 1960.

Table 1. Baker Nunn Sites Showing Percent of Time Lost Due to Clouds

Station Coordinates (Long.)	Lat.		Jan.	Feb.	Mar.	Apr.	May	June	July	Aug.	Sept.	Oct.	Nov.	Dec.
New Mexico		1962	36	25	27	15	5	12	49	32	48	19	26	22
253°27'(E)	+32°25'	1963	34	27	21	29	30	13	48	57	28	16	27	17
South Africa		1962	42	29	31	26	4	6	1	5	8	29	53	37
028°15'(E)	-25°58'	1963	50	23	27	28	15	21	20	2	7	30	55	49
Australia		1962	32	21	21	9	34	12	22	22	27	38	15	18
136°46'(E)	-31°06'	1963	16	22	22	22	51	35	47	21	18	17	18	22
Spain		1962	52	32	81	43	33	15	21	15	34	47	40	43
353°48'(E)	+36°28'	1963	72	49	39	39	35	32	4	19	22	19	60	45
Peru		1962	81	71	56	38	10	2	5	6	35	22	42	55
288°30'(E)	-16°28'	1963	88	95	63	56	23	2	6	15	21	26	13	52
Iran		1962	28	44	33	54	10	1	18	16	03	nil	14	38
052°31'(E)	+29°38'	1963	17	40	30	47	30	7	15	23	1	12	35	22
Curacao		1962	52	43	56	53	74	66	46	38	60	39	45	50
291°10'(E)	+12°05'	1963	70	59	51	68	70	40	64	55	63	50	65	62
Florida		1962	55	40	62	55	36	61	41	55	52	45	55	43
279°53'(E)	+27°01'	1963	57	58	47	28	50	42	44	29	49	32	49	43
Argentina		1962	53	52	38	72	51	27	39	32	22	29	35	43
294°54'(E)	-31°57'	1963	*	35	40	27	39	33	36	32	57	46	46	30
Hawaii		1962	23	41	56	39	33	5	38	18	20	16	26	33
203°45'(E)	+20°43'	1963	59	17	70	78	52	28	29	23	39	39	32	30

*No photography attempted for a 3 week period when the mirror was removed for realuminizing.

EXISTING ASTRONOMICAL OBSERVATORIES

Table 2. Astronomical Optical Telescopes, Aperture ≥ 20 Inches or 50 CM

Observatory	Co-Ord Long., hour Lat., degree	Elev. (m)	Type	Aperture (Inches)	Aperture (cm)	Focus	F/	Accessories	Since
Leuschner Observatory, Berkeley, California, U.S.A.	+ 8:09 +37:52	94	Refl	20	51	Newt Cas	4 16	Pg Pe Sp Mic	1756
Boyden Observatory Bloemfontein, O.F.S., South Africa	- 1:46 -29:02	1387	Refl	60	152	Newt	5.3	Pg Pe Sp	1930
			B-Schm	32 36	81 91	Prime	3.7	Pg Sp	1950
National Observatory, Bosque Alegre Station, Argentina	+ 4:18 -31:36	1250	Refl	61	155	Newt Cas	5 21	Pg Sp	1942
Goethe Link Observatory of Indiana University, Brooklyn, Indiana	+ 5:46 +39:33	300	Refl	36	91	Prime Newt	5	Pg Pe Sp	1939
Mount Stromlo Observatory, Canberra, Australia	- 9:56 -35:20	808	Refl	74	188	Newt Cas Cou	5 18 31	Pg Pe Sp Sp	1955
			Refl	50	127	Greg	18	Pe	1954
			Refl	30	75	Newt Cas	4 18	Pg Pe Sp Pe	1930
			Refl	26	50	Cas	12	Pg Pe	1959
			Pg R	26	66		16.6		1953
			Schm	20 26	50 66	Prime	3.5	Pg	1956
Royal Observatory, Cape of Good Hope, South Africa	- 1:14 -33:56	8	Pg R	24	61		11	Pg Pe	1901
			Refl	40	102	Prime Cas	4.5 20	Pg Pe	1961
Leander McCormick Observatory, Charlottesville, Virginia, U.S.A.	+ 5:14 +38:02	259	Vis R	26	66		15	Pg Pe	1883
Chamberlin Observatory, University of Denver, Denver, Colorado, U.S.A.	+ 7:00 +39:41	1644	Vis R Pg R	20 20	51 51		16 14	Pg Pe Mic	1894
U.S. Naval Observatory, Flagstaff Station, Flagstaff, Arizona, U.S.A.	+ 7:27 +35:11	2310	Refl	40	102	Cas	6.8	Pg Pe Sp Mic IT	1955
Lowell Observatory, Flagstaff, Arizona, U.S.A.	+ 7:27 +35:12	2210	Refl	42	107	Cas Cas Cas	33 23 15	Pg Pe Sp IT	1910
			Vis R	24	61		16	Pg Pe Sp Mic	1896
			Refl	20.8	53	Cas	16	Pe	1953
			Refl	24	61	Cas Cas Cas	16 32 104	Pg Pe Sp IT	1960
McDonald Observatory, Fort Davis, Texas, U.S.A.	+ 6:56 +30:40	2081	Refl	82	208	Prime Cas Cou	4.0 13.6 20.3	Pg Pe Sp Mic IR	1939
Helwan Observatory, Helwan, Egypt	- 2:05 +29:52	115	Refl	30	76	Newt	4.5	Pg Pe	1905
			Refl	74	188	Newt Cas Cou	4.9 18 28.9	Pg Sp	1960
Nizamiah Observatory, Osmania University, *Hyderabad, India*	- 5:14 +17:26	554	Refl	48	122	Newt Cas Cou	4 15 30	Pe	1962
Union Observatory, Johannesburg, South Africa	- 1:52 -26:11	1806	Vis R	26.5	67		16	Pg Mic Int	1925
LaPlata Observatory, LaPlata, Argentina	+ 3:52 -34:54	17	Refl	33	84	Cas	18	Pg Pe Sp	1896
Bosscha Observatory, Lembang, Java, Indonesia	- 7:10 - 6:50	1300	Pg R Vis R	23.6	60		17.9	Pg Pg Mic	1928 1928
			Schm	20 28	51 71	Prime	2.5	Pg	1958
Lisbon Observatory Station, Alfeite, Portugal	+ 0:37 +38:40	45	Refl	20	50	Newt Cas	6 18	Pg	1950
Star Lane Observatory, Louisville, Kentucky, U.S.A.	+ 5:43 +38:08	143	Refl	20.3	51	Newt Cas	5	Pg Pe	1956

Table 2. Astronomical Optical Telescopes, Aperture ≥ 20 Inches or 50 CM (Continued)

Observatory	Co-Ord Long., hour Lat., degree	Elev. (m)	Type	Aperture (Inches)	Aperture (cm)	Focus	F/	Accessories	Since
Lick Observatory, Mount Hamilton, California, U.S.A.	+ 8:07 +37:20	1283	Refl	120	305	Prime Cou	5	Pg Pe Sp	1959
			Refl	36	91	Prime	5.8	Pg Pe Sp	1898
			Vis R	36	91		19	Pg Pe Sp Mic	1888
			Pg R	20	51		7.4	Pg	1940
			Refl	22	56	Cas	11	Pe	1956
Palomar Observatory Mount Palomar, California, U.S.A.	+ 7:47 +33:21	1706	Refl	200	508	Prime Cas Cou	3.3 16 30	Pg Pe Sp Pg Sp	1948
			Schm	48 72	122 183	Prime	2.5	Pg	1948
			Refl	20	51	Cas	12.7	Pg Pe	1951
Mount Wilson Observatory, Pasadena, California, U.S.A.	+ 7:42 +34:13	1742	Refl	100	254	Newt Cas Cou	5 16 30	Pg Pe Sp Pg Sp Sp	1917
			Refl	60	152	Newt Cas	5 16	Pg Pe Pg Sp	1908
Purple Mountain Observatory, Academia Sinica, Nanking, China	- 7:55 +32:04	267	Refl	24	60	Newt Cas	5 16.7	Pg Pe Sp	1935
Dyer Observatory, Nashville, Tennessee, U.S.A.	+ 5:47 +36:03	345	Refl	24 24	61 61	Newt Newt Cas	4.5 3.4 16	Pg Pe	1953
Flower and Cook Observatory, Philadelphia, Pennsylvania, U.S.A.	+ 5:01 +40:00	155	Refl	28	71	Newt Cas Prime	5 15 5	Pe	1956
Radcliffe Observatory, Pretoria, South Africa	- 1:53 -25:47	1542	Refl	74	188	Newt Cas Cou	4.8 18 28	Pg Sp Pe Sp	1948
Observatorio Astronomico Nacional, Universidad de Chile, Santiago, Chile	+ 4:42 -33:24	859	Pg R	24	60		18	Pg Sp	1956
Sproul Observatory, Swarthmore, Pennsylvania, U.S.A.	+ 5:01 +39:54	63	Vis R	24	61		18	Pg Mic	1911
Tokyo Astronomical Observatory, Mitaka, Tokyo-to, Japan	- 9:18 +35:40	59	Pg R	26	65		15	Pg Pe Sp	1930
			Refl	36	90	Prime Cas	5 18	Pg Pe	1961
Okayama Astrophysical Observatory, Kamogata, Okayama-ken, Japan	- 8:54 +34:34	370	Refl	74	188	Newt Cas Cou	4.9 18 29	Pg Pe Sp	1960
			Refl	36	90	Cas	13	Pe	1960
Tonantzintla Observatory, Tonantzintla, Mexico	+ 6:33 +19:02	2193	Schm	26 32	66 81		3.2		1948
Kitt Peak Observatory, Tucson, Arizona, U.S.A.	+ 7:26 +31:57	2090	Refl	36	91	Cas	13.5	Pg Pe Sp	1960
			Refl	84	213	Cas Cou	8 32	Pg Pe Sp Pe Sp	1961
Steward Observatory, Tucson, Arizona, U.S.A.	+ 7:24 +32:14	757	Refl	36	91	Newt Cas Cou	5 15 36	Pg Pe Sp	1922
U. S. Naval Observatory, Washington, D. C.	+ 5:08 +38:55	86	Vis R	26	66		15	Pg Pe Mic	1873
Jones Observatory, Chattanooga, Tennessee, U.S.A.	+ 5:40 +35:01	750	Refl	20.5	52	Cas	17.5		1936
IRSAC Observatory, Elisabethville, Belgian Congo	- 1:50 -11:27	1500	Refl	38.5	98	Prime Cas Cou	2 10 10	Pg Pe Sp	1960
			Schm	26.3 38.5	67 98	Prime	3	Ob Pm	1960
Atmospheric Research Observatory, Arizona State College, Flagstaff, Arizona, U.S.A.	+ 7:27 +35:11	2105	Refl	24	61	Newt Cas	4.5 25		1953

B-Schm = Baker-Schmidt
Cas = Cassegrain
cou = coudé
Greg = Gregorian
IT = Image Tube
Inf = Infinite

Int = Interferometer
IR = Infrared
Mak = Maksutov
Men = Meniscus
Met = Metal
Mic = Micrometer

Nas = Nasmyth
Newt = Newtonian
Ob Pm = Objective Prism
Pe = Photoelectric
Pg = Photographic
Refl = Reflector

R = Refractor
Schm = Schmidt
Sp = Spectrograph
Vis = Visual

EXISTING ASTRONOMICAL OBSERVATORIES

Table 3. Selected Sites for Optical Observations

	Longitude (Hours:Minutes)	Elevation (ft)
National Observatory of Argentina Bosque Alegre Station, Argentina	+4:18	4,100
Radcliffe Observatory Pretoria, South Africa	-1:53	5,060
Nizamia Observatoria Hyderabad, India	-5:14	1,820
Mount Stromlo Observatory Canberra, Australia	-9:56	2,520
Mauna Kea Peak Hawaii	10:35	13,796

EARTH RECEIVING FACILITIES

Optical Communication Site Considerations

LUNAR LASER RANGING SITE

The Catalina Mountains of Arizona have been selected as the site for a laser lunar ranging site.

The Hughes Aircraft Company, under Contract F19628-68-C-0194, from the AF Cambridge Research Lab CRJG, is installing a laser ranging system in the Catalina Mountains of Arizona. This site, operated by the University of Arizona, is located at Lat 32° 26.6' N and Long 110° 44.0' W which means that at moon zenith the site zenith angles will vary over the range of 4 degrees to 60 degrees (90 degrees can, of course, always be found at the lunar setting).

The purpose of the ranging site is to measure the range to the lunar surface to 1.5 meters. This will allow determination of such measures as distance of the site to the axis of the earth, and with other sites on other continents, could directly measure coordinated drift.

The site, at an elevation of 8400 feet, was chosen partly on the freedom it has from cloud cover and has several other astronomical telescopes in addition to the laser ranging instrumentation. Parameters of the ruby laser transmitter, receiver, and optics are noted in the table.

Laser Lunar Ranging Parameters

Mirror diameter	60 inches
Beam-width	1 arc second
Peak Transmitter Power	10^6 kw
Pulse length	10 nanoseconds
Maximum expected received photons	3000
Range accuracy	± 1.5 meters

POTENTIAL OPTICAL SITES IN THE UNITED STATES

Several potential optical sites are given in the southwest United States.

A recent evaluation by Sylvania Electronics Systems[1] of potential sites for optical communications has been made. This evaluation considered the weather conditions on a national, sectional and regional basis. Evaluation of the sites from a topographic nature and the proximity to jet contrail paths was also included.

The report concluded by recommending nine candidate sites for consideration as possible locations for an Optical Communication Facility. They are:

1. Atascosa Peak, Arizona
2. Capitan Mountains, New Mexico
3. Chiracahua Peak, Arizona
4. Chisos Mountains, Texas
5. Guadelupe Mountain Range, New Mexico
6. Kingston Peak, California
7. Mount Wrightson, Arizona
8. Sacramento Mountains, New Mexico
9. White Mountains, California

The limitations of this study did not permit the evaluation of grading of these sites; local unpublished data must be acquired and on-site inspection performed in order that such evaluation and grading of the seeing conditions and other important factors can be accomplished.

It was established that precipitation data is a good relative measure, in the absence of local information, of the probable utilization factor of a site. Of the sites recommended, Atascosa Peak, Capitan Mountains, Chiracahua Peak, and Sacramento Mountains all display a pronounced two-month summer wet season according to the data reported here. Emory Peak and Guadelupe Mountain Range have somewhat more precipitation in summer than in winter. Kingston Peak has no distinct seasonal preference.

It is interesting to compare the dry day averages for these sites first on an annual basis and secondly based on the best 10 months out of the year. The latter gives an indication of the reliability of the site if not used for

---

[1] Final Report "Study on Optical Communication Experimental Facility" NAS 8-20304

spacecraft experiments during the predicted worst two-month period. Judging by any criterion, Kingston, Guadelupe and Atacosa, in that order, show the most promising dry-day records. The other four sites have relatively poorer standing, their standing relative to one another depending on what aspect of the seasonable pattern is stressed. It may be concluded that in the absence of other information, Kingston, Guadelupe and Atascosa should receive prime consideration in subsequent evaluations.

It must be noted that this set of conclusions is predicated on the implementation of a single site for all-year around-the-clock performance. The situation could conceivably be improved if a second site were to be implemented for diversity. Such an alternate site could be chosen with a complementary seasonal pattern, near the coast of upper California for example, to provide true all-year reliable performance, In addition, an alternate site located in a different weather system than the primary site, would provide diversity improvement of the short-term outage times due to weather. The risks can be diminished considerably by limiting the critical experimental phases to the better months of the year, and perhaps by scheduling critical phases for the best hours of the day, which will be determined only by experience with the actual installation.

No site with unusually high year-round reliability has been found, but sites with good probable performance during ten months of the year seem to be available. The requirement for twenty-four hour operation during good seasons implies some compromise between best daytime and best nighttime performance.

It is interesting to compare these sites in the USA southwest to the figure which is a photograph taken by ATS-I on 10 December 1966. This picture shows generally heavy cloud cover but indicates that the southwest United States and Baja, California to be cloud free. This is typical of many such pictures of this area.

POTENTIAL OPTICAL SITES IN THE UNITED STATES

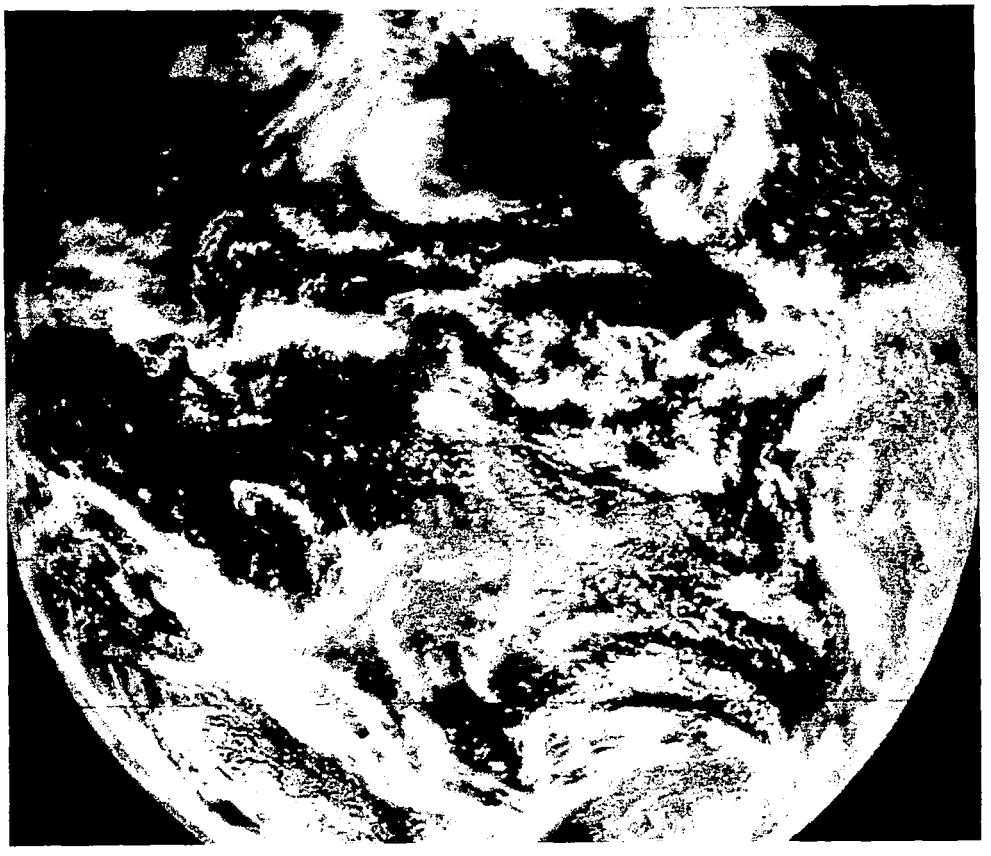

Earth from ATS I

EARTH RECEIVING FACILITIES

Earth Receiving Networks

OPTICAL SITE CONSIDERATIONS

Earth receiving sites for optical communication should favor a convenient site for a pilot station and favor a site with inherent optical performance for an ultimate configuration.

Optical communication can provide high data rate performance for less cost or weight than radio communication for certain missions. This conclusion, documented in other portions of this final report, has given impetus to the development of an optical communication ground network. It is the purpose of this topic to note the major considerations for the placement of stations for such a network.

Function of Optical Communications Earth Site

An optical communication site is not intended to perform all the functions that are presently performed by the radio networks. An optical link is best used as a specialized data link capable of transmitting very high data rates over planetary distances. It is anticipated that the existing radio links will continue to perform functions of trajectory determination, command, and reception of telemetry data from spacecraft status monitors. The choice of an optical site must then consider the proximity to suitable radio facilities as well as conditions suitable for optical communications.

The implementation of an optical facility entails a large expenditure and certainly should be done in phases such that the knowledge obtained with early sites and configurations may be used in later designs. Such a pilot site would be used to determine atmospheric effects upon wide band data transmitted via a laser, effects upon seeing as a function of site surroundings, i.e., mountain side position, plain position or lake mounted position; and statistical effects of the atmosphere as a function of weather patterns, elevation angle and time of year. The effect of the atmosphere upon defraction of the laser beam which acts as a beacon for the spacecraft may also be examined.

In addition to these environmental bounds, mission functions such as the interface between the optical data reception and the world wide communication networks may be exercised.

The pilot station may also carry out experiments with presently planned optical space communication experiments such as the ATS-F & G CO_2 laser communications experiments.

The ultimate use of an optical communication network would be to function the receiving site for extremely high performance communications links. The links of this type are exemplified by a reconnaissance spacecraft orbiting mars. Here very high data rates can be provided by the imagery sensors at planetary ranges. Additionally, if mapping the entire planet is desired, it is possible that there would be periods of time when data interruption would not be objectionable since the same imagery could be obtained on a subsequent orbit. This consideration of non-continuous data, reduces considerably the number of earth stations that would be needed. Further it would reduce the emphasis placed upon an orbiting relay satellite, where the relay satellite receives the optical signal and then relays it to earth on a radio link.

Site Considerations

There are two basic considerations in site selection: convenience and technical suitability.

Convenience relates to the proximity to radio networks such as the Deep Space Network or NASA centers or contractor facilities. In addition to these there are the basic needs of roads, service buildings etc. which must be considered.

Relative to technical performance, the largest single variant is the atmosphere and its constituents. Clearly optical observatory sites are chosen for many of the characteristics needed by laser communications such as a high elevation, having a minimum amount of cloud cover, background light and for generally good seeing. There are additional constraints or degrees of constraints that are required by laser communication. These include the atmospheric defraction, the coherence length and the daytime atmospheric background. Thus it may well be that existing astronomical sites are not the best overall choice for a laser communication.

Conclusion

The need for a development of a laser communication receiving network is based upon the higher performance of lasers in certain missions. The development of a network must be sequential as the knowledge of the desired site characteristics and configuration is developed. Based upon these considerations and upon site location considerations of convenience and technical performance, a pilot site near the STADAN headquarters, the Goddard Space Flight Center, is suggested. Such a site is convenient and can operate with such experiments as the ATS-F and G laser communication experiment.

An ultimate network would have the primary United States sites located in the southwestern portion of the country, near the Goldstone, California DSN Station. Other possible worldwide stations are listed in the table.

Selected Sites for Optical Observations

	Longitude (Hours:Minutes)	Elevation (ft)
National Observatory of Argentina Bosque Alegre Station, Argentina	+4:18	4, 100
Radcliffe Observatory Pretoria, South Africa	-1:53	5, 060
Nizamia Observatoria Hyderabad, India	-5:14	1, 820
Mount Stromlo Observatory Canberra, Australia	-9:56	2, 520
Mauna Kea Peak Hawaii	10:35	13, 796

OPTICAL STATION NETWORK - PROGRAM PLAN

A two phase program plan is presented which outlines the construction of a pilot station and three operating stations for an optical space communications network.

The orderly development of an optical ground network can be done in two phases, an experimental phase and an operational phase. The rationale for such a program was described in the previous topic and the time phasing is presented below and in Figures A and B.

Phase I - Experimental System Development

Figure A is a suggested program plan for the development phase of an optical network. It is the purpose of this phase to develop a ground station design suitable for the operational system, to determine suitable site environmental parameters, and to select sites for the operational network.

In order to accomplish the goals of Phase I, a four part program is suggested: 1) station design and test, 2) optical station integration with the radio network used for scientific satellite testing, STADAN, 3) site atmospheric testing, and 4) operational system site selection. The STADAN radio network was selected as a companion network for the experimental testing since it is likely that space to earth testing would be accomplished using near-earth scientific satellites. Since the STADAN central control is the Goddard Space Flight Center, it is further suggested that the experimental optical site be near GSFC to facilitate integration with STADAN.

Site atmospheric testing will be conducted during the majority of the Phase I period. This will provide data such as optical coherence length, seeing, temperature gradients etc., and possibly correlation of these data to commonly recorded meteorological data for a period greater than one year.

With the atmospheric data it will be possible to analyze prepared sites for the operational system and to plan the operational system and the Deep Space Network (DSN) interface.

It should also be noted that in those instances where manned vehicles use laser communication for deep space missions, e.g., manned landing of mars, that the DSN may temporarily become a part of the manned Space Flight Network (MSFN). Thus the operational network site solution task includes an interface study between the DSN/MSFN.

Phase II - Operational System Development

The time phasing for the operational system development is indicated in Figure B with a summary of Phase I. Phase II of the optical station network begins as soon as Phase I is completed. The summary program plan indicates three sites which are completed four and one half years after the initiation of Phase I. The construction period for the first of these sites is somewhat larger than the second and third to allow for initial contingencies.

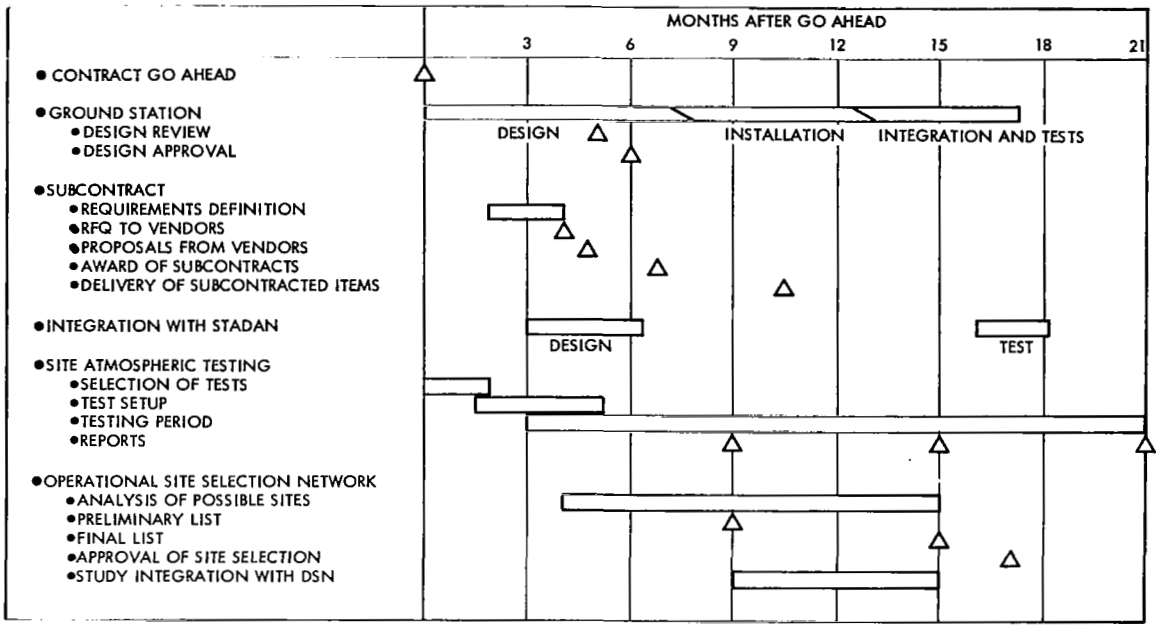

Figure A. Phase I Optical Station Network - Recommended Program Plan

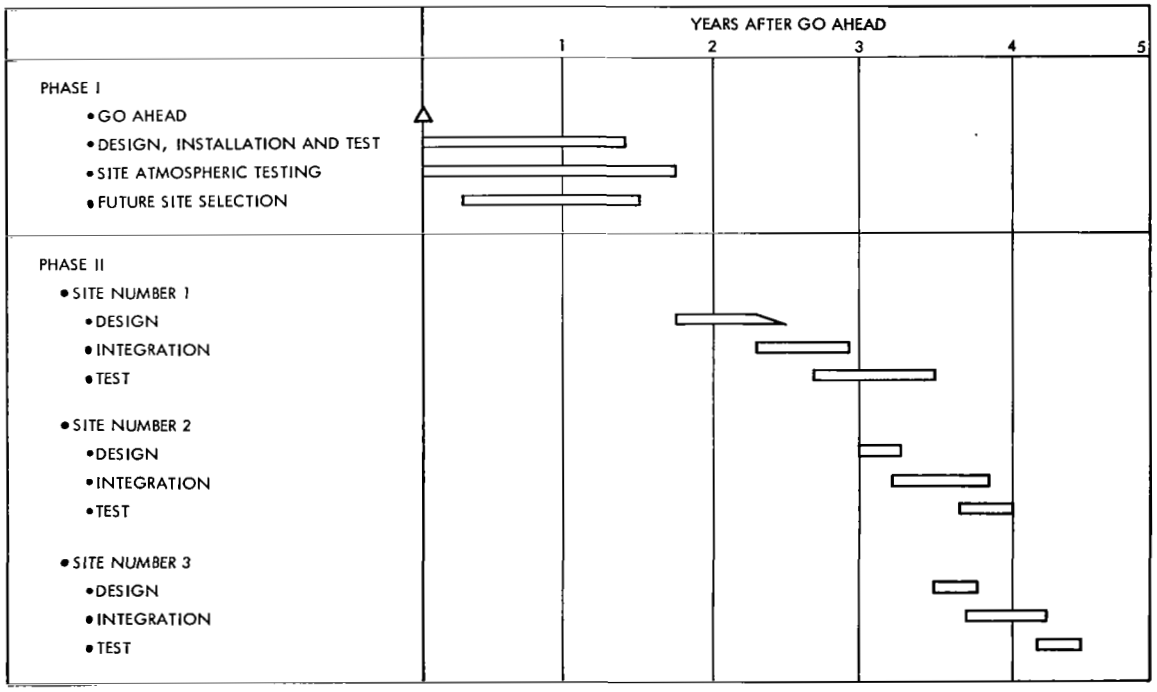

Figure B. Optical Station Network - Summary Program Plan

PART 3 SYSTEMS IMPLEMENTATION

SYSTEMS IMPLEMENTATION

1.0 INTRODUCTION

The purpose of this section, Systems Implementation, is to list tracking and telecommunications parameters of existing deep space probes. Such probes will always be referred to directly or indirectly in any new design or extension of Deep Space communication capability and are included here to aid a designer in making such comparisons.

The telecommunication systems for three probes have been described, the Mariner IV telecommunication link[1] which transmitted photographic and other scientific data from Mars, the Surveyor Spacecraft telecommunication[2] which transmitted photographic coverage of the moon after a successful soft landing and the Lunar Orbiter Spacecraft[6] which transmitted photographic coverage of both the front and back of the moon. In addition overall weight, cost and data rate comparisons are made for several spacecraft.

2.0 MARINER MARS 1964 TELEMETRY AND COMMAND SYSTEM[1]

The primary objective of the Mariner Mars 1964 project was to conduct close-up, fly-by scientific observations of the planet Mars during the 1964-1965 opportunity and to transmit the results of these observations back to earth. Television, cosmic dust, and a complement of fields and particles experiments were carried by Mariner IV. In addition, an occultation experiment was conducted.

A secondary objective was to provide experience and knowledge about the performance of the basic engineering equipment of an attitude-stabilized fly-by spacecraft during a long-duration flight in space farther away from the sun than is the earth.

The Mariner IV spacecraft was launched on November 28, 1964. The spacecraft was fully attitude stabilized, using the sun and Canopus as reference objects. It derived power from photovoltaic cells, arranged on panels having body-fixed orientation, and a battery, which is used for launch, trajectory correction maneuvers, and back-up. The

telecommunication system for the Mariner Mars 1964 Mission was comprised of spacecraft-borne equipment and the NASA Deep Space Net.

Single CW radio-frequency carriers that are transmitted to and from the spacecraft are used for tracking the spacecraft and transmitting the telemetry and command information. The functional arrangement of the spacecraft subsystems utilized to accomplish this is shown in Figure 1. For both the telemetry and command functions, pulse code modulation, phase shift key, and phase modulation (PCM/PSK/PM) techniques in combination with pseudorandom sync codes provide efficient, accurate transmission of the data over interplanetary distances.

The telemetry portion of the system is required to transmit video data in digital form from the vicinity of Mars and both scientific and engineering data during the flight from earth to Mars. Since the rate at which the video data is gathered exceeds the capacity of the telemetry channel, data storage and playback are provided by a synchronous, endless-loop tape recorder capable of storing 20 frames of video data.

2.1 Radio Subsystem

The radio subsystem is required to receive a modulated r-f carrier from stations of the Deep Space Net (DSN), demodulate command and ranging signals, coherently translate the frequency and phase of the r-f carrier by a fixed ratio, modulate the carrier with telemetry and ranging signals, and retransmit it back to earth. It consists of an automatic-phase-control receiver, redundant exciters, redundant power amplifiers, power supplies, low- and high-gain antennas, and associated transmission and control circuits. It operates at S-band frequencies, receiving at 2116 MHz and transmitting at 2298 MHz.

As received from earth, the up-link r-f signal is phase-modulated either singly or simultaneously by a composite command signal and a coded ranging signal. It is of the form

$$S_R = A(\gamma, r) \sin \left[\omega_o t' + \phi_c(t') + \phi_r(t') \right] \qquad (1)$$

$$t' = t - \frac{r(t)}{c} \qquad (2)$$

where

A = received signal level, a function of spacecraft attitude γ and spacecraft earth range r

ω_o = carrier frequency transmitted by the DSN station

ϕ_c = phase modulation by the composite command signal

ϕ_r = phase modulation by the coded ranging signal

$r(t)$ = spacecraft-earth range, a function of time t

c = velocity of propagation.

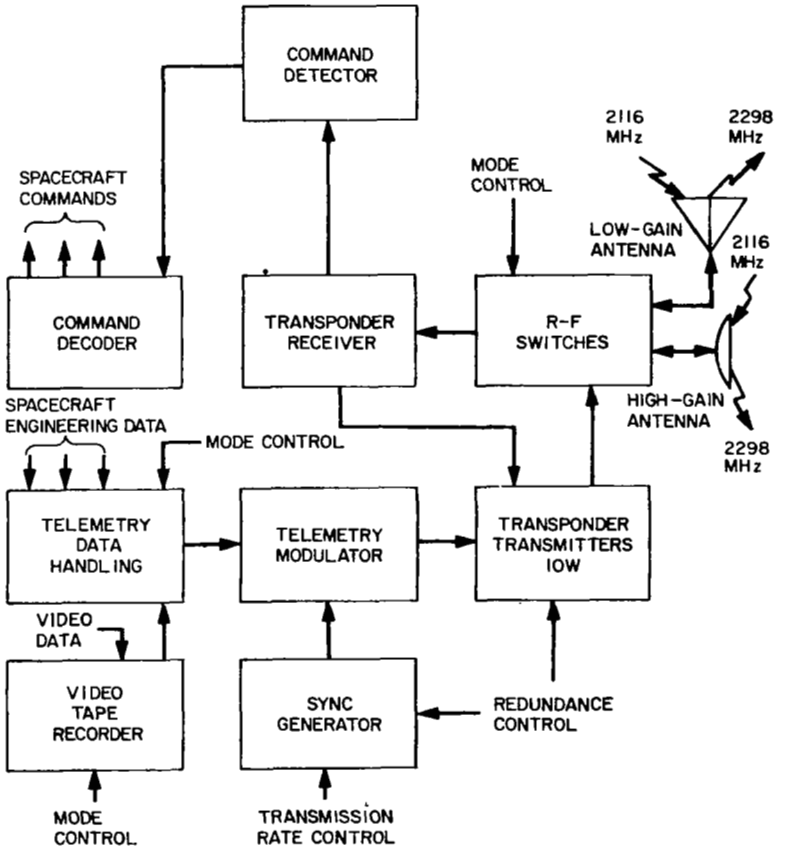

Figure 1. Mariner 1964 Spacecraft Telecommunication System

This signal is demodulated by the automatic phase control, double superheterodyne receiver which tracks the $\omega_o t'$ component of the carrier phase. The composite command modulation and coded ranging signals are sent to the command detector and the exciter phase modulators, respectively. When the receiver is phase-locked to the received signal, it generates for the transmitter exciter a filtered phase reference that is coherent with the $\omega_o t'$ component of the received signal. The phase of the transmitted signal is then related to that of the received signal by a fixed ratio to within an error of less than 1 radian rms. The resulting transfer function is given approximately by

$$\frac{\theta_T}{\theta_R} = \frac{240}{221}\left[\frac{1 + (3/4B)s}{1 + (3/4B)s + 1/2(3/4B)^2 s^2}\right] \qquad (3)$$

where

s = Laplace variable and B = effective noise bandwidth of the receiver phase tracking loop

θ_T = phase of the transmitted signal

θ_R = phase of the received signal

With this relationship the ground stations are provided with a signal that permits two-way Doppler tracking.

The transmitted signal is phase-modulated by a composite telemetry signal and the coded ranging signal. While the telemetry signal modulates the carrier continuously, the ranging modulation can be turned on or off by ground command.

When a signal is not being transmitted to the spacecraft, transmitter frequency control is provided by an auxiliary crystal oscillator. This noncoherent mode of operation permits one-way Doppler tracking, angular position tracking, and telemetry reception by the ground stations.

In order to provide increased reliability over the Mariner II design, redundant exciters, power amplifiers, and power supplies were incorporated in the transmitter. Each exciter consists of an auxiliary

oscillator, a ×4 frequency multiplier, a phase modulator, a ×30 frequency multiplier, and an output isolator. Either exciter can be coupled to either power amplifier by a circulator switching network. Similarly, the input and output circuits of the power amplifiers are coupled through circulator switches.

The control of the switching between these elements is provided by either ground command or on-board failure detection. The modulation, phase reference, and mode control inputs are fed to both exciters in parallel.

The position of the earth as seen from the spacecraft remains within one hemisphere of the spacecraft during the entire flight and within a relatively small angular region during the later portion of the flight; i.e., 130 days before the Mars encounter to 20 days past encounter. A comparison of this characteristic and the required minimum antenna gain vs. time-of-flight showed that the gain requirements could be met with a combination of one low-gain and one high-gain antenna, both of which were fixed relative to the spacecraft (Figure 2). The low-gain antenna provides coverage during the first 70 to 95 days of flight, whereas the high-gain antenna fills in the remaining period until approximately 20 days past encounter.

The low-gain antenna consists of a cruciform aperture at the end of a low-loss circular waveguide, which also functions as the support structure. In order to minimize pattern distortion by reflections from the spacecraft structure, the aperture is mounted well away from the bulk of the spacecraft. This antenna provides a pattern of revolution about the roll axis with a maximum gain of 5.5 db at 2298 MHz in the direction of the -Z spacecraft axis (oriented toward the sun) and a minimum gain of -6 db with respect to circular isotropic over the entire -Z hemisphere. The pattern at 2116 MHz is similar.

Since the thrust vector of the mid-course motor is perpendicular to the -Z axis, the earth can be kept within the -Z hemisphere while the thrust vector is pointed in any arbitrary direction. Thus, the low-gain antenna pattern also meets the requirement for providing coverage during mid-course maneuvers of unrestricted direction.

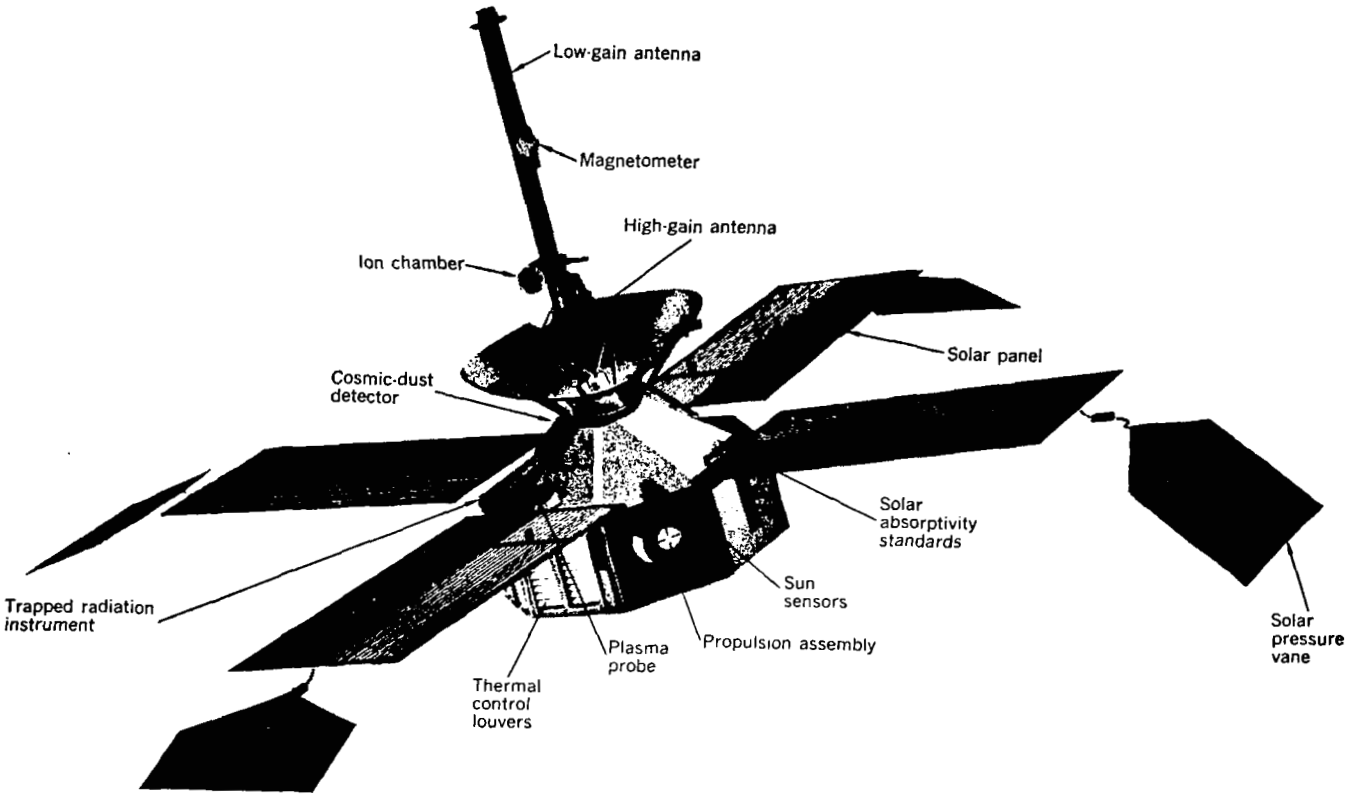

Figure 2. Mariner IV Spacecraft

The high-gain antenna is a 46.0 by 21.2 inch parabolic reflector that is illuminated by a pair of turnstile elements. These elements are arranged so that a right-hand circularly polarized beam is projected with a maximum gain of 23.5 db (at 2298 MHz and a half-power beam width of 13.5° by 7.5°. The beam is positioned so that coverage is provided from approximately 90 days after launch until 20 days past encounter. As a result of using this design as opposed to the one-degree-of-freedom antenna that was used on Mariner II, an estimated 50 pounds of spacecraft weight was saved by the associated reductions in structure, actuator, control electronics, and power requirements.

Three transmitting and receiving modes are available:

1. Transmit low gain, receive low gain.
2. Transmit high gain, receive low gain.
3. Transmit high gain, receive high gain.

These modes provide the required coverage during the acquisition, cruise, mid-course maneuver, and encounter phases of the flight. Selection of the proper mode is controlled by spacecraft programmed commands or ground commands as a backup.

Summaries of the principal radio subsystem transmission and reception parameters are given in Tables 1 and 2, respectively.

2.2 Telemetry Subsystem: Basic Technique

The principal functions of the telemetry subsystem on the spacecraft are to time-multiplex engineering and scientific data samples and to encode them for efficient modulation of the spacecraft-to-earth r-f carrier. A detailed discussion of the telemetry system is given elsewhere.[3-5] The subsystem is specifically required to

1. Transduce engineering parameters into electric signals.
2. Time-multiplex (commutate) engineering and scientific measurement signals.
3. Convert engineering data samples to binary words.
4. Store digitally encoded video data.
5. Phase-shift key a subcarrier with the binary signal.
6. Generate a cyclic, binary, pseudorandom sequence for use in synchronizing the encoding and decoding of the telemetry data.
7. Phase-shift-key a second subcarrier with the sync code.
8. Combine the two subcarriers into a composite telemetry signal.

The basic timing for the subsystem is derived from the 2400 Hz spacecraft power frequency, which is divided down to provide two subcarrier frequencies, one for data and one sync. The frequency divider is arranged to provide two data transmission (bit) rates, 33-1/3 and 8-1/3 bits per second (b/s). While the 33-1/3 b/s rate is used during

Table 1. Spacecraft Radio Transmission Parameters (2998 MHz)

Parameter	Transponder Low-Gain Channel		Transponder High-Gain Channel	
	Value	Tolerance	Value	Tolerance
Total transmitter power [a]	+40.0 dbm	±0.5 db	+40.0 dbm	+0.5 db
Carrier modulation loss [b]	-4.1 db	+0.9 db -1.0 db	-4.1 db	+0.9 db -1.0 db
Transmission circuit loss [c]	-1.7 db	+0.2 db -0.3 db	-1.3 db	+0.2 db -0.3 db
Spacecraft antenna gain [d]	+6.0 db	±1.8 db	+23.2 db	±1.1 db

[a] Ten watts nominal output of traveling-wave-tube amplifier.

[b] Based on modulation indexes of 0.809 rad peak for data subcarrier and 0.451 rad peak for sync subcarrier.

[c] Includes all circuitry between the output of the TWT amplifier and the input to the antenna.

[d] Referenced to perfectly circular isotropic pattern maximum.

Table 2. Spacecraft Radio Reception Parameters (2116 MHz)

Parameter	Transponder Low-Gain Channel		Transponder High-Gain Channel	
	Value	Tolerance	Value	Tolerance
Antenna gain (pattern maximum) [a]	+6.5 db	±1.8 db	+21.8 db	±1.1 db
Receiving circuit loss [b]	-1.0 db	±0.2 db	-0.9 db	±0.2 db
Effective system noise temperature [c]	2700°K	+1700°K -610°K	2700°K	+1700°K -610°K
Carrier APC noise bandwidth ($2B_{LO}$) [d]	20.0 Hz	...	20.0 Hz	...
Carrier threshold SNR in $2B_{LO}$				
Two-way Doppler tracking [e]	+3.8 db	...	+3.8 db	...
Command reception	+8.0 db	±1.0 db	+8.0 db	±1.0 db

[a] Referenced to perfectly circular isotropic pattern maximum.

[b] Includes all circuitry between the antenna and the input to the transponder receiver.

[c] Includes contributions due to antenna temperature, circuit losses, and noise figure at input to preselector, 10 db (+2 db, -1 db).

[d] Tolerance included in uncertainty of system noise figure.

[e] 3.8-db SNR is required for +2.0-db ground receiver degradation.

preflight checkout and the early flight phases up through a first midcourse maneuver, the 8-1/3 b/s rate is used for the remainder of the flight. In-flight selection of the data rate is controlled by ground command and by internal command. Either rate can be selected by ground command, but the internal command only selects the 8-1/3 b/s rate 192 days before encounter. The internal control is to insure that the 8-1/3 b/s rate is used at encounter in the event that command capability is lost.

The square-wave sync subcarrier drives a redundant pair of pseudorandom code generators which generate a cyclic 63-bit code. A set of word gates, in turn, generates bit and word sync pulses that are used to synchronize (1) the stepping of the commutator, (2) the analog-to-digital converters, (3) the readout of data from the data automation system, (4) the readout of the event registers and timers, and (5) the playback of the stored video data. The word sync pulses occur once per cycle of the code, whereas the data-bit sync pulses occur once every nine code bits, or seven times per code cycle. Thus, each data word is seven data bits long.

In order to convey the bit and word sync timing to the ground stations for use in synchronous demodulation of the telemetry subcarrier, the code also phase-shift-keys the sync subcarrier. The resulting composite telemetry signal that modulates the spacecraft-to-earth carrier is given by

$$D(t) = V_d \left[1.79d\left(\frac{2f_d t}{9}\right) \oplus a(4f_d t) + X\left(\frac{f_d t}{2}\right) \oplus a(2f_d t) \right] \qquad (4)$$

where

V_d = amplitude of the complex four-level wave

$d(2f_d t/9)$ = binary telemetry data of amplitude ±1 and bit rate $(2/9)f_d$

$a(ft)$ = symmetrical square wave of amplitude ±1 and frequency f

$X(f_d t/2)$ = cyclic, binary, pseudorandom sequence of amplitude ±1, length 63 bits, and bit rate $f_d/2$

$\oplus$ = modulo 2 addition

At the ground station, a local model of the code in phase-locked to the received code. Word gates identical to those in the spacecraft code generators then produce accurate bit and word sync pulse trains.

Analog engineering measurements are sampled by a solid-state commutator that provides 100 channels, 90 of which are used for measurements and then for synchronization points and subcommutation. These channels are divided among ten decks of ten channels each and are arranged to provide three sampling rates.

The pulse-amplitude-modulated output of the commutator is fed to two analog-to-digital converters, which convert the data samples to serial 7-bit words by a successive approximation technique. The output of the converter forms one of four data sources that comprise the telemetry modes.

Four modes of data transmission are provided for: (1) engineering data, (2) engineering and science data, (3) science data, and (4) stored video data and engineering data. In the first mode, only engineering data from the commutator, event register, event timer, and command monitor are transmitted, primarily for maneuver and checkout phases. In the second mode, both engineering and science data are transmitted in an alternating sequence of 140 engineering data bits followed by 280 science data bits. This mode is intended for most of the cruise phases. In the third mode, only science data are transmitted, as received from the data automation system. This mode is designed for use at planet encounter. In the fourth mode, stored video and engineering data are transmitted in alternating period of approximately 9 and 1.5 hours, respectively. This mode provides for readout of the video data taken during encounter and periodic monitoring of the spacecraft performance after encounter.

Event-type signals that signify the occurence of events such as motor-start, receipt-of-command, or solar-panels-open are accumulated as they occur in four separate registers. Each register

accumulates different types of events, as shown in Table 3, and hold up to eight counts before recycling. The registers are sampled in pairs at the high commutation rate in synchronism with the commutator, so that the state or count of two registers is conveyed by one 7-bit word.

An event timer measures the duration of certain events, such as the mid-course motor firing duration, by dividing the word sync rate by two and accumulating the number of pulses that occur between the start and the end of the event. This number is sampled at the medium rate also in synchronism with the commutator.

During the Mars encounter, a television subsystem which operates under data automation system control periodically generates video data in binary form. These data and the mode 3 instrument data generated at an effective rate of 10,700 b/s are organized in 516,168 bit frames, of which 504,400 bits are TV-related. Since this data rate greatly exceeds the 8-1/3-b/s radio transmission capability at encounter, a data storage subsystem holds the data for postencounter readout.

Data storage is accomplished by an endless-loop tape recorder. This machine records binary data and sync pulses on two tracks, filling

Table 3. Registered Events

Channel	Events
1	Pyrotechnics current pulse Gyro turn-on Solar panel 1 open
2	CC and S events Solar panel 2 open
3	Pyrotechnic arm Pyrotechnic current pulse Solar panel 3 open Recorder end of tape signal
4	Ground command events Sun acquired Solar panel 4 open Scan platform unlatched

one track at a time on each of two consecutive tape cycles. Recording is started and stopped by control signals from the data automation system to coincide with the encounter data frames. In order to prevent overrecording after the two tracks are filled the first time, end-of-tape signals automatically stop the recorder after the second complete tape pass. The tape is then in the correct position for subsequent playback.

Playback, at the 8-1/3-b/s transmission rate and synchronous with the telemetry bit sync pulses, is accomplished by an automatic phase control servo which controls the tape speed so that the recorded bit sync pulses are kept in phase with the telemetry bit sync pulses. By this means the pseudorandom sync signal allows synchronous demodulation of the recorded data at the ground stations. Table 4 summarizes the characteristics of the tape machine. Table 5 lists the principal telemetry subsystem parameters.

2.3 Command Subsystem

Commands are transmitted from DSN ground stations to the spacecraft by two subcarriers, which phase-modulate the earth-to-spacecraft RF carrier. One subcarrier is phase-shift-keyed by serial binary command words, and the other by a pseudorandom sync code in a manner similar to that used for telemetry data transmission.

The command subsystem is required to detect and decode the command words, of which there are two types: direct commands, which result in selected switch closures, and quantitative commands, which convey a magnitude and polarity for spacecraft maneuvers.

Table 6 lists the principal command subsystem parameters.

Table 4. Video Storage Characteristics

Record rate	10,000 b/s
Playback rate (synchronous)	8-1/3 b/s
Storage capacity	5.24×10^6 bits
Number of tracks	2
Type of tape machine	Endless loop

Table 5. Telemetry Parameters

Type of Encoding	Sampled data, digital PSK with pseudonoise sync
Channel requirements: Engineering measurements Event counters	 90 4
Word length	7 bits
Transmission rates	33-1/3, 8-1/3 b/s
Word error probability at threshold	1 word in 28 (bit error probability = 5×10^{-3})
Required $ST/(N/B)^*$ for bit error probability = 5×10^{-3}	$7.6 \frac{\text{db Hz}}{\text{b/s}} \pm 0.7$ db
Data channel modulation loss	-4.6 ± 0.6 db
Sync channel threshold (S/(N/B)	11.0 ± 0.5 db Hz
Sync channel modulation loss	-10 db(+0.2 db, -0.3 db)

*S = signal power; T = time for one bit; N = noise power; B = bandwidth.

2.4 Performance

The telecommunication system is required to provide tracking, telemetry, and command performance from launch to 20 days past encounter, including all of the intermediate phases. In order to reasonably assure this capability, it was desired to choose the system parameters so that the nominal received signal levels exceeded the threshold signal levels by at least the linear sum (in db) of the adverse tolerances. This criterion has been met for all functions and flight phases, except for the telemetry for a period of 10 to 26 days, depending on the launch date.

Figure 3 illustrates, for a typical trajectory, the nominal received carrier level for the spacecraft-to-earth channel vs. time

Table 6. Command Parameters

Number of commands	
Discrete	29
Quantitative	1 address, 3 subaddresses
Modulation type	Digital PSK with PN sync
Word length	26 bits
Transmission rate	1 b/s
Command threshold criteria:	
Probability of correctly executing a discrete command in one attempt	>0.7
Probability of completely executing a quantitative command in one attempt	>0.5
Probability of a bit error in a completely executed quantitative command	$<2 \times 10^{-4}$
Probability of a false discrete or quantitative command being executed when another command is sent	$<2 \times 10^{-9}$
Required carrier SNR in 20 Hz bandwidth at command threshold	+8.0 ± 1.0 db
Required command channel ST/(N/B) at threshold	+15.7 ± 1.0 db
Command channel modulation loss	+8.5 ± 0.6 db
Required sync channel SNR at threshold	+15.7 ± 1.0 db
Sync channel effective noise bandwidth	+2.0 ± 0.8 db
Sync channel modulation loss	+5.5 ± 0.5 db

from launch. The variations are due to both the increasing range and the variable antenna gains, and it is apparent where the performance of the low-gain antenna leaves off and that of the high-gain antenna takes over.

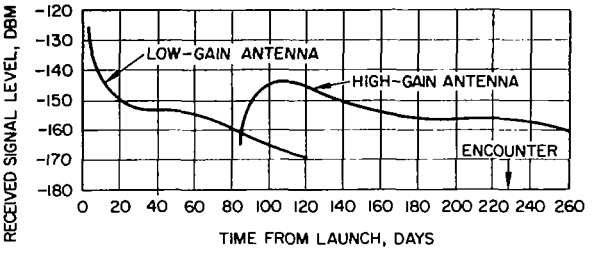

Figure 3. Received Signal Level Versus Time, Spacecraft to Earth

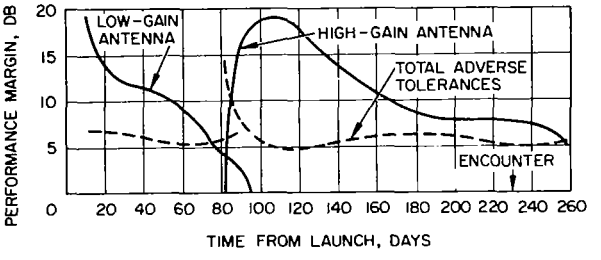

Figure 4. Telemetry Performance Margin Versus Time

Diplexed tracking antenna with maser, 8-1/3 b/s.

For the diplexed tracking feed and maser ground station configuration, the nominal threshold carrier level for telemetry is −164.4 dbm at 8-1/3 b/s. A comparison between this value, the nominal carrier levels, and the system tolerances (Figure 4) shows that the design criterion has been met over most of the flight, and the extent to which it has not been met at the transition region. In the transition region, the telemetry performance may be marginal.

The nominal received carrier levels for the earth-to-spacecraft channels are shown in Figure 5. Since the same spacecraft antennas are used for transmitting and receiving, both up and down channels exhibit similar time variations. A comparison between the command threshold carrier level of −143.3 dbm, the nominal received level, and

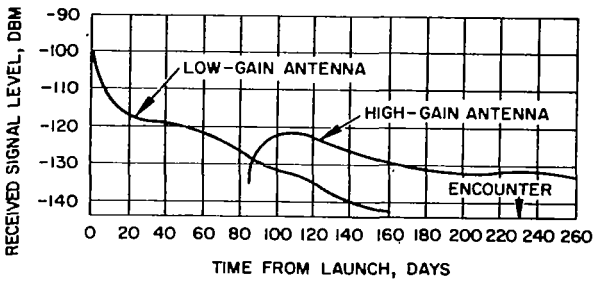

Figure 5. Received Signal Level Versus Time, Earth to Spacecraft

Ground transmission power = 10 kw, command modulation on.

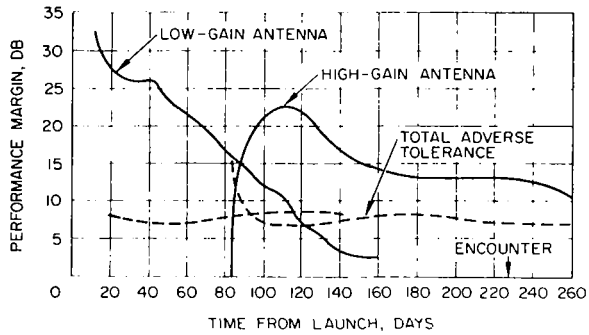

Figure 6. Command Performance Margin Versus Time

Ground transmission power = 10 kw.

the system tolerances (Figure 6) shows that the design criterion for command has been met for all flight phases.

3.0 SURVEYOR TELECOMMUNICATIONS[2]

3.1 Introduction

A basic philosophy incorporated into the Surveyor spacecraft, shown in Figure 7, is one of controlling the spacecraft from the ground to the greatest possible extent. Internal programming is held to a minimum and is allowed only in those instances where events are

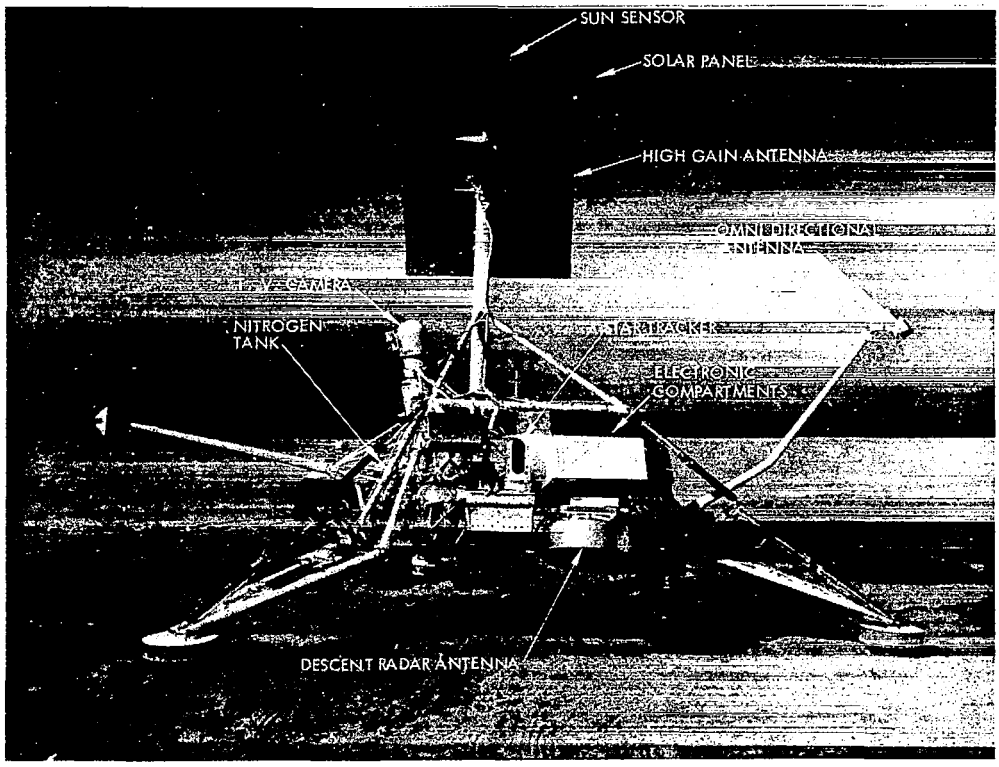

Figure 7. Surveyor Spacecraft

proceeding too rapidly to allow controlling commands to come from the earth. Thus, a heavy reliance is made upon the radio command link to the spacecraft.

The discussion of the Surveyor telecommunications will be presented in three sections. First, a general review of the telecommunications system listing the prominent requirements which it must meet. Secondly, a discussion will be given of the individual subsystems which constitute the telecommunications such as the r-f subsystem, the signal processing subsystem, the TV subsystem, etc. Thirdly, the telecommunications performance will be documented.

3.2 General Telecommunications Requirements

The general design philosophy used in the Surveyor spacecraft design includes the following five points which affect the telecommunications design: (1) As previously mentioned, the spacecraft is to be controlled by the ground to as great an extent as possible. This puts a high performance requirement on the command link but offers considerable flexibility in operating modes and design modifications; (2) During the transit portion of the spacecraft flight, communications must be maintained regardless of the spacecraft attitude; (3) The performance of each configuration of command or data link shall be adequate even in the situation of the simultaneous worst case value for each parameter in the telecommunications link; (4) Complete telecommunication redundancy is to be provided in those parts of the link in which all the data or commands must pass; (5) Only one Surveyor spacecraft will be operating on the lunar surface at a time. Thus, no frequency diversity has been incorporated into the Surveyor design nor has any provision been made for temporarily or permanently disabling a spacecraft.

The overall communication system requirements are summarized in Table 7. These requirements show that the r-f subsystem must

Table 7. Communication System Requirements

- Ground-spacecraft-ground, omni-directional transponder mode for continuous angle two-way doppler tracking to lunar distances
- Highly reliable, omni-directional ground-to-spacecraft command link to lunar distances
- Moderate bandwidth, omni-directional spacecraft-to-ground telemetry link continuously during transmit from injection to lunar distances
- Low power, moderate bandwidth, directional spacecraft-to-ground telemetry link during lunar operations
- High bandwidth, directional spacecraft-to-ground telemetry link for TV video at lunar distances both before and after landing
- Compatibility with the Deep Space Instrumentation Facilities
- High reliability, low power consumption, lightweight

provide a coherent transponder mode for trajectory determination. Due to spacecraft maneuvers and the necessity for maintaining command control, the receiving antenna system must provide a specified gain in all directions from the spacecraft. The gain requirement is greater than -10 db.

Table 7 also indicates the data links used and suggests the relative capacity of each configuration. The relative capabilities of these links result from three basic parameter changes. These are: (1) the variation in range as the spacecraft travels to the moon, (2) the selection of a low or high gain antenna for data transmission and (3) the selection of a low or high transmitting power. The ratio of antenna gains is approximately 35 db and the ratio of transmitted powers is 20 db. The transmitted power and antenna gains are varied as range varies to provide the data handling capability suggested by Table 7. Normally only the power is varied during the transit phase except during terminal descent when TV is transmitted. This requires both high power and the high antenna gain.

As indicated in Table 7, compatibility must be maintained with the Deep Space Instrumentation Facility (DSIF). This is done in two important aspects. The first is that of functional compatibility such as is provided in the transponder function. The second area of compatibility is that of selecting the proper parameters in the spacecraft such that when the gains, the losses, the transmitted power, etc. of the DSIF are considered, the data link is able to provide satisfactory performance. A summary of required DSIF parameters for the Surveyor design is given in Table 8.

A simplified block diagram of the Surveyor telecommunication system is shown in Figure 8. Both the required redundancy and typical signal processing functions are indicated in this diagram. In the command link the redundancy extends from the antennas through the receivers and central command decoders with duplicate units. The individual command decoders do not use redundancy. Similarly, the signal processing uses redundancy from the analog-to-digital converter (for those signals being processed as PCM) through the summing

Table 8. DSIF Parameters

• Transmit Parameters		
R-F Power Output (at Antenna Input)	200 watts to 10 kw	
Frequency Tuning Range	±100 KHz	
Transmitter R-F Losses	0.4 db ± 0.1 db	
• Receive Parameters		
Effective System Noise Temperature		
Maser with Antenna Pointing at Space	$55^{\circ}K \pm 10^{\circ}K$	
Maser with Antenna Pointing at Moon	$165^{\circ}K \pm 35^{\circ}K$	
Paramp with Antenna Pointing at Space	$270^{\circ}K \pm 50^{\circ}K$	
Frequency Tuning Range	±69 KHz with single crystal	
Receive R-F Losses		
With Maser	-0.18 ± 0.05 db	
With Paramp	-0.5 db max	
• Antenna Parameters	Tracking Antenna	Acquisition Antenna
Gain, Transmit	$51.0 \begin{smallmatrix} + 1.0 \\ - 1.5 \end{smallmatrix}$ db	20.0 ± 2.0 db
Gain, Receive	$53.0 \begin{smallmatrix} + 1.0 \\ - 0.5 \end{smallmatrix}$ db	21.0 ± 1.0 db
Beamwidth	0.4 deg	16 deg
Polarization, Overseas	RHCP	RHCP
Polarization, Goldstone	RH and LHCP	RHCP

amplifiers (both for PM and FM summing amplifiers) to the transmitters and antennas. Again each redundant unit is duplicated with the exception of the antenna system which offers the choice of one of two low gain antennas or the high gain planar array antenna.

The signal processing indicated in Figure 8 transmits data in a PCM format or an analog signals. In either case the data is multiplexed using subcarrier oscillators. The subcarrier oscillators in turn may either FM or PM the spacecraft transmitters. These formats are used both by the individual scientific instrument or by spacecraft or "housekeeping" sensors. In addition to these data formats, wideband FM may be used for any scientific sensors and in particular it is used for the television transmission.

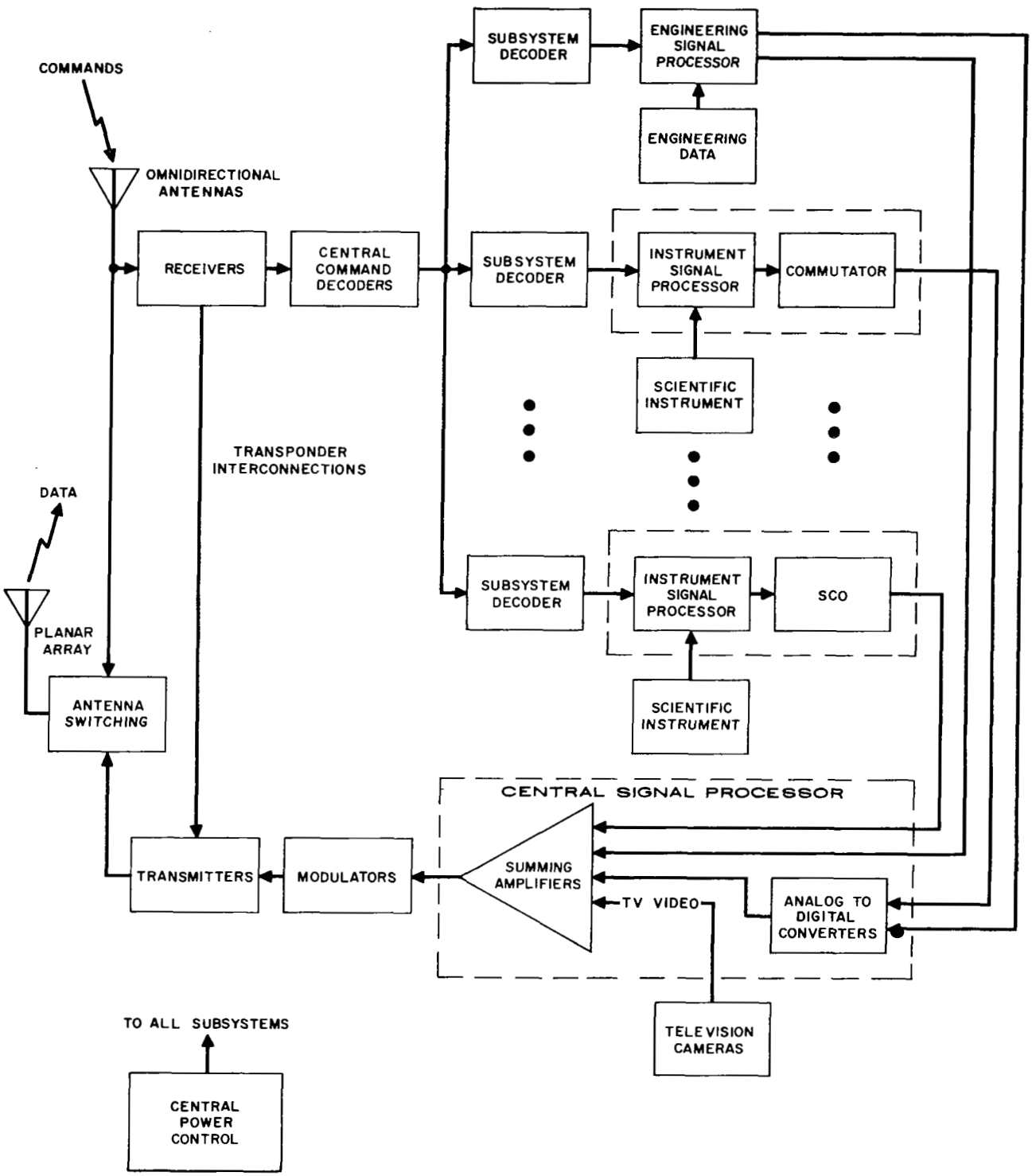

Figure 8. Electronic System Elements

3.3 Individual Subsystems

The component parts of the telecommunication system include the RF subsystem, the command decoding subsystem, the signal processing subsystem, the television subsystem and the scientific instrument subsystem.

The RF Subsystem. The RF subsystem is composed of the receivers, the transmitters, the antennas, and the RF cabling and switching. The functions which are performed by the receiver are those of transponder operation with the DSIF which is done in conjunction with the spacecraft transmitter, and that of receiving commands from the DSIF. The detected commands are sent on to the command decoding subsystem. The functions of the transmitter include providing both phase and frequency modulation capability and operating with the receiver in the transponder mode. In the transponder mode two (not four) combinations are available, receiver A operating with transmitter A and receiver B operating with transmitter B.

The receiver is an all solid state S-band receiver. Key receiver specifications are given in Table 9. Two types of detection are used

Table 9. Surveyor Receiver Specifications

Noise Figure	Less than 13 decibels
Threshold Sensitivity	Less than -110 dbm
Phase-lock Loop Bandwidth	70 ± 20 Hz
Phase-lock Tracking Range	Greater than 70 KHz at threshold, phase modulation index 1.6 radians
I-F Bandwidth (3 db points)	13 ± 0.5 KHz
AGC Dynamic Range	Not less than 40 db
AFC Loop Gain	17 db
AFC Time Constant	15 ± 2 milliseconds
Total Dynamic Range	75 db minimum
Input Frequency	2115 MHz, nominal
Input Impedance	50 ohms
Power Input	
Command Mode	1.43 watts
Phase Tracking Mode	1.8 watts
Weight	3.9 pounds

in the receiver, a phase locked loop detection to track the DSIF carrier for doppler tracking and a frequency discriminator detection for commands from the DSIF. The two methods are needed to achieve the requirements of doppler tracking and low power consumption. The phase locked loop is not needed on the lunar surface and may be disabled at a power savings of 0.37 watts. This is an appreciable savings considering that there are two receivers operating continuously. When the phase locked loop is not locked a frequency locked loop is automatically employed to maintain adequate frequency control.

The transmitter key specifications are given in Table 10. This transmitter uses all solid state components except for the TWT power amplifiers. The transmitter has a nominal output frequency of 2295 MHz which has been multiplied from 19-1/8 MHz. One of three master oscillators is used to supply the 19-1/8 MHz. They are selected on the basis of the desired modulation and the function the transmitter is

Table 10. Surveyor Transmitter Specifications

Transmitter Frequency	2295 MHz, nominal
Output Power	10 watts or 100 milliwatts
Stability	0.002 percent
Total Input Power	
For 10-watt Output	61 watts
For 100 mw Output	4.35 watts
Input Voltage Range	
Wideband FM	0 to 10 volts
Narrowband FM and PM	0 to 5 volts
Weight	6.3 pounds
Volume	325 $in.^3$
Approx. Dimensions	14.9" x 6.75" x 3.25"
Modulation Capability	
Phase Modulation	2.5 radians peak modulation index over an input frequency range of 100 cps to 160,000 cps
Frequency Modulation	
Wideband	Peak deviation 1.5 MHz over an input frequency range of 0 to 220,000 Hz
Narrowband	Peak deviation of 2,200 Hz or 20,000 Hz over an input frequency range of 0 to 1000 Hz

required to perform. Wideband FM is accomplished with one oscillator contained in the transmitter. A second oscillator in the transmitter is used to supply a stable carrier for phase modulation. The third oscillator used to drive the transmitter is supplied by the receiver for the transponder mode. In this mode the transmitter may also be phase modulated.

Two antenna types are used on Surveyor. The first type is a low gain antenna, of which two are used. The second is a high gain planar array antenna. These antennas are shown in Figure 7. Both types of antennas use right hand circular polarization.

Each low gain antenna connects directly to one of the receivers through a diplexer. The transmitter arm of the diplexer goes through r-f switching which allows any of the three antennas to be connected to either transmitter. The requirement for coverage over 4π steradians falls to the two low gain antennas.

The high gain planar array provides a gain of 27 db using a surface of 39" x 39". This design was chosen over a parabolic dish for the following reasons: (1) the efficiency of a planar array can be made higher than a dish of equal aperture (An efficiency of approximately 70% is realized by the Surveyor planar array.) and (2) the planar array requires less volume for a given aperture than a dish. This is an important consideration when mounting the antenna within the limits imposed by the nose shroud.

The antenna array uses seven waveguides side by side to form the radiating surface. These are all driven by another waveguide section. The crossed slots provide circular polarization. The total weight of the antenna is 8.9 lbs.

Command Decoding. The decoding of commands sent to the Surveyor spacecraft from the DSIF is done in two stages. The first stage is completed in the central command decoders. This stage performs the more complicated processes of the decoding such as identifying the sync code, separating the command into its component parts and complement checking the command code. The second stage of the decoding

is done by small subsystem command decoders located throughout the spacecraft. These consist of diode matrices which are set to decode a particular series of pulses from the central decoder.

Two redundant central decoders are used and up to 32 individual non-redundant subsystem decoders may be used. The system is quite flexible in that the subsystem decoders may be added or subtracted quite easily without disturbing the central command decoder. Each subsystem decoder may provide up to 32 individual commands.

Signal Processing. The signal processing used in the Surveyor spacecraft is required to process data from the scientific instruments and from the engineering sensors on the spacecraft. Analog channels and PCM channels are provided and may be transmitted simultaneously by means of subcarriers. Data is transmitted using any of the following methods: FM, FM/FM, FM/PM, PCM/FM/FM, or PCM/FM/PM.

The hardware units which make up the signal processing are in two general categories, those that are basic to the spacecraft on all flights and those that are especially designed for a certain set of scientific or engineering measurements. Included in the first group are the Central Signal Processor (CSP) and the Engineering Signal Processor (ESP). The second group includes the Auxiliary Engineering Signal Processor (AESP), the Low Data Rate Auxiliary (LDRA), and all of the specialized signal processing required for the scientific instruments.

The CSP, as its name implies, is central to the entire signal processing subsystem. It contains summing amplifiers through which all the subcarriers must pass before modulating the transmitter. The CSP also contains two (for redundancy) 10 bit A/D converters. In addition to converting analog signals into a PCM format, the A/D converter supplies timing signals to all the commutations in the signal processing units.

The A/D converter in the CSP has the following characteristics: (1) Bit rates of 4400 b/s, 1100 b/s, 550 b/s, 137.5 b/s and 17.2 b/s are available. (Each of these bit rates drives the appropriate

subcarrier oscillators (SCO) although in the case of a failure of one SCO an alternate SCO, designed for a higher bit rate, may be used.) (2) The PCM word format is an eleven bit word. Ten bits are data bits and one bit is for a parity check. (3) The words are assembled into frames which, depending upon the commutator used, have lengths of 16 words, 50 words, 100 words, and 120 words. Each frame uses as frame sync words, Barker code words. The 100 and 120 word frames use two Barker code words. The Barker code sync words also are generated by the A/D converter. (4) The A/D converter supplies gate timing signals which bypass the A/D conversion process for certain words. These words are then used to transmit on/off signals, with each bit representing a signal rather than each word.

The Engineering Signal Processor (ESP) is the second unit which is basic to all spacecraft. It contains a majority of the commutation circuitry on the spacecraft. Here data from the spacecraft itself, housekeeping data, is commutated into PAM before being sent to the A/D converter for conversion to PCM. Four commutators are contained in the ESP. These are primarily used during four portions of the spacecraft life; transit to the moon (one commutator), terminal descent (two commutators) and operation on the lunar surface (one cummutator). The data sent during each of these periods is pertinent to the operations to be performed. Since the capability of the telecommunications system varies during these four portions of spacecraft life, certain key data is often transmitted several times during a commutation cycle to provide sufficient data samples.

The ESP, in addition to the commutators, contains several subcarrier oscillators (SCO) for transmitting engineering data such as vibration data. The output of these SCO's are summed in the ESP and then sent to the CSP for further summing with other subcarrier oscillators before modulating the transmitter.

The Auxiliary Engineering Signal Processor (AESP) is very similar to the ESP. It is largely an extension of the ESP and is designed as a backup and supplement to the ESP capabilities on early flights of the Surveyor spacecraft.

The Low Data Rate Auxiliary (LDRA) operating in conjunction with the AESP and the CSP, provides low bit rates of 137.5 b/s and 17.2 b/s. An important functional capability has been added by including the LDRA. This is the ability to transmit data continuously from the spacecraft during transit. This is accomplished using the low power transmitter (100 MW) and the low gain antennas.

Television. The television experiment carried by the Surveyor spacecraft gives the spacecraft its name, for the television cameras "survey" the lunar surface. The survey is accomplished when the spacecraft is on the lunar surface. The T.V. experiment will be described from the point of view of its relationship to the telecommunications link and its capability.

The overall capabilities of the T.V. survey cameras are listed in Table 11.

Table 11. TV Capabilities for the Survey Cameras

Azimuth Coverage	360 degrees
Elevation Coverage	65 degrees (-45 to ±20 degrees)
Time per Frame	1 second and 20 seconds*
Resolution per Frame	600 lines and 200 lines*
Wide Angle Viewing Capability	25.4 x 25.4 degrees
Narrow Angle Viewing Capability	6.4 x 6.4 degrees
Focus Range	4 feet to infinity
f-Stop Range	f. 4 to f. 22
Exposure Time	150 ms or "BULB"
Maximum Picture Rate	1 picture per 3.6 seconds
Filter Wheel	One of four filters may be selected

*Emergency Mode Parameters

Two modes are available in the television cameras, a normal mode and an emergency mode. The normal mode results from a 1 second frame with 600 line resolution. This combination yields a video bandwidth of 220,000 cps. The emergency mode is used if the high gain antenna is not available or if the high power transmitters are not available. It has a 1200 cps bandwidth resulting from a 200 line resolution readout in 20 seconds. The video and frame identification for both the normal mode and the emergency mode frequency modulate the spacecraft transmitter. An RF bandwidth of 3 MHz is used for the normal mode and an RF bandwidth of 10 KHz is used for the emergency mode.

Scientific Instruments. Each of the scientific instruments carried by the Surveyor spacecraft forms an interface with the telecommunications system through an especially designed auxiliary unit. This auxiliary unit contains the required command decoding, power switching or power form generation, and signal processing.

The signal processing used by a particular experiment depends upon several considerations. These include the bandwidth required by the experiment, the accuracy required for the data, the length of time the experiment will operate and the relative scientific importance of the experiment with respect to other experiments on the spacecraft. In general, the data received from a scientific experiment may be transmitted using an RF bandwidth up to 3 MHz in either an analog or PCM format.

3.4 Telecommunications Performance

The Surveyor Spacecraft Telecommunications link is required to meet a variety of operating modes. While a detailed listing of these modes is beyond the scope of this discussion, representative operating modes are given in Tables 12 and 13. These tables contain a tabulation of the one way transmission equation listing the parameter values in a

Table 12. Earth to Spacecraft Transmission (Lunar Phase Command Mode)

Parameter	Value	Tolerance
• Signal Power at Receiver		
Total Power Transmitted	10 kw/+70 dbm	+0 -1.0 db
Transmitting Circuit Loss	-0.3 db	±0.1 db
Transmitting Antenna Gain	+50.0 db	±1.0 db
*Antenna cable 8 feet	-0.95 db (max)	
Path Attenuation at carrier MHz, R = 384,500 KM	-211.1 db	±0.4 db
Receiver Antenna Gain	+2.0 db	±2.0 db
Receiver Antenna Polarization Loss	0 db	+0 -6 db
Receiver Circuit Loss	-1.5 db (max)	
Signal Power Available at Receiver	-91.9 dbm	+3.5 -10.5 db
• Noise Power at Receiver		
$T_{eff} = (N.F.-1)290^{o}K + T_s$		
N.F. Noise Figure = +13 ±1 db		
(N.F.-1)290°K = 37.6 ±1 db		
KT_{eff}(Boltzman's constant = -198.6 dbm/deg/kHz	-161.0 dbm/Hz	±1.0 db
Noise Bandwidth, BW 13 kHz	+41.1 db	±0.5 db
Total Noise Power	-119.9 dbm	±1.5 db
• Signal-to-Noise Ratio		
Receiver S/N	+28.0 db	+5 -12.0 db
• Carrier Performance		
Threshold S/N	+10.5 db	±1.0 db
Center Margin	+17.5 db	+6 -13.0 db
Minimum Margin	+4.5 db	

*S/C Functions only

Table 13. Spacecraft to Earth Transmission (Television Transmission - Primary Mode)

Parameter	Value	Tolerance
• Signal Power at Receiver		
Total Power Transmitted	10w/+40 dbm	+1 db -0 db
Transmitting Circuit Loss		
*Cable and transfer switch (A or B)	-0.4 db (max)	
*Interconnecting cable and transfer switch #1	-0.45 db (max)	
Transmitting Antenna Gain	+27 db	±0.5 db
Transmitting Antenna Polarization and/or Pointing Loss	0 db 0 db	±0.1 db +0 -0.1 db
*Antenna cable 16 feet	-1.9 db (max)	
Path Attenuation at carrier MHz, R = 384,500 KM	-211.4 db	±0.4 db
Receiver Antenna Gain	+51.0 db	±0.7 db
Receiver Circuit Loss	-0.5 db	±0.2 db
Signal Power Available at Receiver	-96.65 dbm	+3.9 db -2.0 db
• Noise Power At Receiver		
$T_{eff} = (N.F. - 1)290^{o}K + T_s =$ $160.8^{o}K \pm 1.2$ db		
KT_{eff}(Boltzman's constant = -198.6 dbm/deg/kHz	-176.54 dbm/Hz	±1.2 db
Noise Bandwidth, BW = 3.3 MHz	+65.18 db	
Total Noise Power	-111.36 dbm	±1.2 db
• Signal-to-Noise Ratio		
Receiver S/N	+14.71 db	+5.1 db -3.2 db
• Carrier Performance		
Threshold S/N	+10.5 db	±1.0 db
Center Margin	+4.2 db	+6.1 db -4.2 db
Minimum Margin	0.0 db	

*S/C Functions only

logarithmic form. It is required of the telecommunications links that the sum of the worst case margins on each parameter value be subtracted from the nominal value of the output signal to noise ratio and that the resulting signal to noise ratio be above the required threshold value.

4.0 THE LUNAR ORBITER TELECOMMUNICATIONS SYSTEM[6]

4.1 Introduction

The primary purpose of the Lunar Orbiter Program is to obtain lunar topographic data to assist in selecting an Apollo landing site. It accomplished this by taking high-resolution photographs from lunar orbit at an altitude of about 25 miles. The photographs will be obtained using a film-type camera, the pictures developed onboard, and then scanned and transmitted to earth.

Tracking of the Lunar Orbiter will yield information concerning the size and shape of the moon and its gravitational field. In addition, the spacecraft will carry a limited number of sensors which will provide some data on the lunar environment.

4.2 Spacecraft Configuration

Figure 9 shows the general configuration of the 850-pound spacecraft which is about 5-1/2 feet high and 5 feet in diameter, excluding the solar panels and antennas. The span across the deployed antenna booms is about 18-1/2 feet.

With the exception of the rocket engine and its fuel tanks, which are used for midcourse maneuvers and deboost into lunar orbit, essentially all of the major spacecraft components are attached to an equipment mounting plate. That mounting plate, the underside of which remains oriented toward the sun at all times except when the spacecraft is maneuvering, provides thermal control for the components attached to it.

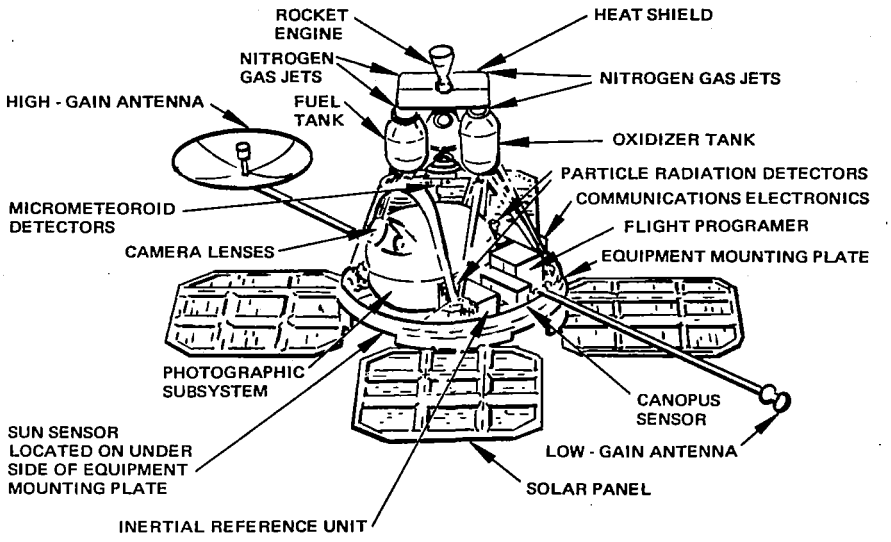

Figure 9. Spacecraft Configuration

The spacecraft power system is a conventional solar array/storage battery type. A 12 ampere-hour nickel cadmium battery will be used to supply the spacecraft power requirements during the launch phase prior to solar array deployment and during those periods of the lunar orbit when the spacecraft is in the moon's shadow. When the solar array is in sunlight a maximum of about 375 watts is available to handle all power demands including battery recharging.

The star Canopus and the sun are the primary references for spacecraft attitude orientation. For maneuvering, or when those references are occulted, a strapped-down gyro system is used. Attitude control is accomplished by a cold-gas system.

The spacecraft camera system employs two lenses which take simultaneous pictures on a roll of 70-mm-wide aerial film. One of the lenses nas a 24-inch focal length and can take pictures from an altitude of 46 km with a resolution of about 1 meter. The other lens, which has

a focal length of about 3 inches, will take pictures with a resolution of about 8 meters. The film is developed onboard using a method which presses the film into contact with a web that contains a single-solution processing chemical. After the film has been dried, it is ready for readout and transmission to the ground.

Figure 10 is a drawing of the readout system. The light source for film scanning is a line-scan tube. The tube itself sweeps the beam of light through an excursion of 0.1 of an inch in a direction parallel to the film travel. An optical system sweeps the beam of light across the film in a transverse direction and also serves to focus that spot of light. As the figure shows, scanning with sweeps of 0.1 inch begins at one edge of the film and continues across the film until the opposite edge is reached. At that time the film is advanced 0.1 inch and the film is scanned in the opposite direction. This sequence is repeated, with the scan rates being such that 43 minutes are required to scan about 1 foot of film which contains one high-resolution and one medium-resolution photograph. Collecting optics direct the transmitted light into a photomultiplier, and the resulting electrical signal is conditioned and mixed with synch and blanking pulses and fed to the communication system modulator.

The spacecraft "brain" is a programer which accepts inputs from the earth via the command system. That programer is essentially a digital data processing system and will control about 65 functions within the spacecraft.

4.3 Telecommunication System

Design Objectives and Constraints. The basic functions assigned to the Lunar Orbiter communication system include data transmission (telemetry and video data), command reception, and measurement of Doppler and range.

The design of a system to satisfy those basic functional requirements was constrained by a number of factors, including the following:

1. Compatibility with the DSIF Stations.
2. Each RF link to have a nominal performance margin of not less than 6 dB.
3. Video (photographic data) to be transmitted in analog form.
4. Video (data rate) to be approximately 250 KHz.
5. Ability to transmit telemetry data during video transmission.
6. Provide a video data output S/N ratio of not less than 33 dB, p-p/rms.
7. Provide a command link having a bit error rate not greater than 10^{-5}.
8. Provide a telemetry bit error rate not greater than 10^{-5}.
9. Provide a spacecraft antenna system which, at lunar distance, would enable command capability and telemetry reception for any spacecraft orientation.
10. Have an overall reliability of not less than 95 percent for the first 30 days of the mission.
11. Use existing, space-qualified, hardware components wherever possible.
12. Provide for on-off control from the earth for all spacecraft RF emissions.
13. Minimize system power consumption.
14. Sideband energy outside of 3-1/3 MHz channel bandwidth to be at least 30 dB down.
15. Avoid the use of RF power switches in the spacecraft.
16. Provide for two-way Doppler tracking.
17. Provide for ranging measurements using the JPL Pseudo Noise ranging system.

Modulation Techniques. Vesgitial sideband-amplitude modulation (VSB-AM) was chosen for Lunar Orbiter primarily on the basis of containing more of the radiated energy within the allotted 3.33-MHz spaceband channel. That consideration was imposed as a design constraint due to the possibility of other spacecraft operating in an adjacent channel.

The video data, which occupy a frequency spectrum from 0 to 230 KHz, are first double-sideband, suppressed-carrier modulated onto a 310-KHz subcarrier, and then the upper sideband removed by filtering. A 38.75-KHz pilot tone is derived from the 310-KHz subcarrier oscillator and is transmitted for use by the ground demodulator for subcarrier reinsertion. The 50 bps PCM telemetry data are biphase modulated (0° or 180°) onto a 30-KHz subcarrier. The video, pilot tone, and telemetry signals are then summed, and the resulting composite signal phase modulates the S-band carrier. The frequency spectrums of the video and composite signals are shown in Figure 11. The effective modulation indices are: video - 3.6 radians peak, pilot tone - 0.47 radian peak, and telemetry - 0.2 radian peak. When transmitting video data, the spacecraft operates on a 10-watt transmitter and a directional antenna with a gain of 23.5 dB.

When video is not being transmitted, the spacecraft operates on a 0.5-watt transmitter to conserve battery power. Doppler tracking, ranging, and telemetry transmission can be accomplished in this low-power mode using the low-gain antenna. The same 50 bps PCM telemetry data are telemetered to earth on a 30-KHz subcarrier as during video transmission. However, while operating in the low power mode, the modulation index is increased from 0.2 radian peak to 1.5 radians peak to enhance the output S/N ratio at the receiving station. In all cases the telemetry bit error rate is expected to be 10^{-5} or less. Ranging is accomplished using the JPL turnaround ranging system. The pseudo noise ranging code is phase modulated onto the up-link S-band carrier with an index of 1.2 radians peak. After detection in the transponder, the code is then remodulated on the down-link carrier with an index of 0.41 radian peak and is transmitted simultaneously with telemetry.

Several subcarriers are used in the command transmission system. The digital command word is frequency-shift-keyed onto one of the subcarriers. All of the subcarriers utilized are phase modulated on the up-link carrier, each with an index of 0.7 radian peak. To insure that commands are received correctly, the command words are telemetered back to the DSIF via one of the data slots in the 50 bps telemetry frame before the commands are executed by the spacecraft.

Block Diagram. The spacecraft telecommunication system block diagram, Figure 12, except for the periods of video transmission, the spacecraft will operate with the transponder exciter and low-gain antenna. For video transmission, the spacecraft effective radiated power will be increased by a TWT RF amplifier and high-gain antenna.

The appropriate spacecraft emission mode will be selected by earth command: (1) telemetry and ranging, (2) video and telemetry, or (3) telemetry alone.

High-Gain Antenna. The high-gain antenna is a 36-inch parabolic dish of lightweight honeycomb construction. It is attached to the end of a 52-inch boom which acts as a coaxial transmission line. The antenna is deployed from its stowed position at spacecraft shroud ejection in the same manner as the low-gain antenna. Some of the pertinent characteristics of this antenna are:

Gain:	23.5 dB
Beamwidth:	10^{o}
Efficiency:	61 percent
Bandwidth:	2290 to 2300 MHz
Feed Type:	Turnstile with cup-shaped reflector
Focal Length:	12 inches
Polarization:	Right-hand elliptical
Axial Ratio:	<1.59:1

VSWR:	<1.3:1
Weight:	2.3 lb (dish and feed)

An unusual feature of the Lunar Orbiter use of this antenna is the method of pointing it toward the earth using rotation about only one axis. When the attitude reference system is locked on the sun and Canopus the antenna boom is approximately perpendicular to the ecliptic plane. Therefore, as the moon traverses its orbit, it is necessary only to rotate the antenna about the boom axis to direct the pattern toward the earth.

Transponder. The Lunar Orbiter transponder is basically an extension of the coherent transponder used on Mariner 4 and makes use of the standard modules developed by JPL.

The transponder will operate in a noncoherent mode using a self-contained crystal-controlled auxiliary oscillator until an up-link carrier is received with sufficient signal strength to switch to the coherent VCO. Coherent operation will translate the up-link carrier frequency by the exact ratio 240/221 for retransmission.

For lunar distances, it was found that the loop noise bandwidth of the transponder could be increased from the 20 cps required by Mariner to 100 cps and still have a receiving threshold which would allow the communications link to perform as planned. By increasing the loop noise bandwidth to 100 cps, the capability to coherently track greater Doppler rates is provided, allowing two-way Doppler tracking during the worst-case spacecraft accelerations.

Other transponder characteristics are:

Threshold:	-142 dBm
Noise figure:	12 dB
Exciter power output:	500 mw
Modulation sensitivity:	2 rad/volt
Weight:	12.75 lb
Power consumption:	Less than 17 watts

The Lunar Orbiter TWT RF amplifier uses an existing space-proven tube, the Hughes 349H. The prime reason for selecting this device rather than another power amplifier, such as a triode cavity or amplitron, was its proven long life.

Some of the other characteristics of the TWT RF amplifier are:

Power Output:	10-13 watts
RF Gain:	27 dB
Noise Figure:	38 dB
Overall Efficiency:	24 percent
D-C Power Required:	54 watts, maximum
Weight:	5.5 lb

Command Decoder. The command decoder contains the demodulators for the command subcarriers, the command-data shift registers, and other circuits used for address recognition and code verification.

When a command is received, it is temporarily stored in the data shift registers so that the multiplexer encoder can nondestructively sample the command word and telemeter it to earth for verification. Upon verification on earth that the correct command is being held in the registers, the command word is transferred to the spacecraft programer to be acted upon immediately or to be stored and acted upon at a designated later time. If a wrong command is being held, the register can be cleared and the command retransmitted.

The command transmission rate on the up-link carrier is 20 bps.

Multiplexer Encoder. The multiplexer encoder is essentially a standard PCM encoder consisting of analog and digital multiplexers, an analog to digital converter (ADC), and several registers.

The encoder converts analog and digital input data into a 50 bps serial NRZ bit train. Each frame is equivalent to 128 9-bit words, thereby providing one complete frame every 23 seconds. Each frame contains 78 analog channels, 127 1-bit "event" channels, 9 digital channels and a 43-bit Legendre frame synch word.

4.4 Ground System Description

The Lunar Orbiter uses the Deep Space Stations at Goldstone, Madrid, and Woomera. The equipment configuration employed at those stations consists of both standard station equipment and special Lunar Orbiter project equipment.

When the spacecraft operates in the low-power mode, Doppler tracking and carrier demodulation is accomplished by the DSIF phase-lock receiver. The 30-KHz telemetry subcarrier is taken from the telemetry output of the DSIF receiver and is then demodulated telemetry demodulator. After detection and decommutation, the PCM bit train is entered into an SDS-920 computer. The computer edits the telemetry data, inserts GMT, and formats the data for transmission to the SFOF via high-speed-data and teletype lines.

During transmission of video data, the DSIF receiver operates in a noncoherent mode since the modulation index of 3.6 radians often produces phase reversal of the carrier and prevents carrier tracking. The receiver gain and VCO frequency are controlled manually during this type operation. The 10-MHz IF output of the receiver is demodulated by an FMFB demodulator. Coherent detection of the 310-KHz video subcarrier takes place in the video subcarrier detector, from whence the video data are fed to the video data photographic recorder where the pictures are reproduced.

The DSIF transmitter produces up to 10 kW of S-band power and can be phase modulated up to 3.0 radians peak. The phase-lock, double-superheterodyne receiver has a traveling wave maser front end with an equivalent noise temperature of 55° Kelvin. The threshold loop noise bandwidth ($2\ B_{LO}$) of the carrier tracking loop is 12 cps.

Both transmitting and receiving are accomplished using an 85-foot-diameter, Cassegranian fed, parabolic antenna with a gain of 53 dB. When pointed at the Lunar disk, the antenna adds another 110°K to the system noise temperature.

An FMFB demodulator is used instead of a standard FM discriminator to detect video data because of its threshold improvement characteristics. The demodulator thresholds at a C/N ratio of 7.0 dB measured in a 3.3-MHz bandwidth. It utilizes an internal IF of 45 MHz with a feedback factor of 9.5 dB, an IF noise bandwidth of 1.0 MHz, and a loop noise bandwidth of 600 KHz.

The command words are frequency modulated onto a subcarrier and then mixed with other command system subcarriers. This combined signal is then fed to the DSIF transmitter modulator, where it is phase modulated onto the S-band carrier. When the command word is returned via telemetry from the spacecraft, it is routed into the command equipment. There it is automatically compared with the transmitted word, and, if the two are identical, an execute command is sent to the spacecraft, completing the command cycle.

4.5 Communications Link Design

Shown in Table 14 is a summary of the Lunar Orbiter Communications link design for operation at lunar distance. The analysis is based on a system noise temperature of 165°K for the DSIF receiver and 3400°K for the transponder receiver. The thresholds for carrier tracking are the signal-to-noise ratio which produce a 30° rms phase jitter in the phase-lock loop. The minimum margin above threshold is 6.7 dB in the video link. With a PM noise improvement factor of 17.8 dB, the output signal-to-noise ratio for the video data is 36.8 rms/rms in an output at bandwidth of 310 KHz, assuming a noiseless input signal from the spacecraft photo subsystem. Normally the signal from the photo subsystem has a signal-to-noise ratio of 24-dB peak-to-peak/rms; thus, the communications system noise has little

Table 14. Communications Link Design

Parameter	Command	Telemetry	Video
Transmitter power	70.0 dBm	26.0 dBm	40.0 dBm
Transmitting antenna gain	51.0*	0.0	23.5
Space loss	-210.7	-211.4	-211.4
Circuit loss	-3.4	1.8	-2.6
Receiving antenna gain	-3.0	53.0	53.0
Total received power	-96,1 dBm	-134.2 dBm	-97.5 dBm
Carrier tracking PLL:			
Modulation loss	-2.2	-5.8	
Received carrier power	-98.3 dBm	-140.0 dBm	
Loop noise bandwidth	20.0	10.8	Not applicable
Threshold S/N ratio	9.0	14.0	
Threshold power	-134.3 dBm	-151.6 dBm	
Performance margin	36.0	11.6	
Data channel:			
Modulation loss	-7.9	-3.2	0
Received data power	-104.0 dBm	-137.5 dBm	-97.5 dBm
Noise bandwidth	24.0	17.0	65.2
Threshold S/N ratio	12.0	10.3	7.0
Threshold power	-127.3 dBm	-149.1 dBm	-104.2 dBm
Performance margin	23.3	11.6	6.7
Output S/N ratio	61.8 rms/rms	21.9 rms/rms	36.8 rms/rms

*All values in dB unless otherwise noted.

Note: All values nominal.

effect on the noise content of the reconstructed pictures. Though not shown in the table, in the high-power mode the telemetry output S/N ratio is 44.9-dB rms/rms in a 50-Hz bandwidth, and the pilot tone S/N ratio is 51.9-dB rms/rms in a 1-Hz bandwidth.

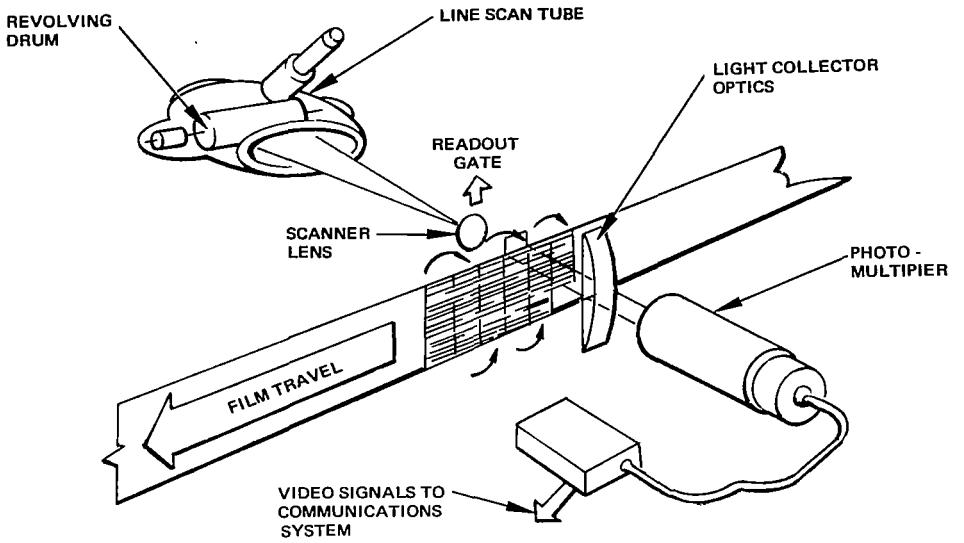

Figure 10. Photographic Readout System

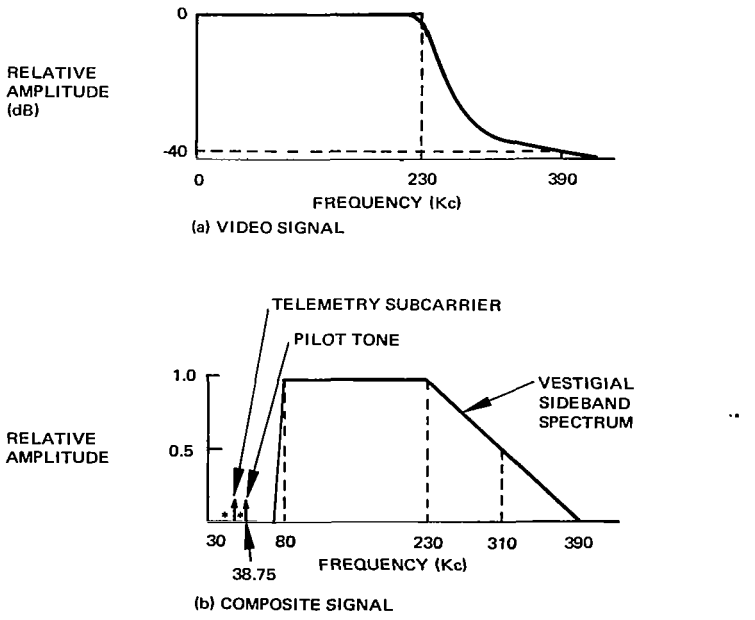

Figure 11. Frequency Spectra

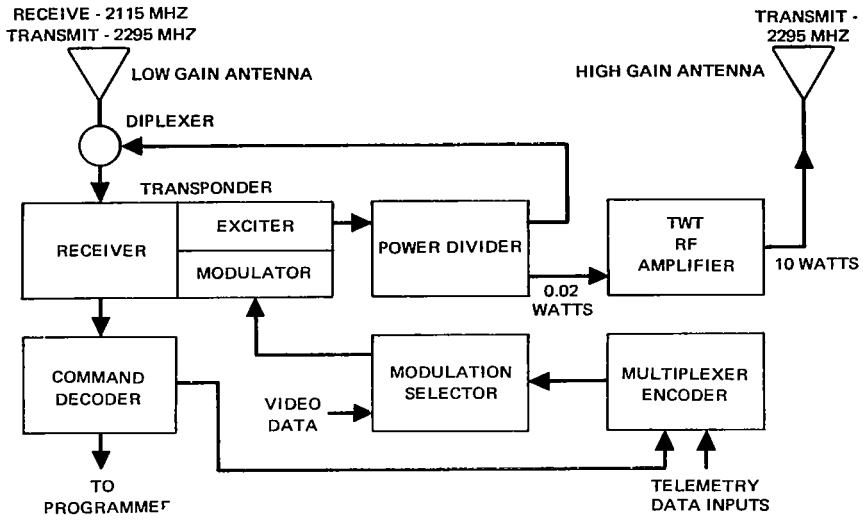

Figure 12. Spacecraft Communications System

5.0 OVERALL SPACECRAFT PERFORMANCE

The overall spacecraft performance is given in this section in terms of spacecraft weight, cost, and data rate. The communications methodology, developed during this contract, determines the parameters for the communication link to meet the required data rate performance for a minimum cost or weight of the communication equipment. It remains then to relate the communications system weight and cost to the overall spacecraft weight and cost. While establishing this relationship was beyond the scope of the contract, a correlation between the communications system weight and the total spacecraft weight may be made for actual spacecraft. Such a tabulation is given in Table 15[7]. This table indicates that between 40 and 65 percent of the total spacecraft weight is due to components described by the communications system methodology (i.e., communications, timing, data handling and electric power). Therefore doubling the spacecraft weight estimates given by the methodology weight, gives a fair estimate of the total spacecraft weight.

Table 15. Interplanetary Spacecraft Weight Allocations

	Pioneer V	Mariner II	Mariner IV	Pioneer VI
Percentable of total weight allocated to:				
Scientific experiments	10	11	11	25
Communications, timing, and data handling	30	16	18	25
Electric power	35	24	26	20
Structure, pyro, cabling, and thermal control	25	30	26	24
Attitude control and propulsion	0	19	19	6
Total spacecraft weight, pounds	95	445	575	140

Table 16. Approximate Costs of Selected Automated Spacecraft

Launch-vehicles costs not included. Cost of instruments included.

Spacecraft	Number of Flight Units	Total Cost (Including Development), $M	Cost per S/C, $M	Weight-Pound (Excluding Propellants)	Cost per Pound, $K	Repeat Cost Per S/C, $M
Mariner II	3	30	10	450	22	10
Mariner IV	3	85	28	575	50	17
Ranger	9	170	19	675-800	25	16
Surveyor	7	450	64	760	85	33
Orbiter	5	150	30	570	53	15
OSO	8	80	10	500	20	10
OAO	5	310	62	3600	17	45
OGO	6	210	35	1000	35	26
Nimbus	4	200	50	900	56	45
Biosatellite	6	130	22	950-1250	21	12

Table 16[8] gives cost data for various spacecraft, including the cost per pound. These cost per pound values may be compared with optimization results from the communications methodology given earlier in this final report. Typically these results indicated a cost of $20,000 per pound which compares favorably with the values noted in Table 16.

As an indication of the general performance for spacecraft data rate, Figure 13[7] is given. This indicates the continual performance improvement as a function of time.

6.0 NOMENCLATURE

A	received signal level, a function of spacecraft attitude γ and spacecraft earth range r
ω_o	carrier frequency transmitted by the DSN station
ϕ_c	phase modulation by the composite command signal
ϕ_r	phase modulation by the coded ranging signal
$r(t)$	spacecraft-earth range, a function of time t
c	velocity of propagation
V_d	amplitude of the complex four-level wave
$d(2f_d t/9)$	binary telemetry data of amplitude ±1 and bit rate $(2/9)f_d$
$a(ft)$	symmetrical square wave of amplitude ±1 and frequency f
$X(f_d t/2)$	cyclic, binary, pseudorandum sequence of amplitude ±1, length 63 bits, and bit rate $f_d/2$

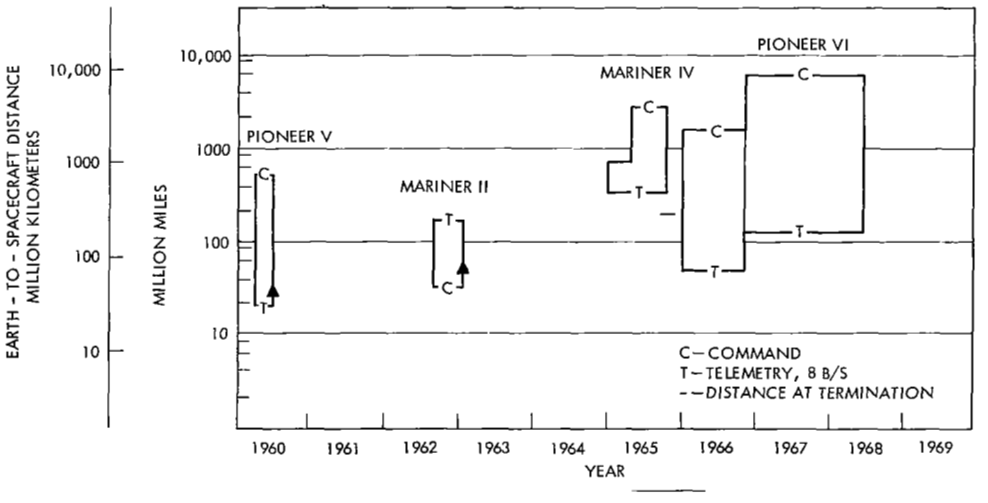

Figure 13. Interplantary Telecommunication Capability

$\oplus$	modulo 2 addition
S	signal power
T	time for one bit
N	noise power
B	bandwidth

7.0 REFERENCES

1. Mathison, R.P., "Mariner Mars 1964 Telemetry and Command System," IEEE Spectrum, July 1965.

2. Stokes, L.S., "Telecommunications From a Lunar Spacecraft," AIAA Unmanned Spacecraft Meeting, Los Angeles, California March 1-4, 1965.

3. Martin, B.D., "The Mariner Planetary Communication System Design," Tech. Report 32-85 (Rev. 1), JPL, May 15, 1961.

4. Springett, J.C., "Command Techniques for the Remote Control of Interplanetary Spacecraft," Technical Report 32-314, JPL, Aug. 1, 1962.

5. Springett, J.C., "Pseudo Random Coding for Bit and Work Synchronization of PSK Data Transmission Systems," presented at International Telemetering Conference, London, England, 1963.

6. Bundick, W.T., Green, C.H., and Brummer, E.A., "The Lunar Orbiter Telecommunication System," presented at International Space Electronics Symposium, November 1965.

7. Reiff, G.A., "Interplanetary Spacecraft Telecommunications Systems," IEEE Spectrum, April 1966.

8. Cortright, E.M., "Automated Spacecraft Cone of Age," Astronautics and Aeronautics, January 1967.